



# Thermal Extraction and Delivery from Advanced Reactor Systems

September 2023

*Changing the World's Energy Future*

Daniel Mark Mikkelson, Vaclav Novotny, Logan David Williams, Junyung Kim, Sarah Elizabeth Creasman, Nipun Popli, Aidan Christopher George Rigby, Kyle Russell Costanza



#### **DISCLAIMER**

This information was prepared as an account of work sponsored by an agency of the U.S. Government. Neither the U.S. Government nor any agency thereof, nor any of their employees, makes any warranty, expressed or implied, or assumes any legal liability or responsibility for the accuracy, completeness, or usefulness, of any information, apparatus, product, or process disclosed, or represents that its use would not infringe privately owned rights. References herein to any specific commercial product, process, or service by trade name, trade mark, manufacturer, or otherwise, does not necessarily constitute or imply its endorsement, recommendation, or favoring by the U.S. Government or any agency thereof. The views and opinions of authors expressed herein do not necessarily state or reflect those of the U.S. Government or any agency thereof.

# **Thermal Extraction and Delivery from Advanced Reactor Systems**


**Daniel Mark Mikkelsen, Vaclav Novotny, Logan David Williams, Junyung Kim,  
Sarah Elizabeth Creasman, Nipun Popli, Aidan Christopher George Rigby, Kyle  
Russell Costanza**

**September 2023**

**Idaho National Laboratory  
Idaho Falls, Idaho 83415**

**<http://www.inl.gov>**

**Prepared for the  
U.S. Department of Energy  
Under DOE Idaho Operations Office  
Contract DE-AC07-05ID14517**



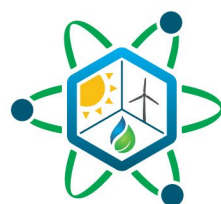
# Thermal Extraction and Delivery from Advanced Reactor Systems

---

*September | 2023*

*Logan Williams, Vaclav Novotny, Junyung Kim, Sarah Creasman,  
Nipun Popli, Aidan Rigby, Kyle Costanza, Daniel Mikkelsen*

*Idaho National Laboratory*



**IES**

Integrated Energy Systems

#### **DISCLAIMER**

This information was prepared as an account of work sponsored by an agency of the U.S. Government. Neither the U.S. Government nor any agency thereof, nor any of their employees, makes any warranty, expressed or implied, or assumes any legal liability or responsibility for the accuracy, completeness, or usefulness, of any information, apparatus, product, or process disclosed, or represents that its use would not infringe privately owned rights. References herein to any specific commercial product, process, or service by trade name, trademark, manufacturer, or otherwise, does not necessarily constitute or imply its endorsement, recommendation, or favoring by the U.S. Government or any agency thereof. The views and opinions of authors expressed herein do not necessarily state or reflect those of the U.S. Government or any agency thereof.

# **Thermal Extraction and Delivery from Advanced Reactor Systems**

**Logan Williams, Vaclav Novotny, Junyung Kim, Sarah Creasman,  
Nipun Popli, Aidan Rigby, Kyle Costanza, Daniel Mikkelsen**

**Idaho National Laboratory**

**September 2023**

**Idaho National Laboratory  
Integrated Energy Systems  
Idaho Falls, Idaho 83415**

**<http://www.ies.inl.gov>**

**Prepared for the  
U.S. Department of Energy  
Office of Nuclear Energy  
Under DOE Idaho Operations Office  
Contract DE-AC07-05ID14517**

*Page intentionally left blank*

## **ABSTRACT**

This document presents a preliminary thermodynamic analysis of thermal extraction and delivery from advanced nuclear reactors. Light-water, high-temperature gas-cooled, sodium fast, and molten-salt reactors are templated and analyzed for thermal extraction from nominal steam production conditions. Uncontrolled, controlled, and partial admission steam extraction methods are described and analyzed to show the differences in system impact as a result of the various methods. The thermal delivery modeling results reflect comparisons made possible thanks to the computational capabilities of the thermal delivery model. Due to the significant degrees of freedom of the problem, specific cases are used to compare the thermodynamic costs of heat transport using various heat transfer fluids. All this work was conducted using Modelica models, enabling future application of models in dynamic analyses beyond the steady-state calculations presented in this report. The appendices describe additional capabilities and methods that can help users analyze complex problems by using the HYBRID models developed in Modelica.



*Page intentionally left blank*

# CONTENTS

|  |     |
|--|-----|
| ABSTRACT.....  | iii |
| LIST OF ACRONYMS .....   | x   |
| 1 INTRODUCTION.....  | 1   |
| 2 BALANCE OF PLANT MODELING AND NOMINAL CONDITIONS .....           | 2   |
| 2.1 Three-Section Turbine – Open Feedwater Heating.....            | 3   |
| 2.2 Three-Section Turbine – Closed Feedwater Heating .....         | 7   |
| 2.3 Advanced Light-Water Reactor Nominal Conditions.....           | 10  |
| 2.4 High-Temperature Gas-Cooled Reactor Nominal Conditions .....   | 11  |
| 2.5 Sodium-Cooled Fast Reactor Nominal Conditions.....             | 12  |
| 2.6 Molten-Salt Reactor Nominal Conditions.....                    | 14  |
| 3 THERMAL EXTRACTION ANALYSIS .....                                | 14  |
| 3.1 General Consideration of Thermal Extraction Steam Cycles ..... | 15  |
| 3.2 Heat Supply Interface.....                                     | 15  |
| 3.3 Steam Extraction Configurations and Turbine Models.....        | 16  |
| 3.4 Uncontrolled Steam Extraction and Modelica Turbine Model ..... | 16  |
| 3.5 Partial Admission.....   | 17  |
| 3.6 Multiple Extraction Points for Single Demand.....              | 17  |
| 3.7 Controlled Extraction.....                                     | 18  |
| 3.8 Workflow Using RAVEN.....                                      | 19  |
| 4 THERMAL EXTRACTION RESULTS.....                                  | 20  |
| 4.1 Uncontrolled Extraction.....                                   | 20  |
| 4.2 Controlled Extraction.....                                     | 26  |
| 5 THERMAL DELIVERY MODELING .....                                  | 34  |
| 5.1 Modeling Theory.....   | 35  |
| 5.1.1 Piping Geometry Description.....                             | 36  |
| 5.1.2 Heat Transfer Fluid .....                                    | 36  |
| 5.1.3 Thermal Losses .....   | 37  |
| 5.1.4 Pump Selection .....   | 38  |
| 5.2 Results.....   | 38  |
| 5.2.1 Nominal Setup Results.....                                   | 38  |
| 5.3 Parameter Sweep: Pipe Geometry.....                            | 39  |
| 5.3.1 Data Generation .....  | 40  |
| 5.4 HTF Comparison.....  | 42  |
| 6 FUTURE WORK.....   | 45  |
| 7 CONCLUSIONS.....   | 45  |

|   |                        |    |
|---|------------------------|----|
| 8 | ACKNOWLEDGEMENTS ..... | 46 |
| 9 | REFERENCES.....        | 47 |

## FIGURES

|   |    |
|---|----|
| Figure 1. Conceptual energy flows within integrated energy systems, including nuclear reactors. ....  | 1  |
| Figure 2. Block diagram of a BOP featuring a three-section turbine with OFWHs. ....   | 3  |
| Figure 3. Results of the design thermodynamic model of the three-section turbine (with OFWHs)<br>BOP model. ....  | 6  |
| Figure 4. Three-stage BOP (with OFWHs) for mixing bypass streams and feedwater.<br>NHES.Systems.BalanceOfPlant.RankineCycle.Models.SteamTurbine_L3_HPOFWH. ....   | 7  |
| Figure 5. Block diagram of the BOP three-section turbine with CFWHs. ....   | 8  |
| Figure 6. Results of the design thermodynamic model of the BOP three-section turbine with<br>CFWHs. ....  | 8  |
| Figure 7. Three-stage BOP model with a closed feedwater heat exchanger for heating the<br>feedwater via the turbine bypass.<br>NHES.Systems.BalanceOfPlant.RankineCycle.Models.SteamTurbine_L3_HPCFWH. ....                         | 10 |
| Figure 8. BOP test model connecting the three-stage BOP model with the A-LWR model.<br>NHES.Systems.PrimaryHeatSystems.SMR_Generic.SMR_Test_3ST. ....   | 11 |
| Figure 9. BOP test model connecting the three-stage BOP model with the HTGR model.<br>Shortened path:<br>HTGR.RankineCycle.Examples.Rankine_HTGR_ThreeStageTurbine_OFWHextractio<br>n. ....   | 12 |
| Figure 10. SFR test for the nominal BOP. Note that SFR systems include intermediate sodium<br>loops to isolate primary coolant from steam.<br>NHES.Systems.PrimaryHeatSystem.SFR.SFR_Example3TSBOP. ....                            | 13 |
| Figure 11. MSR-BOP test including the intermediate loop which isolates primary reactor coolant<br>loop from the BOP. NHES.Systems.PrimaryHeatSystem.MSR.PFL_PCL_BOP. ....   | 14 |
| Figure 12. Illustration of a typical configuration of a CHP BOP with a backpressure turbine and<br>condensing extraction turbine with a feedwater tank at the heat utilization pressure. ....                                       | 15 |
| Figure 13. Illustration of the expansion curve for a single-section and a two-section turbine<br>expansion in h-s and T-s diagrams, all sections having constant isentropic efficiencies.<br>Parameters correspond to the SFR. .... | 16 |
| Figure 14. Flow schematic of the condensing steam turbine, using two uncontrolled extraction<br>openings to provide process steam [7]. ....   | 17 |
| Figure 15. Illustration of controlled extraction from the turbine [7]. ....   | 18 |
| Figure 16. BOP with controlled extraction realized by a valve before the LPT (left), and by LPT<br>PA (right). ....   | 19 |
| Figure 17. Thermal extraction analysis workflow using RAVEN. ....   | 20 |
| Figure 18. Snippet of the whale chart. ....   | 21 |
| Figure 19. Extraction pressures for required demand steam flow and demand pressure. ....  | 22 |
| Figure 20. Thermal efficiency as a function of demand and extraction pressure. ....   | 22 |
| Figure 21. Whale chart of the OFWH BOP with A-LWR conditions. ....  | 24 |
| Figure 22. Whale chart of the OFWH BOP with HTGR conditions. ....   | 24 |

|  |    |
|--|----|
| Figure 23. Whale chart of the CFWH BOP with HTGR conditions.....   | 25 |
| Figure 24. Whale chart of the OFWH BOP with SFR conditions. ....   | 25 |
| Figure 25. Whale chart of the OFWH BOP with MSR conditions.....  | 26 |
| Figure 26. Whale chart of uncontrolled extraction for SFR parameters, overlaid with several<br>controlled extraction cases.....  | 28 |
| Figure 27. Valve-controlled extraction for a range of design extraction pressures and three<br>different demand pressures. ....  | 29 |
| Figure 28. Comparison of valve- and PA-controlled extraction over the full explored range, with a<br>demand pressure of 1 bar.....   | 30 |
| Figure 29. Comparison of PA- and valve-controlled extraction for a minimal (0.5 bar) design<br>pressure difference between extraction and demand. Parameters for the SFR steam<br>cycle.....   | 31 |
| Figure 30. CHP efficiency, parameters for SFR steam cycle. ....  | 32 |
| Figure 31. CHP efficiency for SFR steam cycle in uncontrolled extraction.....  | 32 |
| Figure 32. Comparison of PA- and valve-controlled extraction for a minimal (0.5 bar) design<br>pressure difference between extraction and demand. Parameters for the LWR<br>oversimplified steam cycle. ....   | 33 |
| Figure 33. Comparison of PA- and valve-controlled extraction for a minimal (0.5 bar) design<br>pressure difference between extraction and demand. Parameters for the HTGR<br>oversimplified steam cycle. ....  | 33 |
| Figure 34. Comparison of PA- and valve-controlled extraction for a minimal (0.5 bar) design<br>pressure difference between extraction and demand. Parameters for oversimplified<br>MSR steam cycle. ....   | 34 |
| Figure 35. Possible future IES model, using the heat transport model to model long-distance heat<br>transport for IES applications. The yellow box shows the thermal delivery location and<br>integration. ....  | 35 |
| Figure 36. NHES.Systems.HeatTransport.HeatTransport_withCS (some conditional connections<br>are not shown). ....   | 35 |
| Figure 37: Pipe geometry parameter input GUI.....  | 36 |
| Figure 38. HTF menu in the model parameter GUI.....  | 37 |
| Figure 39: Heat transfer paths for heat loss. ....   | 37 |
| Figure 40: Pumps tab in the parameter GUI. ....  | 38 |
| Figure 41. The initial test harness for the heat delivery model involves setting the inlet pressure<br>and energy conditions, the heat removal rate at the delivery point, and pressure at the<br>condensate return. The model is found at<br>NHES.Systems.HeatTransport.Examples.HTtest6..... | 39 |
| Figure 42. Pressure drop calculations sweeping across various pipe lengths and diameters.....  | 40 |
| Figure 43: The effect of velocity on thermodynamic losses for steam transport.....   | 42 |
| Figure 44: Comparison of multiple HTFs over a range of pipe diameters. ....  | 42 |
| Figure 45: Effect of velocity on pressure loss for several HTFs.....   | 43 |

|  |    |
|--|----|
| Figure 46: Effect of velocity on power loss for several HTFs.....  | 43 |
| Figure 47: Power loss of steam per unit length, with different power delivery rates. ....  | 44 |
| Figure 48: Power loss of CO <sub>2</sub> across different power rates and temperatures. Note that only one<br>line is visible, as the values are nearly identical..... | 44 |
| Figure 49: Power loss from sodium delivering power at various temperatures.....  | 45 |

## TABLES

|  |    |
|--|----|
| Table 1. Steady-state thermodynamic model inputs. Cycle Design Point refers to Figure 2 and<br>Figure 3..... | 4  |
| Table 2. Modelica three-section turbine model inputs (open feedwater heating).....                           | 6  |
| Table 3. Modelica three-section turbine model inputs (closed feedwater heating).....                         | 8  |
| Table 4. A-LWR nominal conditions.....   | 10 |
| Table 5. HTGR nominal conditions.....  | 11 |
| Table 6. SFR nominal conditions.....   | 12 |
| Table 7. MSR nominal conditions. ....  | 14 |
| Table 8: Nominal parameters for the heat transport model.....  | 39 |
| Table 9. Heat transport input parameters for steam. ....   | 40 |
| Table 10. Heat transport input parameters for carbon dioxide.....  | 41 |
| Table 11. Heat transport input parameters for sodium.....  | 41 |

## LIST OF ACRONYMS

|       |   |
|-------|---|
| A-LWR | advanced light-water reactor                          |
| BOP   | balance of plant                                      |
| CFWH  | closed feedwater heater                               |
| CHP   | combined heat and power                               |
| FORCE | Framework for Optimization of Resources and Economics |
| HERON | Holistic Energy Resource Optimization Network         |
| HPT   | high-pressure turbine                                 |
| HTF   | heat transfer fluid                                   |
| HTGR  | high-temperature gas-cooled reactor                   |
| IES   | integrated energy system                              |
| LPT   | low-pressure turbine                                  |
| LWR   | light-water reactor                                   |
| MSR   | molten-salt reactor                                   |
| OFWH  | open feedwater heater                                 |
| PA    | partial (arc) admission                               |
| RAVEN | Risk Analysis Virtual Environment                     |
| RL    | reinforcement learning                                |
| SFR   | sodium-cooled fast reactor                            |

*Page intentionally left blank*



# 1 INTRODUCTION

There is growing interest in how nuclear reactors can be used primarily as heat generators and integrated into thermal demand processes [1]. As relatively low-quality heat generators (producing lower temperatures available to thermal-to-electric conversion equipment) relative to carbon sources, nuclear reactors have lower thermal-to-electric efficiencies than carbon-burning systems such as coal and natural gas plants. Because of this, the overall energy utilization for nuclear systems is lower than that for carbon-burning systems when generating electricity. This reduced conversion efficiency impacts economics, leading to less favorable electricity operation for nuclear reactors. Nuclear systems are closer to parity with carbon emitting energy sources, based on the cost of thermal generation. With the ongoing push to decarbonize energy use across all sectors, interest has been renewed in how nuclear reactors can be designed to operate to generate heat instead of baseload electricity (this includes load-following and combined heat and power [CHP] operations). These new dynamic operating capabilities should enable the nuclear core to operate at nominal full neutron power while dynamically dispatching thermal power to one or more energy consumers. In relation to Figure 1, this document presents work analyzing the arrows located between the separate subsystems.

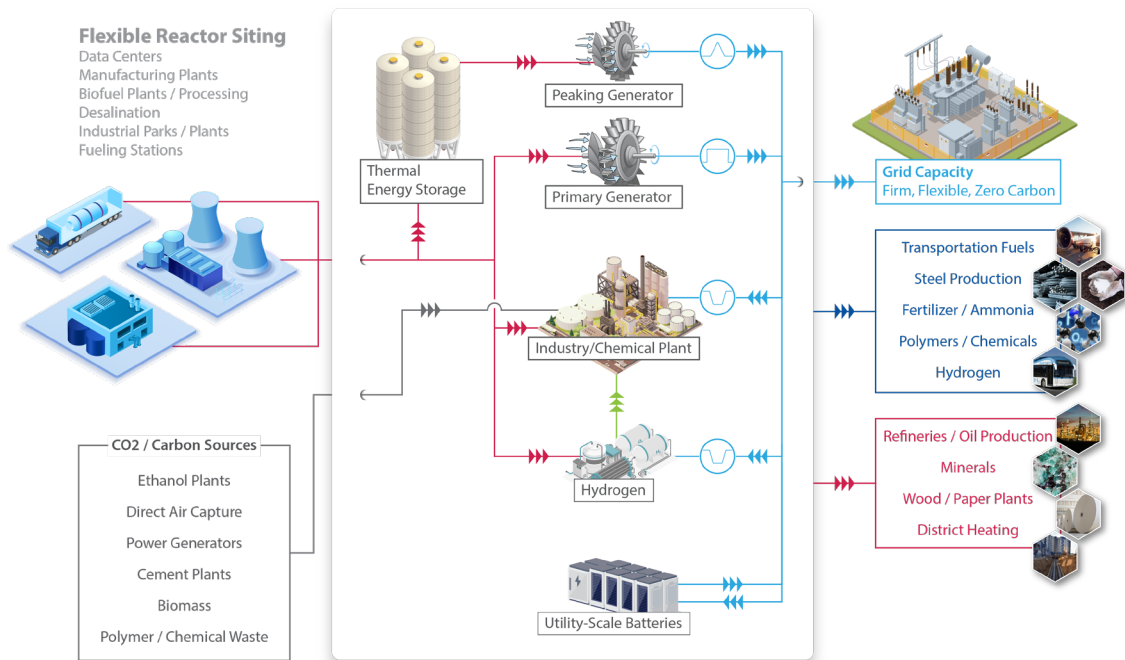


Figure 1. Conceptual energy flows within integrated energy systems, including nuclear reactors.

Understanding how thermal energy can be extracted from the electricity-generating balance of plant (BOP) system of advanced reactors is key to proposing new opportunities for nuclear heat generators. In power plants, the nominal BOP system is set up to produce steam and run it through a turbine to produce electricity [2]. Nominally, electricity production is expected to continue for nuclear reactors, both now and in the future. Thus, this is the general design focus for advanced reactor vendor companies, and in turn for the U.S. Department of Energy's Integrated Energy Systems (IES) program as well. The present report demonstrates a new model for calculating nominal and atypical conditions in turbo-generator systems. Additionally, solution maps show how thermal-to-electric efficiency changes when varying amounts of steam are withdrawn from the system. These maps also show the relationship between design turbine extraction pressure and the application pressure, illustrating how much mass is accessible to a given thermal application case when paired with a specific reactor type. In anticipation of dynamic CHP

operation, the present report makes comparisons between simple uncontrolled extraction, controlled extraction (in which upstream pressures are controlled via internal valving), and partial admissions (PA) systems (in which pressures are maintained via swallowing capacity decreases). Thermodynamic efficiency is crucial for economic operation of large energy systems. While this report does not investigate economic details pertaining to operation, understanding the thermodynamic opportunity cost of different design choices is the first step toward advising how advanced reactor BOP systems can best be designed to participate in CHP operations.

The second physical system needed for CHP operation is the thermal integration network. The piping network connecting thermal generators and thermal consumers is anticipated to function as a relatively simple system during operation, but requires care during the design phase in order to optimize the interface capabilities. Operating power, distance, temperatures, schedule, and interface fluids are all variables that factor into the thermodynamic impact of transporting heat. Alternate choices not only carry different upfront costs for installation, but will alter the operating revenue, reliability, and control of the system at large. The present report offers a model that can be sampled to calculate the thermodynamic cost of transporting heat across a significant distance, and the results can later be used to generate cost curves for various deployment scenarios. The multiphysics approach presented herein combines the energetic and momentum losses to ensure that, as distances continue to expand and the adiabatic and isothermal assumptions become less valid, the combined impact of momentum and energy losses are accounted for. At this stage, result tables and maps are generated that can then be inquired of for specific deployment scenarios.

All modeling described in this report is consistent with the dynamic Modelica modeling of the HYBRID repository [3]. The IES program’s modeling repository contains a wide variety of models—spanning multiple languages and modeling software programs—intended to aid analysts in evaluating possible IES configurations and their physical constraints, efficiencies, and control strategies. The model diagrams contained in the figures in this report (with the file path included in the figure caption) can be found in the online repository located at <https://github.com/idaholab/HYBRID>.

Two appendices are included at the end of this report to document the progress made in HYBRID modeling functionality. Appendix A discusses the reinforcement learning of a Modelica model applying various Python libraries. While the methods proposed in Appendix A are not yet fully integrated into the Framework for Optimization of Resources and Economics (FORCE), they may provide a blueprint for future integration of reinforcement learning into Idaho National Laboratory (INL)’s IES tools. Appendix B directs INL IES users on how to integrate the Risk Analysis Virtual Environment (RAVEN) and Dymola when using the high-performance computing system at INL.

## **2 BALANCE OF PLANT MODELING AND NOMINAL CONDITIONS**

BOP models of simplified plant configurations have been created that can operate in multiple operating paradigms. BOP systems, also termed secondary systems of nuclear plants, encompass equipment such as the feedwater system, turbines, steam treatment equipment, and various control/safety valves, all of which combine to distribute energy as needed. In the present work, extraction points found between significant turbine stages are investigated in light of extraction steam that can be delivered to industrial processes.

Within the context of this report, the BOP system’s on-design operation is considered to equate to a dedicated thermal-to-electric conversion system that uses all heat for electricity generation. If heat is extracted, either via an extraction stage or from piping between turbines, the operation will then shift from on-design to off-design. The standard BOP models developed for the HYBRID repository allow for on-design and off-design operation calculations with different configurations. Here, the term “standard” is used to describe the BOP system model itself, which can be reconfigured to reflect the electric-generation capabilities of various advanced nuclear reactors. These models are not intended to define the entire suite

of possible BOP configurations, as this would exceed the analysis goals of the project. Two BOP models are presented in this report, the main difference between them being the feedwater heating method: closed vs. open. Closed feedwater heating uses a heat exchanger to pass heat from a hot stream—nominally a turbine bypass stream—to heat the feedwater. Open feedwater heating mixes turbine bypass streams into the feedwater stream. There are design advantages to both systems. Closed systems allow for much greater dynamic flexibility and for mismatched pressures within the turbine bypass streams and feedwater system. Open feedwater systems are thermodynamically more efficient, as mixing the streams effectively functions as a perfect heat exchanger. Typical current systems use a single open feedwater heater (OFWH) that also acts as a deaerator (i.e., a tank for removing ingress air from the condenser), along with at least four closed feedwater heaters.

Details on the design differences between the open and closed feedwater heating systems are given in Sections 2.1 and 2.2. The nominal designs are then parameterized to match the HYBRID template reactor models; these values are reported in Sections 2.3–2.6.

## 2.1 Three-Section Turbine – Open Feedwater Heating

An updated three-section turbine model was created using the previous three-section model described in INL/RPT-23-03062 [2]. The input data block was simplified to make parameterization, nominal physical characterization of the system, easier. A second OFWH was added to more accurately reflect a real Rankine cycle, and one feedwater heater was moved in order to utilize steam offtake bypassed upstream of the high-pressure turbine (HPT), so as to be able to reach higher feedwater temperatures, even though this configuration affords no thermodynamic benefit. Figure 2 is a block diagram of this model.

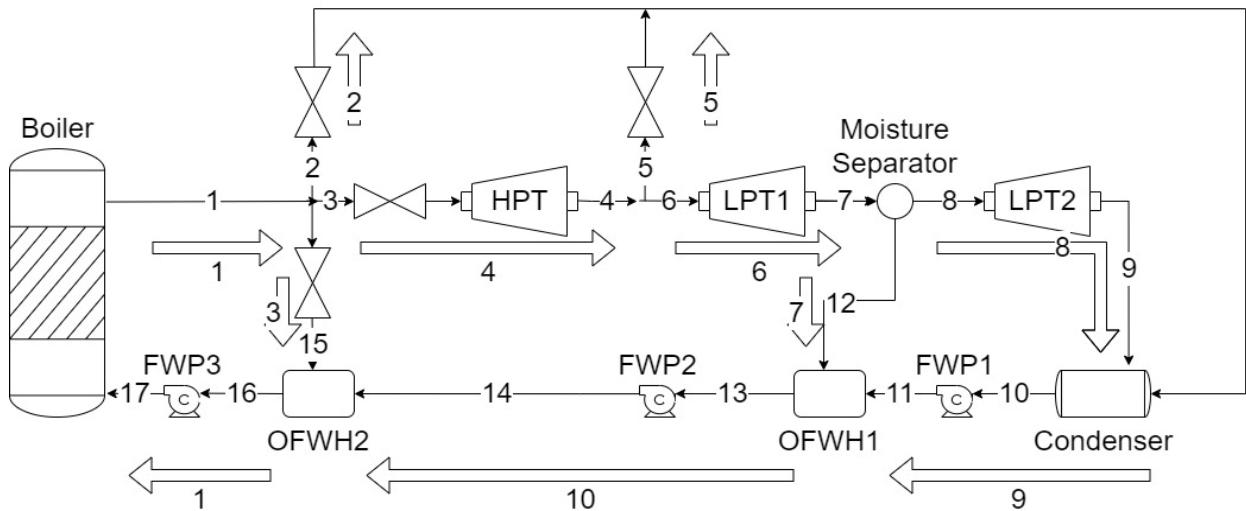


Figure 2. Block diagram of a BOP featuring a three-section turbine with OFWHs.

This configuration was considered because it can provide a variety of insights into BOP design (insights that legacy HYBRID models are unable provide), yet also correspond to a reasonable computational time. By changing the conditions at points 3–5, the impacts of different extraction conditions can be observed throughout the BOP. The moisture separator is regularly installed equipment for ensuring sufficient liquid content within LPT2. Note that controls implemented in these BOP systems act to moderate the steam generator pressure, steam temperature, feedwater flow rate, and feedwater temperature. These values are considered safety relevant and are thus functions of the nominal reactor design. Throughout the analysis covered in this report, operating conditions under which the control system failed to maintain

nominal conditions were considered invalid and thus disregarded. In addition, any piping losses were assumed negligible relative to the large changes occurring in the heat exchangers, pumps, and turbines.

Table 1 lists the major BOP model parameters. The Excel sheet shown in Figure 3 uses the set of inputs shown in Table 1 to give nominal steady-state conditions for each component in the cycle.

Table 1. Steady-state thermodynamic model inputs. Cycle Design Point refers to Figure 2 and Figure 3.

| Parameter           | Description                             | Unit | Cycle Design Point |
|---------------------|---|------|--------------------|
| Power <sub>th</sub> | Core Thermal Power                      | MW   | 1                  |
| T <sub>steam</sub>  | Inlet Steam Temperature                 | °C   | 1, 2               |
| T <sub>feed</sub>   | Feedwater Temperature                   | °C   | 18                 |
| P <sub>in</sub>     | HPT Impulse Pressure                    | Bar  | 2, 3               |
| P <sub>i1</sub>     | Low-Pressure Turbine 1 Impulse Pressure | Bar  | 5                  |
| P <sub>i2</sub>     | Low-Pressure Turbine 2 Impulse Pressure | Bar  | 6, 7               |
| P <sub>cond</sub>   | Condenser Pressure                      | Bar  | 8                  |
| Eta <sub>t</sub>    | Turbine Isentropic Efficiency           | %    | 3, 5, 6            |
| Eta <sub>p</sub>    | Pump Isentropic Efficiency              | %    | 9, 12, 15          |
| Eta <sub>mech</sub> | Turbine Mechanical Efficiency           | %    | 3, 5, 6            |

The steady-state (design) thermodynamic model of the Rankine cycle was created in Excel alongside the Dymola BOP models in order to enable easy parameterization. These values were used to find the system's nominal conditions, which in turn informed the initial reference point for the Modelica model and enabled off-design performance of the turbines to be calculated. The Excel design thermodynamic model assumes steady-state conditions with no pressure drop across valves or the reactor, and ideal moisture separation. The thermodynamic state for each component is calculated and the mass flow rates through each component are listed. These values and all the others outlined in thick, green-colored boxes in Figure 3 were used as nominal conditions within the parameterization data block in the Modelica model.

The properties for state 1 (all states refer to the numbered locations in Figure 1), which is the steam coming from the steam generator, were calculated using the reference input values for the steam temperature (T<sub>in</sub>) and steam pressure (P<sub>in</sub>). The conditions for state 2 and state 3 were identical those of state 1, as any valve losses were assumed negligible. State 4 was calculated by using Eq. 1, with input pressure P<sub>in</sub> and outlet pressure P<sub>i1</sub>. State 5 and state 6 were considered identical to state 4, with the mass flow from state 4 being split between state 5 and state 6. State 7 was calculated via Eq. 1, using inlet pressure P<sub>i1</sub> and outlet pressure P<sub>i2</sub>. State 8 and state 12 were calculated using the mass balance in Eq. 2 and the moisture separation energy balance in Eq. 4. The moisture separator assumes perfect separation, but if the incoming steam is superheated, the liquid flow is set to zero and the steam outlet conditions are set to equal the inlet conditions. State 9 again used the turbine energy balance in Eq. 1. with the inlet pressure being equal to P<sub>i2</sub> and the outlet pressure being equal to the condenser set pressure (P<sub>cond</sub>). The condenser exit, state 10, was assumed to be a saturated liquid at the condenser pressure. The properties at state 11 were calculated using the pump equation, Eq. 5. The feedwater energy balance was calculated via Eq. 5. The feedwater at state 11 was pumped to P<sub>i2</sub>, where it mixed with the liquid from the moisture separator, state 12. The outlet of the first OFWH, state 13, was calculated based on the energy and mass balances, Eq. 2 and Eq. 3. State 14 was calculated using the pump equation, Eq. 5. State 15 was set to have the same enthalpy as state 1 but at a lower pressure, P<sub>i1</sub>. State 14 and state 15 were mixed in the second feedwater heater, with Eq. 2 and Eq. 3 being used to calculate state 16. State 17 was calculated via Eq. 5 to give the feedwater conditions based on the inputs.

$$h_{t,o} = h_{t,i} - \eta_t \left( h_{t,i} - h \left( P_{t,o}, s(P_{t,i}, h_{t,i}) \right) \right) \quad (1)$$

$$\sum \dot{m}_i - \sum \dot{m}_o = 0 \quad (2)$$

$$\sum \dot{m}_i \cdot h_i - \sum \dot{m}_o \cdot h_o = 0 \quad (3)$$

$$\dot{m}_i \cdot h_i + \dot{m}_g \cdot h_g(P) + \dot{m}_f \cdot h_f(P) = 0 \quad (4)$$

$$h_{p,o} = h_{p,i} + \frac{\left( \left( h_{p,i} + v(P_{p,i}, h_{p,i}) \cdot (P_{p,o} - P_{p,i}) \right) \right) - h_{p,i}}{\eta_p} \quad (5)$$

where  $h_{t,o}$  is the turbine outlet enthalpy,  $h_{t,i}$  is the turbine inlet enthalpy,  $\eta_t$  is the assumed turbine isentropic efficiency,  $P_{t,o}$  is the turbine outlet pressure,  $P_{t,i}$  is the turbine inlet pressure,  $h()$  and  $s()$  are enthalpy and entropy functions,  $\dot{m}_i$  is an inlet mass flow,  $\dot{m}_o$  is an outlet mass flow,  $h_i$  is an inlet enthalpy, and  $h_o$  is an outlet enthalpy. The subscripts  $g$  and  $f$  on the mass flow rates and enthalpy functions indicate the saturated vapor and fluid states, respectively.  $h_{p,o}$  and  $h_{p,i}$  are the pump outlet and inlet enthalpies, respectively, and  $v()$  is a specific volume function.  $P_{p,i}$  and  $P_{p,o}$  are the pump inlet and outlet pressures, respectively, and  $\eta_p$  is the assumed pump efficiency.

The overall flow rate ( $\dot{m}_1$ ) at state 1 was calculated via Eq. 6, using the thermal power rating ( $\dot{Q}_{th}$ ) and the steam and feed conditions. The flow rates at state 2 and state 5 were set by the user. The flow rate at state 7 was found by using the moisture separator equations (Eq. 2 and Eq. 4). The flow rate at state 3 was solved iteratively to obtain the correct feedwater conditions. All the other flow rates were found by using the mass balance equation (Eq. 2).

$$\dot{m}_1 = \frac{\dot{Q}_{th}}{h_1 - h_{17}} \quad (6)$$

where  $h_1$  and  $h_{17}$  are the enthalpy values at state 1 and state 17, respectively.

The turbine work was calculated using Eq. 7, and the pump work was calculated using Eq. 8. The net work and thermal power of the cycle was used to calculate the electrical efficiency by using Eq. 9.

$$\dot{W}_t = \dot{m} \cdot \eta_{mech} \cdot (h_{t,i} - h_{t,o}) \quad (7)$$

$$\dot{W}_p = \dot{m} \cdot (h_{p,o} - h_{p,i}) \quad (8)$$

$$\eta_{th} = \frac{\sum \dot{W}_t - \sum \dot{W}_p}{\dot{Q}_{th}} \quad (9)$$

where  $\dot{W}_t$  is the turbine work,  $\eta_{mech}$  is the assumed mechanical-to-electric efficiency value,  $\dot{W}_p$  is the pump work, and  $\eta_{th}$  is the thermal efficiency value of the system.

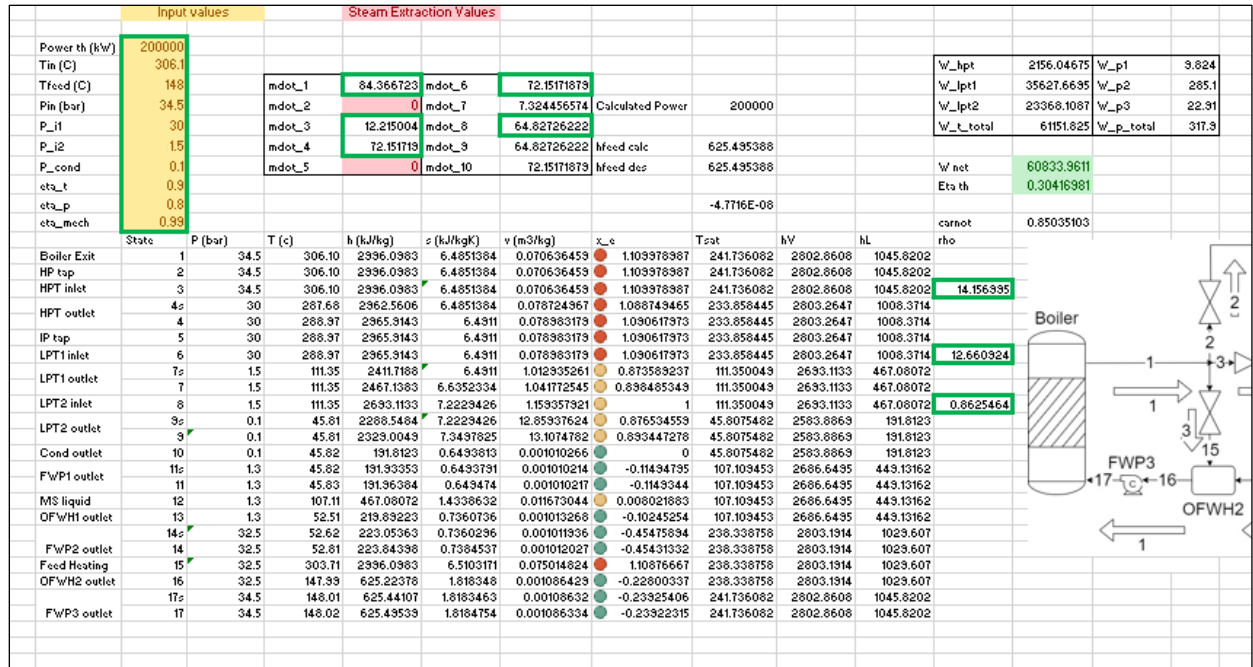


Figure 3. Results of the design thermodynamic model of the three-section turbine (with OFWHs) BOP model.

All the parameters needed for the Modelica model can be determined based on the design thermodynamic model. The list of necessary parameters is shown in Table 2. Using these inputs, the Modelica model shown in Figure 4 can be parameterized. The values for these parameters vary greatly depending on reactor type and the corresponding steam and feedwater conditions.

Table 2. Modelica three-section turbine model inputs (open feedwater heating).

| Parameter             | Description                                   | Unit              |
|-----------------------|---|-------------------|
| Power <sub>nom</sub>  | Nominal Electric Power                        | MW                |
| T <sub>steam</sub>    | Inlet Steam Temperature                       | °C                |
| T <sub>feed</sub>     | Feedwater Temperature                         | °C                |
| P <sub>in</sub>       | HPT Impulse Pressure                          | Bar               |
| P <sub>i1</sub>       | Low-Pressure Turbine 1 Impulse Pressure       | Bar               |
| P <sub>i2</sub>       | Low-Pressure Turbine 2 Impulse Pressure       | Bar               |
| P <sub>cond</sub>     | Condenser Pressure                            | Bar               |
| P <sub>dump</sub>     | Turbine Bypass Relief Valve Set Pressure      | Bar               |
| P <sub>use</sub>      | Application Demand Pressure                   | Bar               |
| d <sub>HPT in</sub>   | HPT Inlet Density                             | kg/m <sup>3</sup> |
| d <sub>LPT1 in</sub>  | Low-Pressure Turbine 1 Inlet Density          | kg/m <sup>3</sup> |
| d <sub>LPT2 in</sub>  | Low-Pressure Turbine 2 Inlet Density          | kg/m <sup>3</sup> |
| Mdot <sub>total</sub> | Nominal Total Mass Flow Rate                  | kg/s              |
| Mdot <sub>fd</sub>    | Nominal Feed Heating Mass Flow Rate           | kg/s              |
| Mdot <sub>HPT</sub>   | Nominal HPT Mass Flow Rate                    | kg/s              |
| Mdot <sub>LPT1</sub>  | Nominal Low-Pressure Turbine 1 Mass Flow Rate | kg/s              |
| Mdot <sub>LPT2</sub>  | Nominal Low-Pressure Turbine 2 Mass Flow Rate | kg/s              |





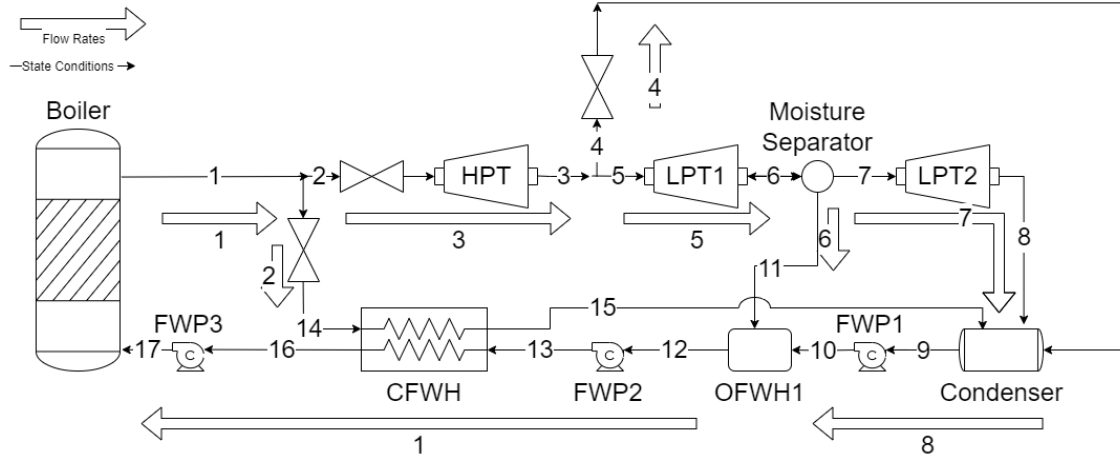


Figure 5. Block diagram of the BOP three-section turbine with CFWHs.

The input parameters for the design thermodynamic model remain the same as for the model of the OFHW system seen in Figure 6. Among the Modelica model parameters (see Table 3) are a few additional inputs in comparison to the OFWH model. The Modelica model is shown in Figure 7.

| Input values   |        | Steam Extraction Values |        | HX model assumes 10 degree difference between T14 and T16 with no pressure drop |            |             |              |
|----------------|--------|-------------------------|--------|---|------------|-------------|--------------|
| Power th (kW)  | 100000 |                         |        |   |            |             |              |
| Tin (C)        | 515    |                         |        |   |            |             |              |
| Tfeed (C)      | 208    |                         |        |   |            |             |              |
| Pin (bar)      | 140    |                         |        |   |            |             |              |
| P_i1           | 8      |                         |        |   |            |             |              |
| P_i2           | 1.5    |                         |        |   |            |             |              |
| P_cond         | 0.1    |                         |        |   |            |             |              |
| eta_t          | 0.9    |                         |        |   |            |             |              |
| eta_p          | 0.8    |                         |        |   |            |             |              |
| eta_mech       | 0.99   |                         |        |   |            |             |              |
| State          |        | P (bar)                 | T (c)  | h (kJ/kg)   | s (kJ/kgK) | v (m3/kg)   | x_e          |
| Boiler Exit    | 1      | 140                     | 515.00 | 3366.01291  | 6.4468498  | 0.023229243 | 1.68207388   |
| HP tap         | 2      | 140                     | 515.00 | 3366.01291  | 6.4468498  | 0.023229243 | 1.68207388   |
| HPT inlet      | 3      | 140                     | 515.00 | 3366.01291  | 6.4468498  | 0.023229243 | 1.68207388   |
| HPT outlet     | 4s     | 8                       | 170.41 | 2673.07297  | 6.4468498  | 0.229200538 | 0.953484973  |
| IP tap         | 5      | 8                       | 170.41 | 2742.36696  | 6.60307142 | 0.237297119 | 0.987331754  |
| LPT1 inlet     | 6      | 8                       | 170.41 | 2742.36696  | 6.60307142 | 0.237297119 | 0.987331754  |
| LPT1 outlet    | 7s     | 1.5                     | 111.35 | 2454.77201  | 6.60307142 | 1.035337781 | 0.89293002   |
| LPT2 inlet     | 8      | 1.5                     | 111.35 | 2483.5315   | 6.6778682  | 1.050302639 | 0.905849641  |
| LPT2 outlet    | 9s     | 0.1                     | 45.81  | 2288.54839  | 7.22294257 | 12.85937624 | 0.876534559  |
| Cond outlet    | 10     | 0.1                     | 45.82  | 2329.00487  | 7.34978248 | 13.1074782  | 0.893447278  |
| FWP1 outlet    | 11s    | 1.3                     | 45.82  | 191.933527  | 0.64937906 | 0.001010214 | -0.114947947 |
| MS liquid      | 12     | 1.3                     | 107.11 | 467.080724  | 1.43386321 | 0.011673044 | 0.008021883  |
| OFWH1 outlet   | 13     | 1.3                     | 50.24  | 210.397088  | 0.70683174 | 0.001012195 | -0.106696142 |
| FWP2 outlet    | 14s    | 138                     | 50.73  | 224.233797  | 0.70767186 | 0.001006835 | -1.239353779 |
| Feed Heating   | 15     | 138                     | 514.11 | 3366.01291  | 6.45279095 | 0.023568492 | 1.669099242  |
| HX exit        | 16     | 140                     | 61.56  | 269.354745  | 0.84313681 | 0.001011755 | -1.219551604 |
| HX feed outlet | 17     | 138                     | 207.96 | 892.940182  | 2.38617272 | 0.001156735 | -0.62030927  |
| FWP3 outlet    | 18s    | 140                     | 207.99 | 893.171529  | 2.38617385 | 0.001156589 | -0.635023838 |
|                | 18     | 140                     | 208.01 | 893.229366  | 2.38629399 | 0.001156609 | -0.634969644 |

Figure 6. Results of the design thermodynamic model of the BOP three-section turbine with CFWHs.

Table 3. Modelica three-section turbine model inputs (closed feedwater heating).

| Parameter | Description                             | Unit |
|-----------|---|------|
| Power nom | Nominal Electric Power                  | MW   |
| T steam   | Inlet Steam Temperature                 | °C   |
| T feed    | Feedwater Temperature                   | °C   |
| P in      | HPT Impulse Pressure                    | Bar  |
| P i1      | Low-Pressure Turbine 1 Impulse Pressure | Bar  |



Table 3. (continued).

| Parameter                 | Description                                      | Unit              |
|---------------------------|--|-------------------|
| P <sub>i2</sub>           | Low-Pressure Turbine 2 Impulse Pressure          | Bar               |
| P <sub>cond</sub>         | Condenser Pressure                               | Bar               |
| P <sub>dump</sub>         | Turbine Bypass Relief Valve Set Pressure         | Bar               |
| P <sub>use</sub>          | Application Demand Pressure                      | Bar               |
| d <sub>HPT in</sub>       | HPT Inlet Density                                | kg/m <sup>3</sup> |
| d <sub>LPT1 in</sub>      | Low-Pressure Turbine 1 Inlet Density             | kg/m <sup>3</sup> |
| d <sub>LPT2 in</sub>      | Low-Pressure Turbine 2 Inlet Density             | kg/m <sup>3</sup> |
| Mdot <sub>total</sub>     | Nominal Total Mass Flow Rate                     | kg/s              |
| Mdot <sub>fd</sub>        | Nominal Feed Heating Mass Flow Rate              | kg/s              |
| Mdot <sub>HPT</sub>       | Nominal HPT Mass Flow Rate                       | kg/s              |
| Mdot <sub>LPT1</sub>      | Nominal Low Pressure Turbine 1 Mass Flow Rate    | kg/s              |
| Mdot <sub>LPT2</sub>      | Nominal Low Pressure Turbine 2 Mass Flow Rate    | kg/s              |
| Mdot <sub>ext</sub>       | Extraction Mass Flow Rate                        | kg/s              |
| Eta <sub>t</sub>          | Turbine Isentropic Efficiency                    | %                 |
| Eta <sub>p</sub>          | Pump Isentropic Efficiency                       | %                 |
| Eta <sub>mech</sub>       | Turbine Mechanical Efficiency                    | %                 |
| Heater <sub>NTU</sub>     | Number of Transfer Units of the Feedwater Heater | —                 |
| Heater <sub>K-tube</sub>  | K Value of the Tube in the Feedwater Heater      | 1/m <sup>4</sup>  |
| Heater <sub>K-shell</sub> | K Value of the Shell in the Feedwater Heater     | 1/m <sup>4</sup>  |
| Heater <sub>V-tube</sub>  | Tube-Side Volume of the Feedwater Heater         | m <sup>3</sup>    |
| Heater <sub>V-shell</sub> | Shell-Side Volume of the Feedwater Heater        | m <sup>3</sup>    |

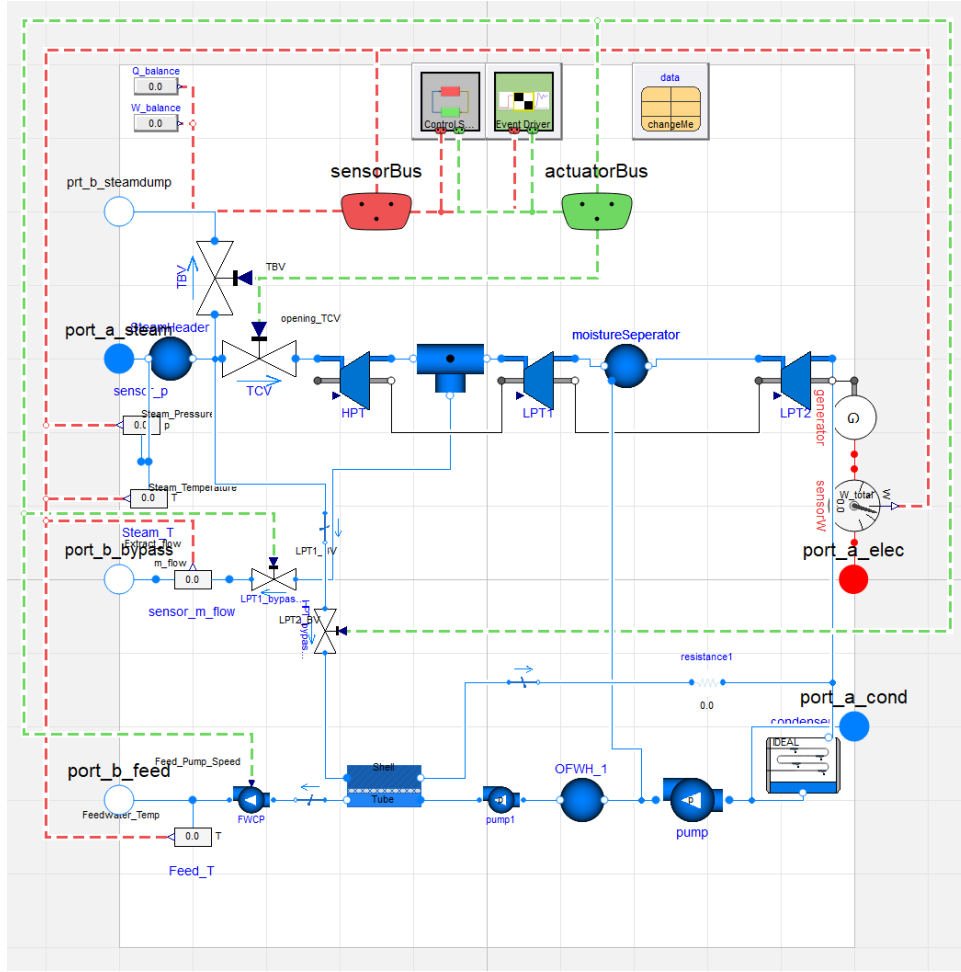


Figure 7. Three-stage BOP model with a closed feedwater heat exchanger for heating the feedwater via the turbine bypass. NHES.Systems.BalanceOfPlant.RankineCycle.Models.SteamTurbine\_L3\_HPCFWH.

## 2.3 Advanced Light-Water Reactor Nominal Conditions

Table 4 shows the input conditions for the advanced light-water reactor (A-LWR), a natural-circulation integral pressurized-water reactor. Figure 8 shows the Modelica template of the coupled light-water reactor (LWR) and BOP models.

Table 4. A-LWR nominal conditions.

| Parameter           | Value | Unit            |
|---------------------|-------|-----------------|
| Power <sub>th</sub> | 200   | MW <sub>t</sub> |
| T <sub>steam</sub>  | 306.1 | °C              |
| T <sub>feed</sub>   | 148   | °C              |
| P <sub>in</sub>     | 34.5  | Bar             |
| P <sub>i1</sub>     | 3     | Bar             |
| P <sub>i2</sub>     | 1.5   | Bar             |
| P <sub>cond</sub>   | 0.1   | Bar             |
| Eta <sub>t</sub>    | 0.9   | —               |
| Eta <sub>p</sub>    | 0.8   | —               |

| Parameter | Value | Unit |
|-----------|-------|------|
| Eta_mech  | 0.99  | —    |

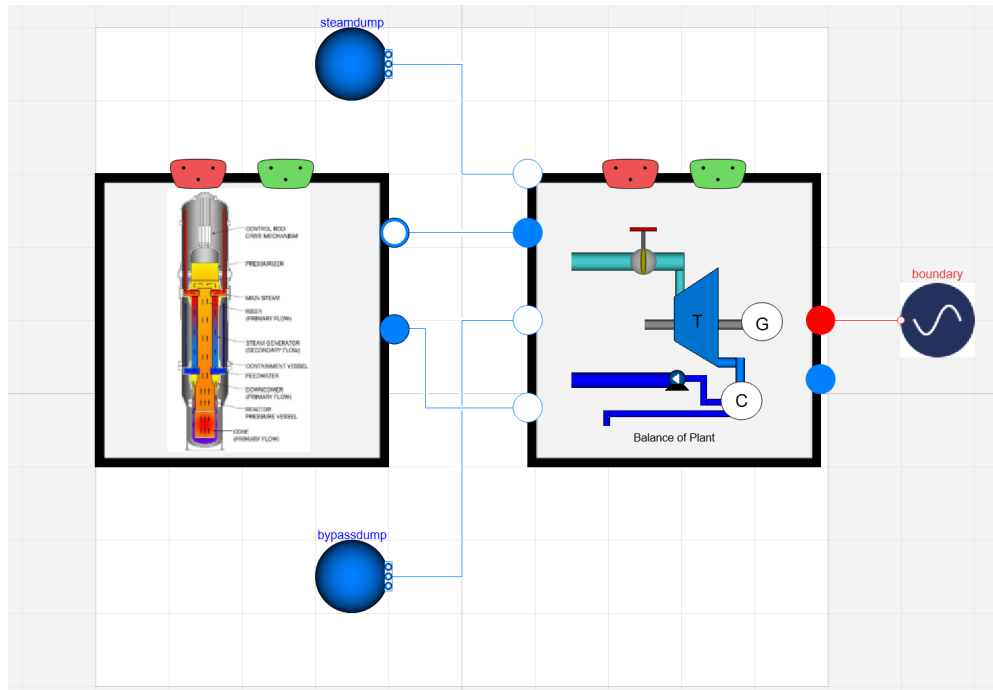


Figure 8. BOP test model connecting the three-stage BOP model with the A-LWR model.  
NHES.Systems.PrimaryHeatSystems.SMR\_Generic.SMR\_Test\_3ST.

## 2.4 High-Temperature Gas-Cooled Reactor Nominal Conditions

Table 5 shows the input conditions for the high-temperature gas-cooled reactor (HTGR), a helium-cooled pebble-bed-style reactor. Figure 9 shows the Modelica models of the coupled HTGR and BOP models.

Table 5. HTGR nominal conditions.

| Parameter           | Value | Unit            |
|---------------------|-------|-----------------|
| Power <sub>th</sub> | 100   | MW <sub>t</sub> |
| T <sub>steam</sub>  | 515   | °C              |
| T <sub>feed</sub>   | 208   | °C              |
| P <sub>in</sub>     | 140   | Bar             |
| P <sub>i1</sub>     | 3     | Bar             |
| P <sub>i2</sub>     | 1.5   | Bar             |
| P <sub>cond</sub>   | 0.1   | Bar             |
| Eta <sub>t</sub>    | 0.9   | —               |
| Eta <sub>p</sub>    | 0.8   | —               |
| Eta <sub>mech</sub> | 0.99  | —               |

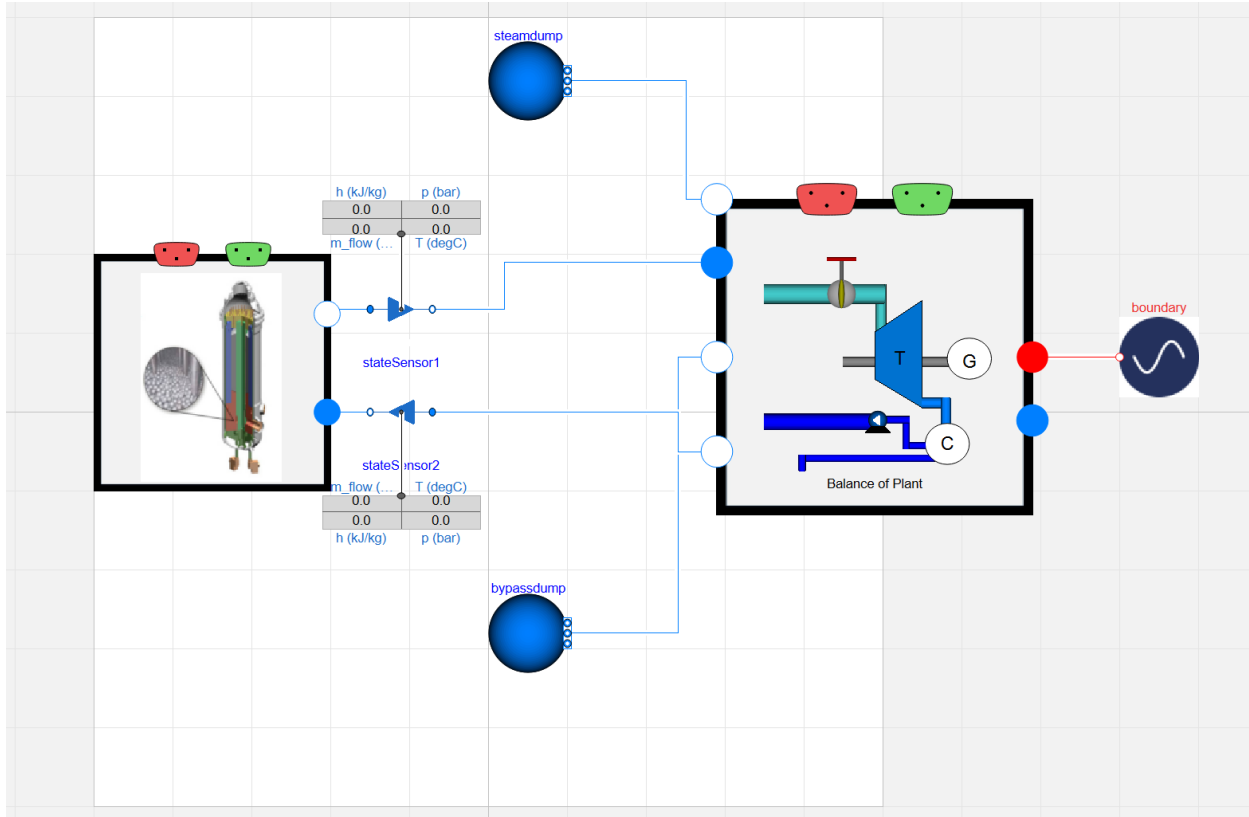


Figure 9. BOP test model connecting the three-stage BOP model with the HTGR model. Shortened path: HTGR.RankineCycle.Examples.Rankine\_HTGR\_ThreeStageTurbine\_OFWHextraction.

## 2.5 Sodium-Cooled Fast Reactor Nominal Conditions

Table 6 shows the input conditions for the sodium-cooled fast reactor (SFR) system. Figure 10 shows the Modelica model of the full system which includes the SFR, intermediate sodium loop, and BOP models.

Table 6. SFR nominal conditions.

| Parameter           | Value | Unit            |
|---------------------|-------|-----------------|
| Power <sub>th</sub> | 100   | MW <sub>t</sub> |
| T <sub>steam</sub>  | 364   | °C              |
| T <sub>feed</sub>   | 210   | °C              |
| P <sub>in</sub>     | 123   | Bar             |
| P <sub>i1</sub>     | 3     | Bar             |
| P <sub>i2</sub>     | 1.5   | Bar             |
| P <sub>cond</sub>   | 0.1   | Bar             |
| η <sub>t</sub>      | 0.9   | —               |
| η <sub>p</sub>      | 0.8   | —               |
| η <sub>mech</sub>   | 0.99  | —               |

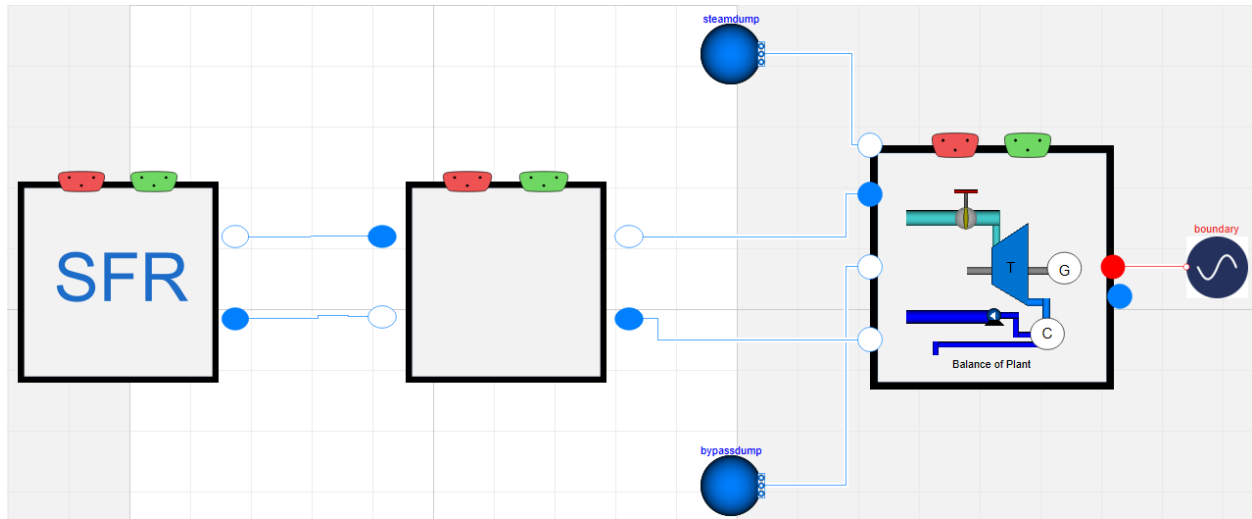


Figure 10. SFR test for the nominal BOP. Note that SFR systems include intermediate sodium loops to isolate primary coolant from steam. NHES.Systems.PrimaryHeatSystem.SFR.SFR\_Example3TSBOP.

## 2.6 Molten-Salt Reactor Nominal Conditions

Table 7 shows the input conditions for the molten salt reactor (MSR) system. Figure 11 shows the Modelica model of the MSR primary fuel loop, primary coolant loop, and BOP models. The present research has extended some work previously conducted for another Modelica library [4].

Table 7. MSR nominal conditions.

| Parameter           | Value | Unit |
|---------------------|-------|------|
| Power <sub>th</sub> | 750   | MWt  |
| T <sub>steam</sub>  | 540   | °C   |
| T <sub>feed</sub>   | 200   | °C   |
| P <sub>in</sub>     | 120   | Bar  |
| P <sub>i1</sub>     | 20    | Bar  |
| P <sub>i2</sub>     | 1.5   | Bar  |
| P <sub>cond</sub>   | 0.1   | Bar  |
| Eta <sub>t</sub>    | 0.9   | —    |
| Eta <sub>p</sub>    | 0.8   | —    |
| Eta <sub>mech</sub> | 0.99  | —    |

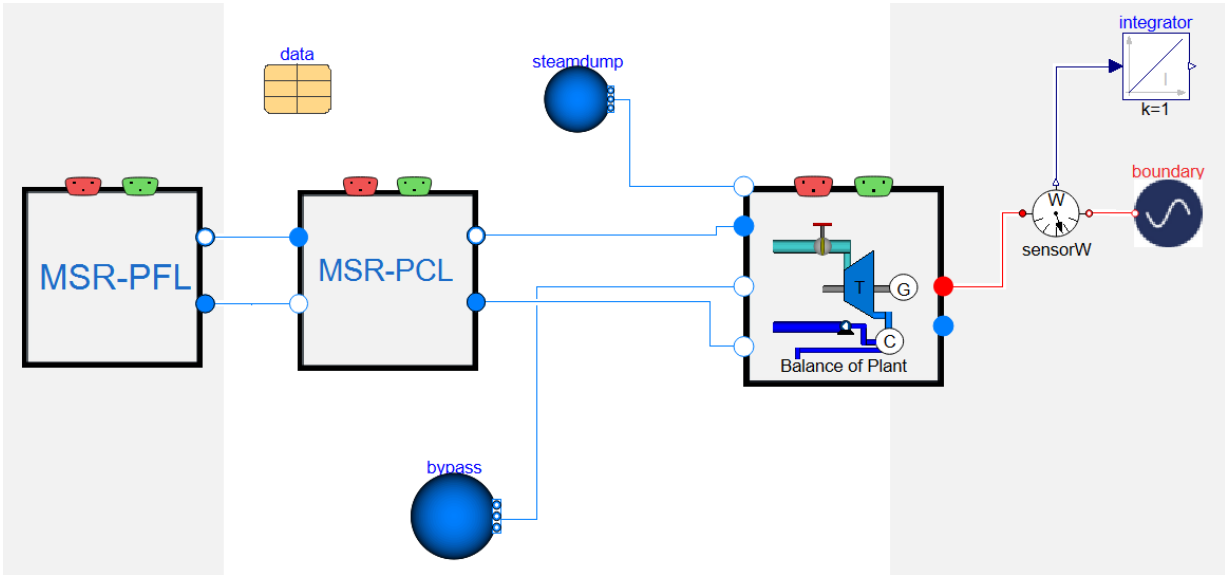


Figure 11. MSR-BOP test including the intermediate loop which isolates primary reactor coolant loop from the BOP. NHES.Systems.PrimaryHeatSystem.MSR.PFL\_PCL\_BOP.

## 3 THERMAL EXTRACTION ANALYSIS

In general, higher flexibility in power and heat dispatch leads to drops in efficiency as well as negative impacts on other performance metrics, and necessitates a more complex design. The prior designs discussed in Section 2 were based on uncontrolled extraction. Section 3 presents several other technical solutions of various complexity are presented for CHP applications. Simplified models of these solutions were developed in Modelica. A sensitivity analysis pertaining to varying the thermal extraction

rate and pressure was then performed on several of them, using steam cycle parameters from advanced nuclear reactor concepts.

### 3.1 General Consideration of Thermal Extraction Steam Cycles

When considering the deployment of nuclear systems for CHP applications, inspiration can be taken from fossil-fired (primarily coal) CHP plants. These plants often include both a backpressure turbine and a condensing extraction turbine, as shown in Figure 12. The backpressure turbine is designed to meet the minimal heat demand, and extraction from the condensing turbine is used to supplement this heat to reach the maximum demand.

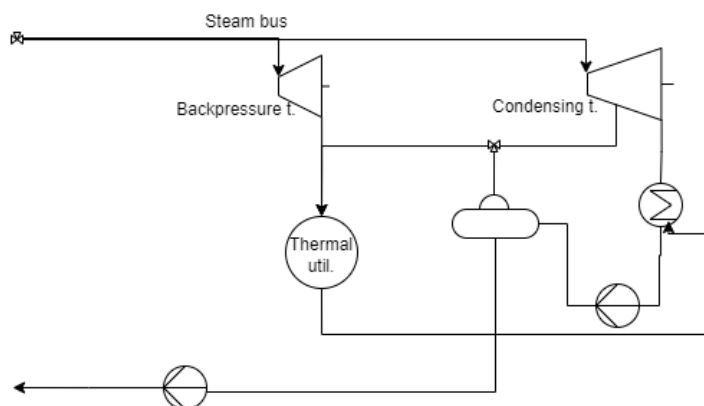


Figure 12. Illustration of a typical configuration of a CHP BOP with a backpressure turbine and condensing extraction turbine with a feedwater tank at the heat utilization pressure.

This configuration works well—from an efficiency standpoint—when the heat input can be modulated, as the turbine inlet pressures and temperatures can be maintained near nominal values. Typically, there are even multiple boilers for supplying steam into a common bus. To further extend the operation range into the high-efficiency region, PA is not uncommon at the inlet of the condensing turbine. Controlled extraction is also commonly considered in regard to ensuring that the demand pressure is met during off-design operation.

Nuclear plants, in which the reactor serves as the primary heat source, are typically intended to operate constantly at nominal power and deems operation shown in Figure 12 to be unfeasible. The only exceptions are when a thermal energy storage system is available to buffer the reactor and the conversion system, or in reactor concepts designed specifically for flexible dispatch. Still, many of the features of this multipoint extraction method find good application in nuclear CHP system design.

### 3.2 Heat Supply Interface

Only rarely do thermal distribution systems directly apply turbine-expanded steam to industrial processes and heating networks. The exceptions are either relatively smaller systems (no more than several MWe of power production) with lower pressures/temperatures in the steam cycle, or when the steam demand is for indirect heating with immediate colocation to the steam cycle.

Typically, even if steam is distributed further, an intermediate loop is used. The reasons for this include:

- Chemical treatment of water for high-temperature/pressure steam cycles is unsuitable for low-pressure steam distribution. The deionized water and pH is guards against any fouling on the most

stressed components, but requires specific and costly materials to prevent corrosion from occurring.

- The deionized and specifically treated water is also relatively expensive when used in a system in which losses or contamination may occur. To prevent contamination due to leakage across the heat exchanger, intermediate heat transfer loops are sometimes considered.
- This system isolation heat exchanger ensures that only a small degree of thermal potential is lost, as the heat transfer coefficients of condensation (and eventually boiling) are very high. Nor does the size of this heat exchanger need to be especially high.

The return condensate can then be entered back into the steam-cycle feedwater system at a suitable point based on its temperature. Returning condensate to the feedwater system may require additional control within the nuclear BOP, or guarantee by design that the condensate will not prevent feedwater conditioning. If no heat is left in the condensate, it would be introduced into the condenser.

### 3.3 Steam Extraction Configurations and Turbine Models

The two principal options for steam extraction—controlled and uncontrolled—are differentiated by the possibility of controlling the extraction pressure at partial-load operation. Additional flexibility and improved performance can be achieved by implementing PA of the turbine (instead of throttling), creating a network of extraction points at different points in the turbine so as to maintain the required extraction pressure at varying load.

### 3.4 Uncontrolled Steam Extraction and Modelica Turbine Model

The first and most simple configuration is uncontrolled extraction, which simply entails creating a side branch from the main steam flow. This branching can be implemented between turbine stages or between turbine sections. This solution is typically used for the feedwater heating train. When used for varying the extraction thermal load, the decreased flow rate in the cascade downstream of the extraction causes the extraction pressure to drop. As currently implemented in the models, and as also seen above in Figure 7, the extraction is realized by a T-junction between turbine sections, each with a specified isentropic efficiency. This effect can cause a discrepancy between the efficiency of the entire expansion and that of each section, as illustrated in the T-s and h-s diagrams shown in Figure 13.

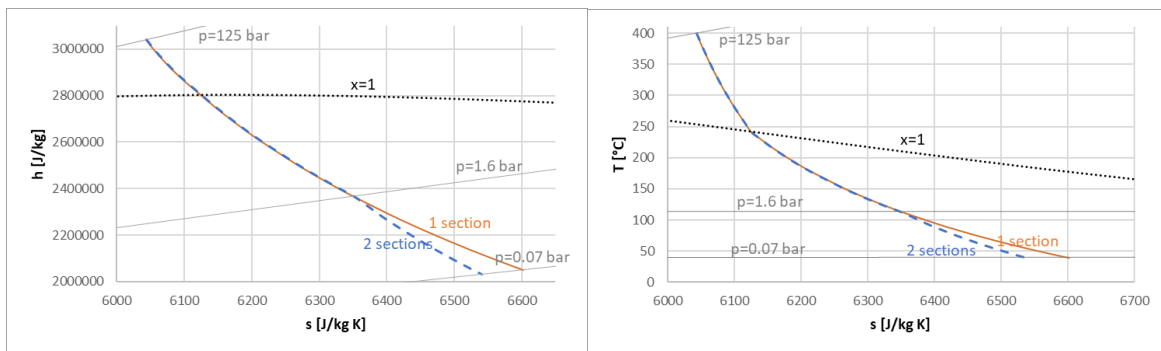


Figure 13. Illustration of the expansion curve for a single-section and a two-section turbine expansion in h-s and T-s diagrams, all sections having constant isentropic efficiencies. Parameters correspond to the SFR.

The turbine model follows the Stodola equation, an industry standard since the 1920s [5]. The Stodola equation models an infinite number of turbine stages. At highly off-design conditions, the turbine model does not account for potentially choked flow conditions, despite the Stodola equation remaining



numerically consistent. Thus, for any deviations in which the HPT relative pressure ratio across the turbine exceeds the critical pressure ratio, the results may not be physically accurate. As choking can be expected at the outlet of the HPT, its backpressure would be higher than at the extraction point. A shock expansion, dissipating the energy, would occur between these points, reducing delivered power. Note that the extent of off-design turbine performance would also result in different (typically lower) isentropic efficiency, which is here maintained constant.

### 3.5 Partial Admission

Higher flexibility in combination with limiting off-design operation of the turbine can be achieved through multiple adjustments to the system configuration. PA is a method of controlling the turbine via a governing impulse stage at its inlet, when large changes in load are desired. Valves that allow vapor admission into distinct groups of nozzles of the impulse stage inlet are incrementally closed or opened, reducing or increasing the effective inlet area and swallowing capacity of the turbine. The main features of PA and its resulting performance can be summarized as follows:

- A governing stage is needed at the inlet
- The cycle operates at nominal pressure, maintaining nominal efficiency even at reduced loads
- The turbine efficiency decreases slightly; however, the impact is typically smaller than the drop in cycle efficiency that would otherwise occur at partial load

In the scope of CHP steam cycles for nuclear plants, PA downstream of the extraction point is implemented as a method for controlled extraction while maintaining high efficiency. For more details on PA, refer to [6].

### 3.6 Multiple Extraction Points for Single Demand

If uncontrolled extraction is desired, the configuration in Figure 14 offers the potential to maintain lower extraction pressures during low extraction demand (limiting throttling losses, as steam expands in the turbine to lower the pressure prior to extraction) by utilizing Extr. 1 (Figure 14). At higher extraction requirements—exceeding the capacity of Extr. 1—the extraction point upstream in the turbine (Extr. 2) is utilized (alone, or in combination with Extr. 1 to ensure the process demand is met while also maximizing power production).

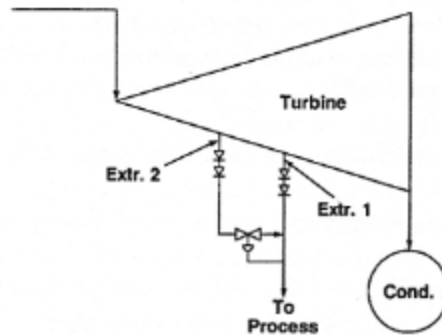


Figure 14. Flow schematic of the condensing steam turbine, using two uncontrolled extraction openings to provide process steam [7].

This configuration has been modeled as a proof-of-concept, but was deemed unsuitable for this general analysis, as it would be best assessed on a specific case of thermal demand and range of extraction points and operating conditions. This task will likely be considered as a possible optimal solution in future specific deployment cases.

### 3.7 Controlled Extraction

The other option is controlled extraction, as illustrated below in Figure 15. Controlled extraction uses a control element such as a valve (in practical terms, a screen inside the turbine casing) between turbine sections downstream of the extraction junction in order to prevent the extraction pressure from dropping below the desired level. With this configuration, the extraction flow rate is theoretically unlimited, ranging from zero to 100%. In actual systems, a 10–15% steam flow rate must typically pass through the downstream turbine to provide cooling, as the ventilation losses could overheat the turbine.

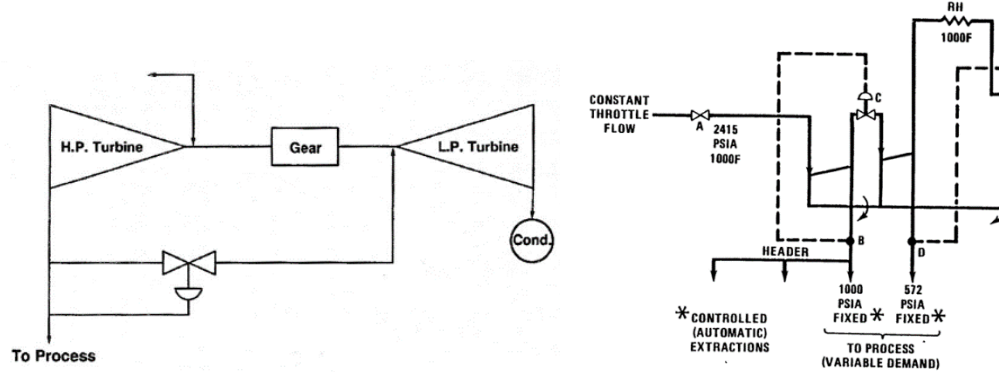


Figure 15. Illustration of controlled extraction from the turbine [7].

To avoid throttling, the low-pressure section can, theoretically, also operate with PA. Eventually, if multiple parallel casings are used, controlled routing of the steam into these separate turbine sections becomes possible.

Previous BOP models were modified to include controlled extraction (see Figure 16). In this model, the valve on the extraction line is still used to control the steam flow rate. PA of the low-pressure turbine (LPT) or the extraction control valve is controlled to maintain a constant small pressure difference (0.5 bar) across this valve. This effectively keeps the extraction pressure constant when the system operates with the controlled extraction valve partially opened. In the regime in which the controlled extraction valve or PA would be fully opened, the extraction flow rate remains controlled by a valve on the extraction line, just the same as with uncontrolled extraction.

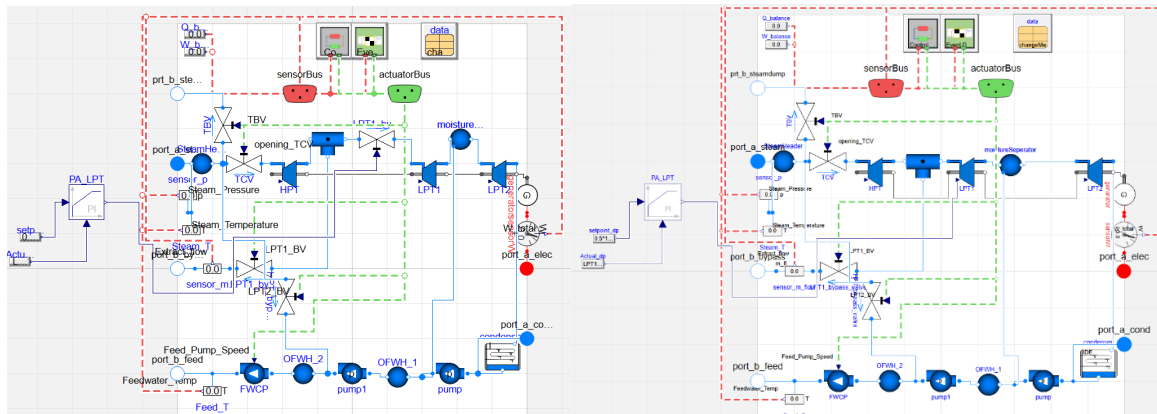


Figure 16. BOP with controlled extraction realized by a valve before the LPT (left), and by LPT PA (right).

### 3.8 Workflow Using RAVEN

To understand the effects of thermal extraction on the system, a thermal extraction analysis workflow was created to flex the system models with a large set of parameters. The analysis required a parametric study accomplished by running the Modelica models with different sets of input parameters. RAVEN was used to perform these tasks. Figure 17 shows a thermal extraction analysis workflow using RAVEN [8].

First, the system specifications, including control setpoints such as thermal power, feedwater temperature, and steam generator outlet pressure, were input to the design thermodynamic model, which also received a set of design extraction pressure, demand pressures, and extraction flow rates from the RAVEN sampler. The nominal fluid density at the extraction point (i.e., input parameter of the LPT) was then taken by the RAVEN sampler as input process variables of the Modelica model, prior to running it. As such, the steady state model was flexed using the RAVEN sampler, and the response surface analysis and its visualization were performed next.

To identify operational ranges (i.e., extraction pressure and extracted steam mass flow), given a demanded pressure for heat demand, two separate thermal extraction analyses were performed. First, the demand pressure was set to 1 bar, the lowest demand pressure considered, as demand temperatures below 100°C were ignored. The simulation was then run using a range of different extraction pressure and mass flow rates, going from minima (zero mass flow rate, 1 bar extraction pressure) up to their physical maximums. A physical maximum is considered the point at which nominal design values within the steam generator (steam pressure, feedwater temperature, and steam temperature) can no longer be met during operation. Multiple demand pressures were not needed for this set of runs, as the demand pressure did not affect the resulting thermal efficiency of the system (it only affected the cutoff point, beyond which more steam cannot be extracted using the current configuration). Second, the extraction mass flow rate was set as the total nominal flow rate of the system (i.e., all steam passing through the HPT), with a set of different extraction and demand pressures. When the system could not meet key design points, the flow rate was deemed to be the maximum extraction flow rate. This was repeated to find the maximum flow rate for each set of pressures. In the second analysis, only simulations in which the extraction pressure exceeded the demand pressure were run. All results from the first and second analyses were compiled into a 2D map, with contour lines for both the extraction and demand pressures. Due to its appearance this type of map is known as a “whale chart.”

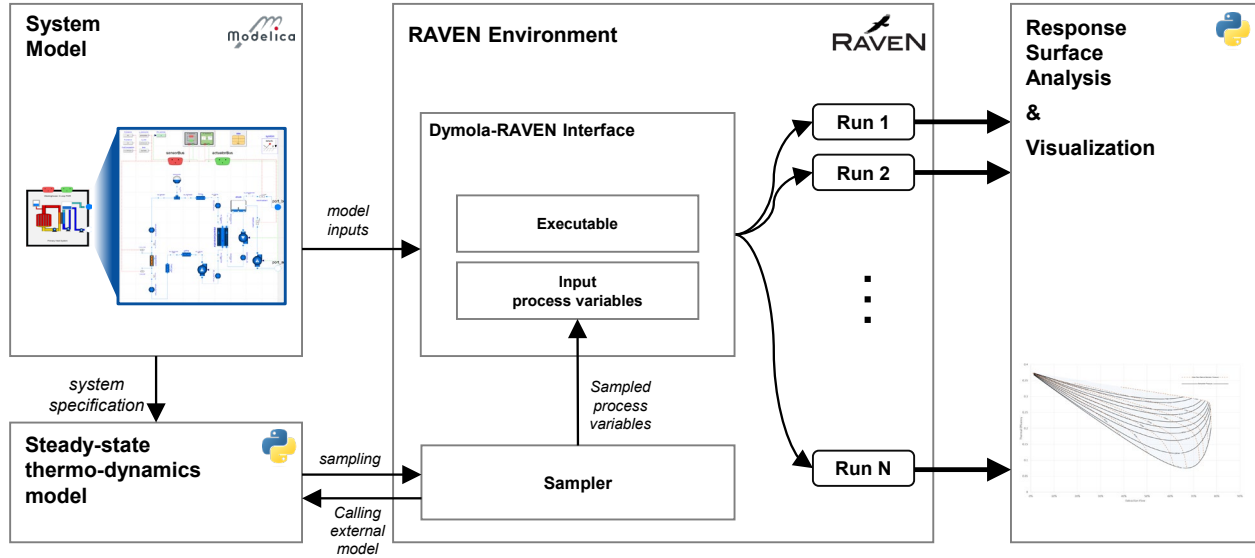


Figure 17. Thermal extraction analysis workflow using RAVEN.

## 4 THERMAL EXTRACTION RESULTS

Thermal extraction analyses were performed for each of the reactor types shown in Sections 2.3–2.6. Some of the detailed reactor models were replaced with heated volumes and hydraulic resistances in order to improve computational speed. The heated volumes and resistances simulate the steam generator at steady-state operation. Where the pressure and feedwater conditions are met with design values, a nominal nuclear heat generation rate is well estimated by a constant heat rate imparted on the secondary-side flow. It is important to note that the results of these analyses are steady-state results; therefore, steady-state simplifying assumptions can appropriately describe the system. The detailed steam generation and nuclear steam supply system modeling will be reinstated before any transient analyses are completed.

### 4.1 Uncontrolled Extraction

Figure 18 shows as an illustrative example of several specific curves of flow rate and extraction pressure—and not the full range for illustrating the entire whale chart—to help inform readers of how to read the full whale chart. Two kinds of curves are plotted: the solid black lines show the thermal-to-electric efficiency of the BOP at a dictated design extraction pressure. This pressure can be thought of as, effectively, the pressure at the inlet of the LPT. The orange dashed lines show the maximum mass flow rate that can be extracted with a given thermal demand pressure outside of the BOP. Due to pressure losses across different components, these extraction flow rate lines are necessarily below the extraction pressures of the same value. The key points on the whale chart are where the dashed lines cross over the solid lines. These indicate extraction flow rates from an extraction pressure to a demand pressure. In Figure 18, this means that, with extraction pressures of 35, 50, and 110 bar, the maximum flow rates that can be extracted to a 20 bar process are around 41%, 58%, and 80% of the nominal steam flow. These values are specific to the BOP system being analyzed: feedwater heating methods and setpoints, along with the design steam pressure influence the line contours on the whale charts.

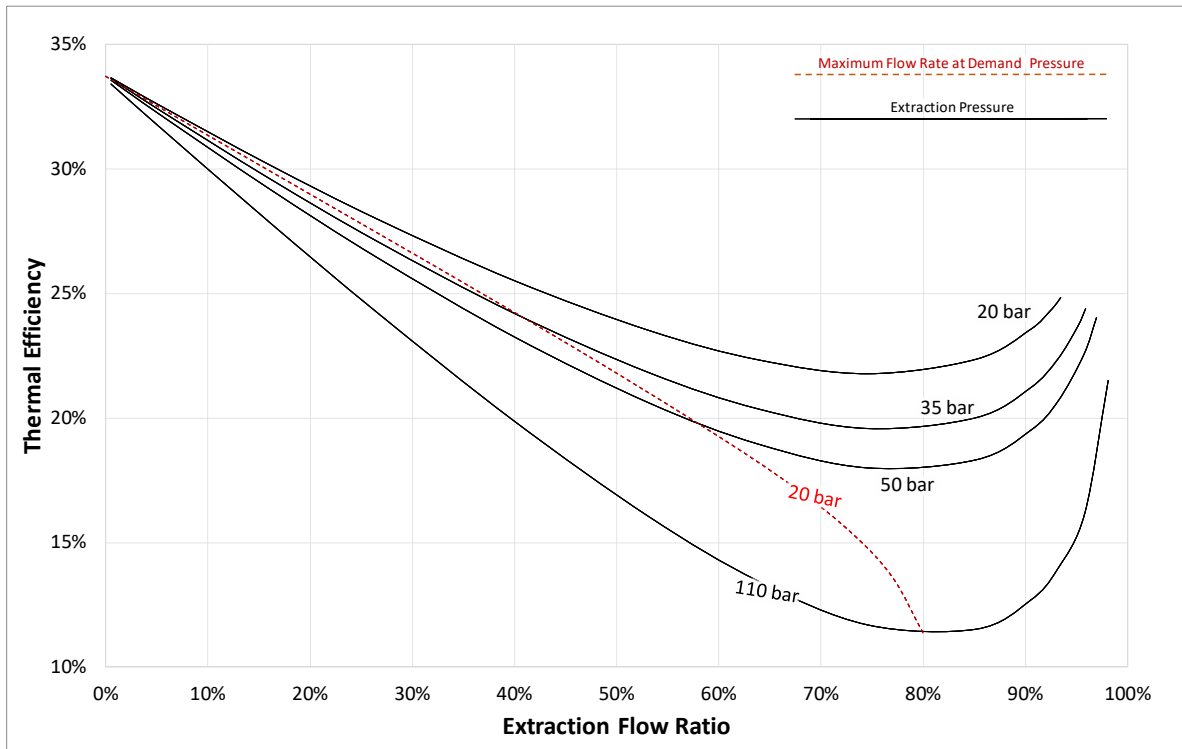


Figure 18. Snippet of the whale chart.

To better explain the pressure parameters within the system and their impact on performance, Figure 19 shows the relationship between the maximal extraction steam flow and the required extraction nominal pressure for given demand pressure. The ends of the curves in Figure 19 (for a given extraction pressure) indicate that removing additional mass flow from the system will cause the BOP to fail to meet design setpoints. Figure 20 shows the thermal efficiency of the system that combines nominal extraction with the desired delivery demand pressures. Though the curves in Figure 20 are not on the whale chart, the chart demonstrates how a single-rule solution (e.g., always minimize the design extraction pressure relative to the demand pressure) is insufficient to describe all systems.

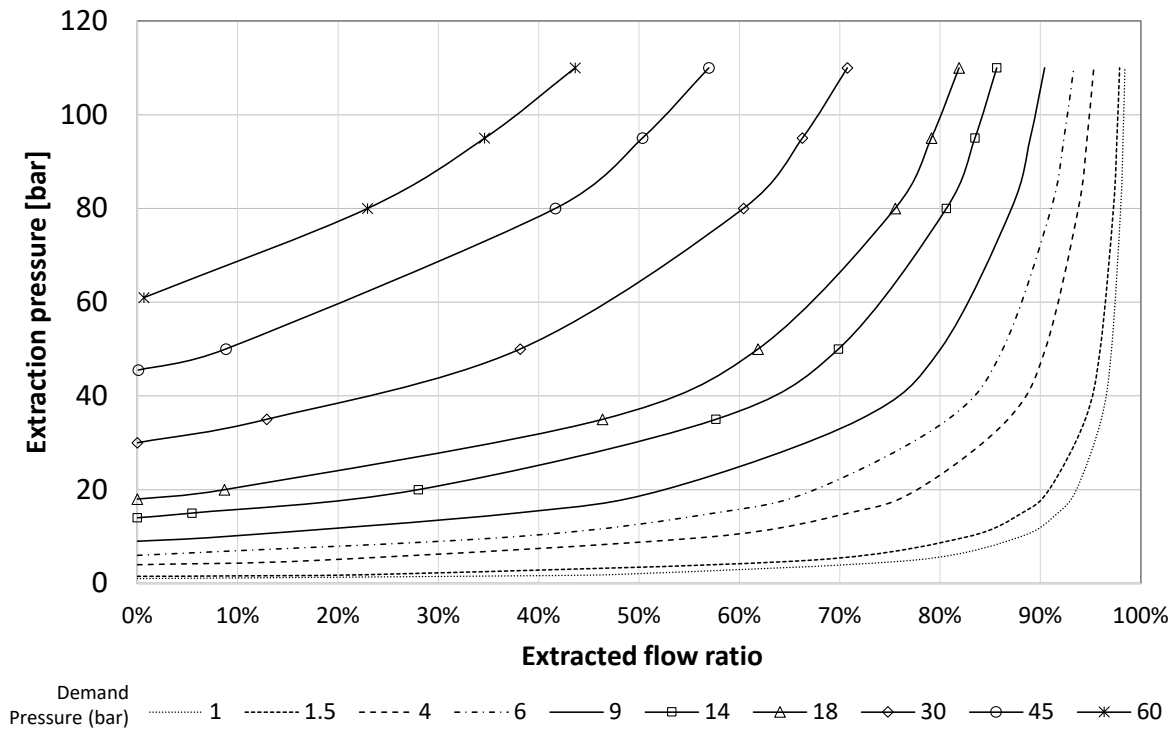


Figure 19. Extraction pressures for required demand steam flow and demand pressure.

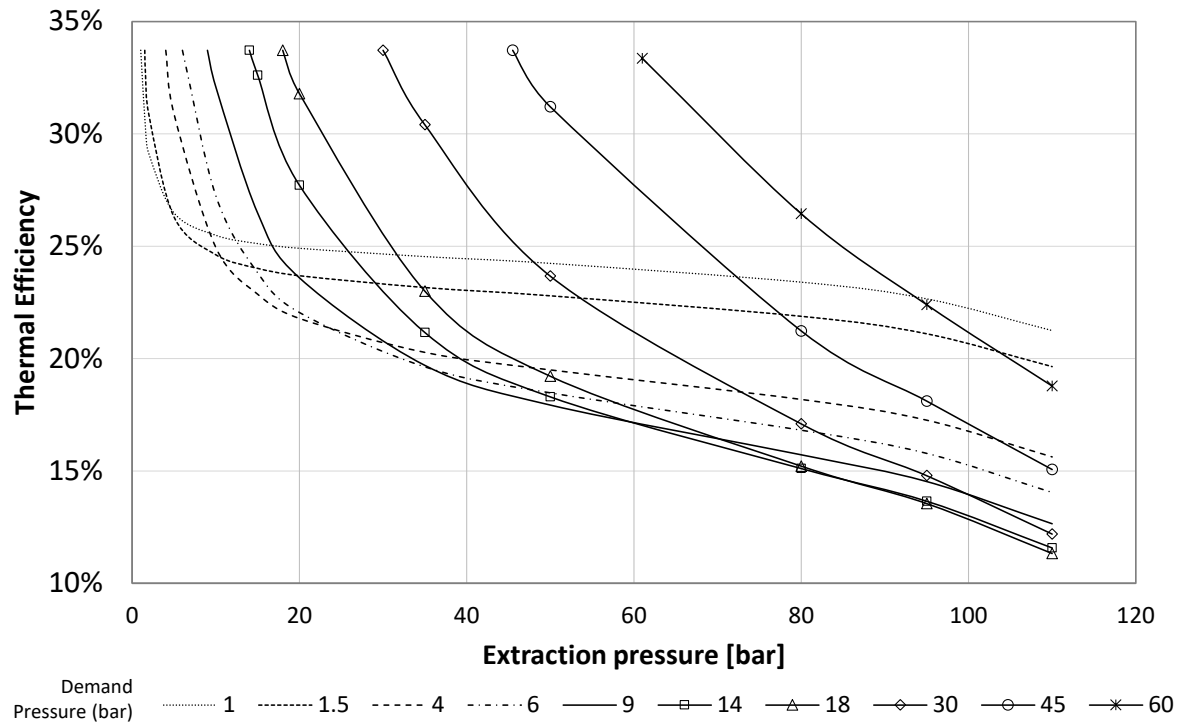


Figure 20. Thermal efficiency as a function of demand and extraction pressure.

The whale charts in Figure 21–Figure 24 were generated from these results. These figures show the relationships among extraction pressure, demand pressure, extraction flow rate, and thermal efficiency. The mass flow rate is given as a ratio of the extraction flow rate over the HPT inlet mass flow rate. Thermal efficiency does not account for the thermal utilization of the steam application, but only the net electrical work of the Rankine cycle.

Figure 21 shows the whale chart for the OFWH BOP with A-LWR conditions. Figure 22 and Figure 23 show the whale charts for the HTGR with the OFWH and the CFWH BOPs. Little difference is observed between the different feedwater configurations, which is why repeated presentations of the OFWHs and CFWHs for other reactor systems are not included. Note that reduced thermal efficiency can be observed in the HTGR with CFWHs. Figure 24 shows the whale chart of a SFR BOP. Note that for the SFR BOP, the highest extraction pressure in the explored range was relatively low compared to the HPT inlet pressure in other cases, causing the whale shape to be visually narrower. This is due to the lower steam pressure in SFRs than in HTGRs, combined with high feedwater temperatures relative to A-LWRs. Figure 25 shows the whale chart for the MSR BOP. As with the SFR case, the MSR also had a lower steam pressure.

The dashed orange lines are extraction contours of the maximum flow ratio that can be extracted at a given demand pressure. The operating pressure at the extraction point must exceed the demand pressure. The limit is the point at which the actual extraction pressure decreases to the level of the demand pressure (plus the pressure drop across the extraction valve). As more flow is extracted, the flow rate through the LPTs (with original full-flow-rate swallowing capacity) is reduced, in turn decreasing the pressure at the extraction point. For any given demand pressure, the system can only operate below the dashed line. The solid black line shows the system's thermal efficiency at a given extraction pressure and flow rate. The demand pressure has no effect on the electrical efficiency of the system—only the extraction pressure and flow rate do. The demand pressure need only be below the operational (off-design) extraction pressure. Any difference between these two pressures occurs as a pressure drop across the extraction valve.

In addition to the work potential lost due to the steam extracted at the demand pressure, two other losses also result from the off-design system operation. As the intermediate pressure at the extraction point is decreased, the turbine can handle a larger flow rate (higher pressure difference). Since a larger flow rate is unavailable with the fixed amount of thermal power from the reactor, the pressure at the HPT inlet must be decreased by closing the turbine control valve. The second loss results from throttling across the valve controlling the steam extraction. This throttling loss occurs every time there is a difference between the operation extraction pressure and the demand pressure, as the extraction valve reduces the pressure sent to the theoretical process demand. Extraction throttling decreases with additional mass extraction as the extraction pressure decreases to match the demand pressure. This decrease in extraction pressure means that the full amount of steam in the HPT section expands across a larger pressure difference. The throttling losses are not easily noticeable in the whale charts.

It may initially appear counterintuitive that the thermal efficiency in the system increases at very high thermal extraction rates. This effect occurs as the specific enthalpy converted into electricity increases within the HPT as the pressure ratio across the HPT increases. Initially, the increase in per-unit energy conversion does not overcome the mass flow reduction that exists within the LPT. Eventually, the increase in the energy withdrawal in the HPT overcomes the reduction of energy withdrawal in the LPT as the pressure ratio within the HPT becomes very high. Note that all the nominal mass flow continues to flow through the HPT, regardless of the steam extraction rate—only its backpressure is changing based on the extraction rate.

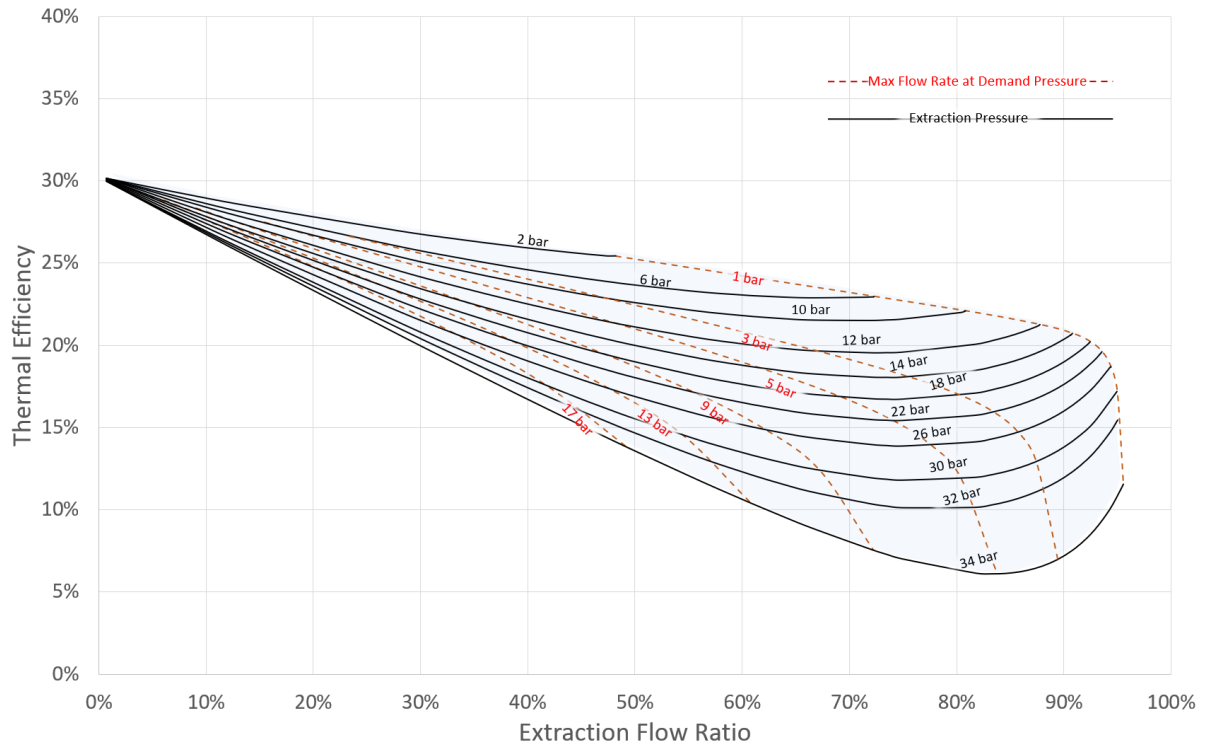


Figure 21. Whale chart of the OFWH BOP with A-LWR conditions.

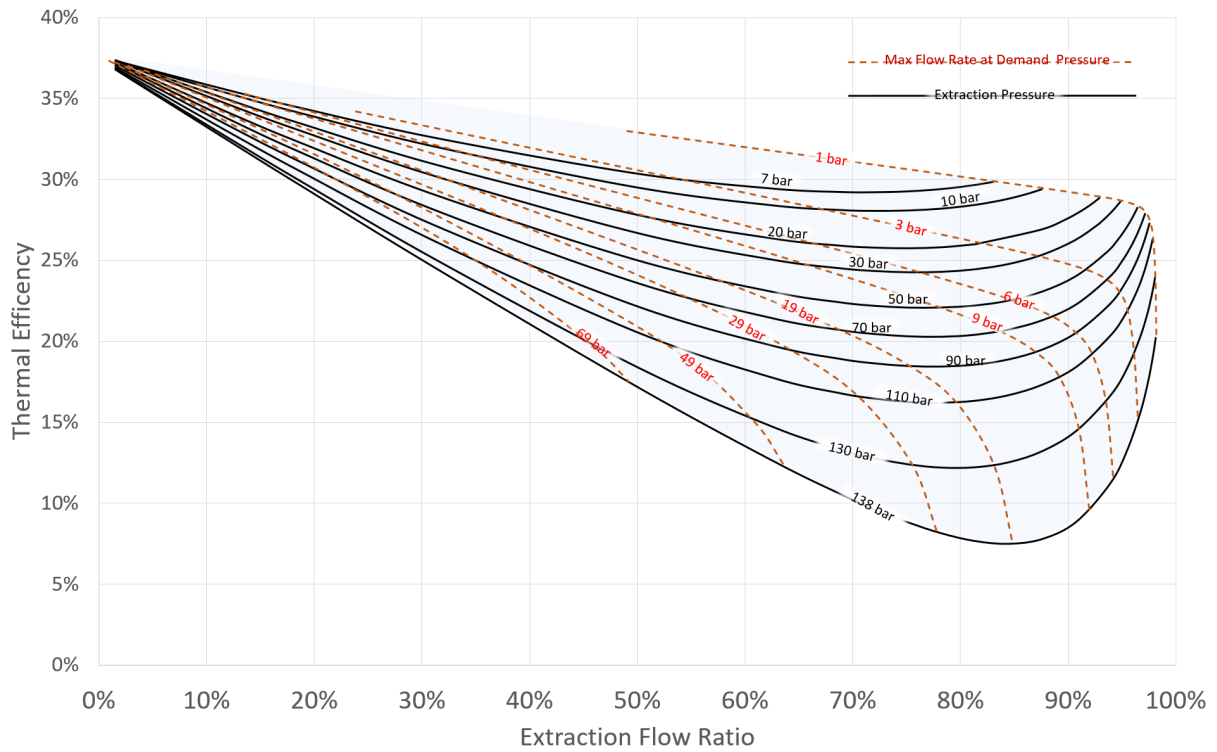


Figure 22. Whale chart of the OFWH BOP with HTGR conditions.



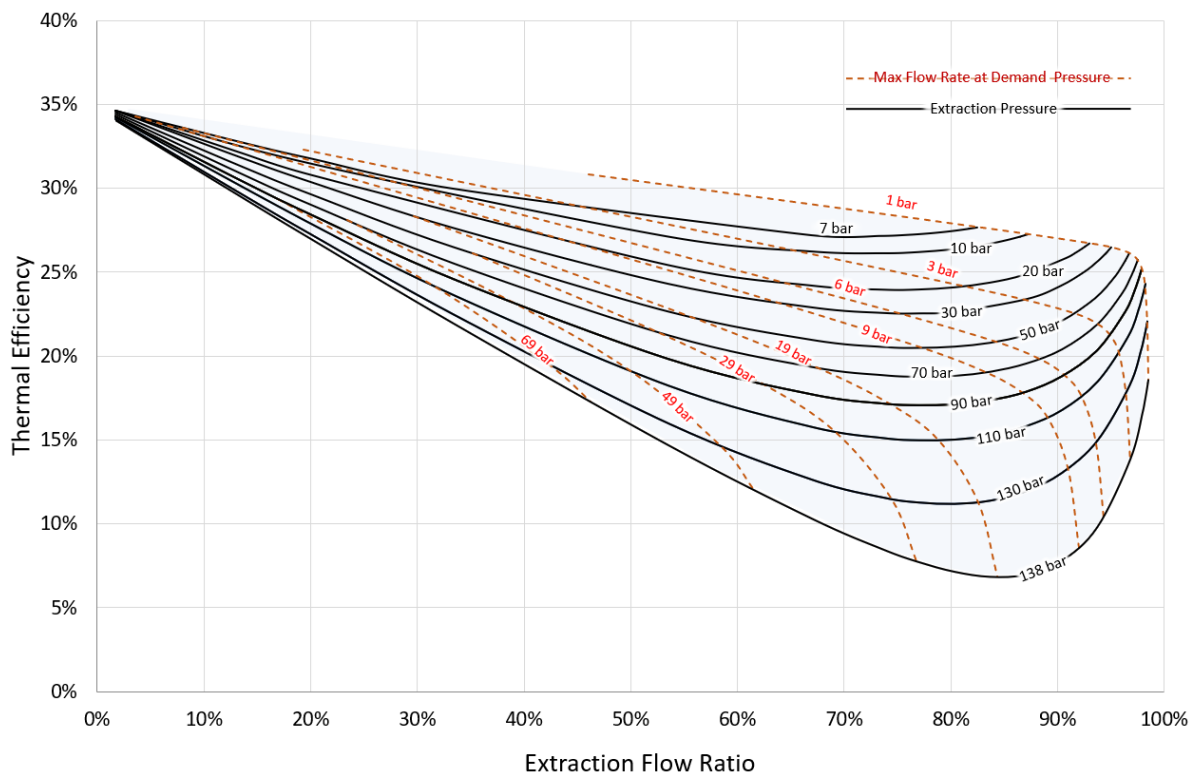


Figure 23. Whale chart of the CFWH BOP with HTGR conditions.

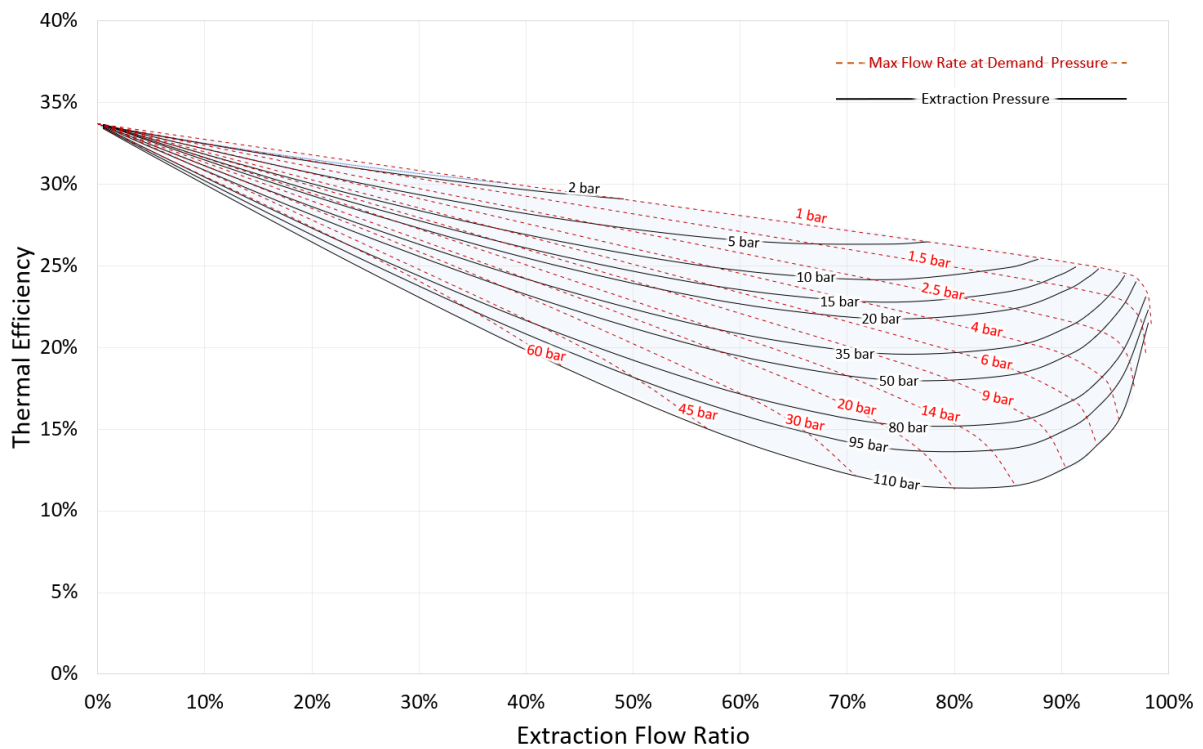


Figure 24. Whale chart of the OFWH BOP with SFR conditions.

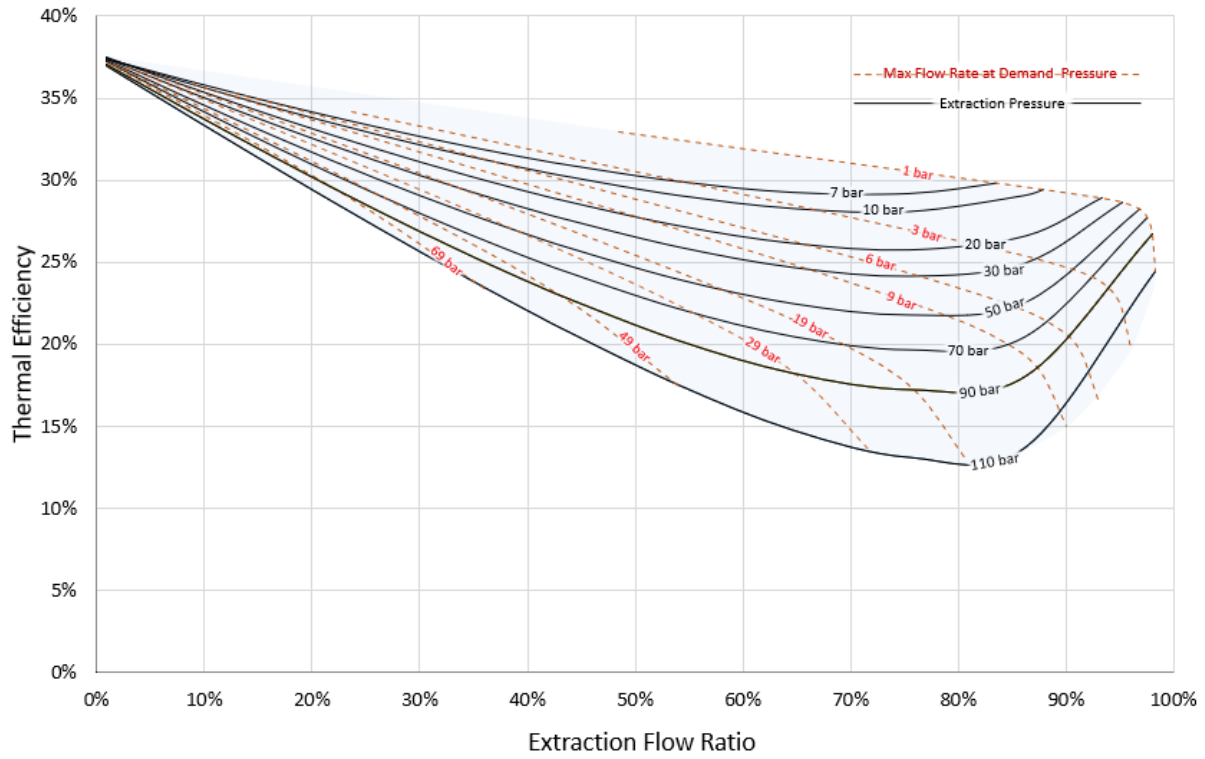


Figure 25. Whale chart of the OFWH BOP with MSR conditions.

## 4.2 Controlled Extraction

The results of the models' analysis are, again, first illustrated in a larger depth on a SFR BOP. After this, the main results are then presented for the remaining reactors. First, a 3-bar demand pressure

case is presented for controlled extraction reflected in the previously developed whale chart in

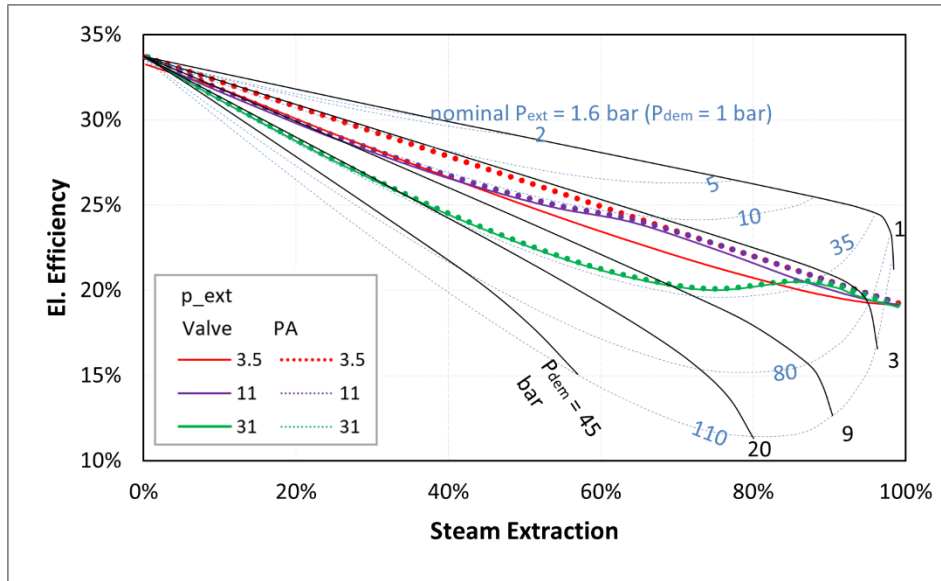


Figure 26. The highest efficiency was achieved for the PA case, with the design extraction pressure being as close as possible to the demand pressure, as all throttling losses are minimized. A slightly lower value from the original whale chart line for the 3-bar demand (which was constructed from multiple uncontrolled extraction designs, connecting maximal points for a range of design extraction pressures) was caused by the considered 0.5 bar pressure drop on the extraction line, pushing the actual extraction pressure to the specified 3.5 bar value.

When the design extraction pressure is higher, for 11- and 31-bar extraction pressures, we see that, at lower extraction flow rates, the curves follow the whale chart for constant extraction pressure. At this point, the PA is fully open, and the system is actually in the uncontrolled extraction regime. Once the limit of uncontrolled extraction is reached, the PA starts controlling the pressure and the curves start to follow the ideal case of PA at 3.5 bar.

The results are somewhat different for valve-controlled extraction, as the remaining flow rate after the turbine is throttled, meaning adding a loss. As the extraction at 3.5 bar means throttling from the beginning of extracting any flow rate, the efficiency is notably lower. Only at 100% extraction would the curves meet, as there is no (throttled) flow rate going through the downstream sections of the turbine.

When the design extraction pressure is higher, the corresponding curves again follow the whale chart until the need for closing the control valve is reached. One interesting feature is that, when assuming constant turbine off-design efficiency, a certain region of thermal efficiency exceeds the design point at 3.5 bar. Also note that all these cases assume the design point of the turbine to be zero extraction (full swallowing capacity of the LP section downstream of extraction). Creating a specific design based around the most frequent operation regimes can decrease this loss.

Note also that some slight efficiency differences in the chart stem from the modeling approach, in which each turbine section has a constant isentropic efficiency. Cascading multiple turbine sections at different intermediate sections correspond to different overall efficiencies of the expansion.

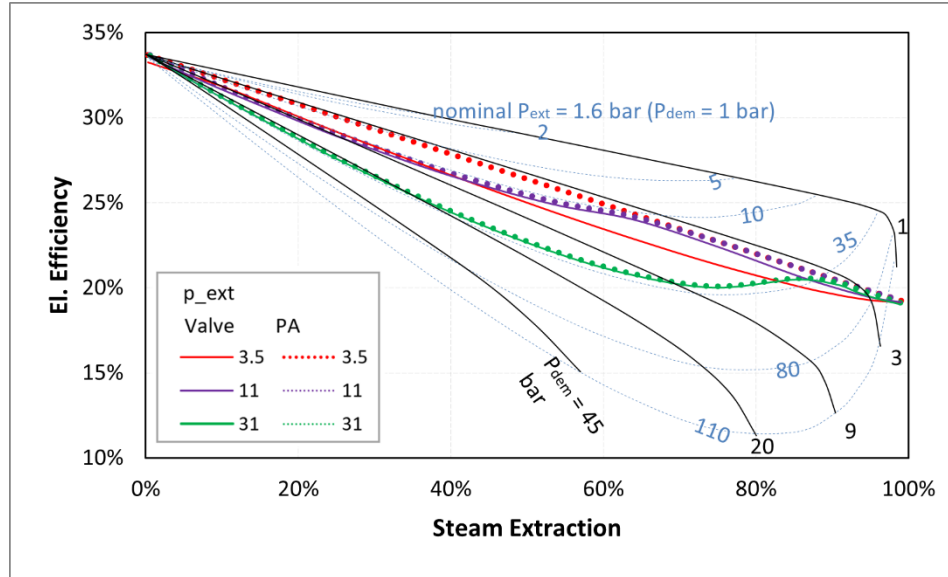


Figure 26. Whale chart of uncontrolled extraction for SFR parameters, overlaid with several controlled extraction cases.

The full range of parameters for multiple extraction pressure options can be plotted for each demand pressure. A selection for demand pressures of 1, 5 and 30 bar are presented in a single figure for valve-controlled extraction (see Figure 27). For the higher-than-demand extraction pressures, the curves are identical for each until reaching the aforementioned cutoff limit for uncontrolled extraction.

Note the difference in starting point for the low extraction pressure—specifically visible for the 1.6 bar extraction pressure. This is due to the model considering separate turbine models, each with constant isentropic efficiency from its inlet. Adding the multiple turbine models works effectively to improve overall expansion efficiency. It is less significant when the last turbine sections come to similar pressures, as the efficiency increases from the third section diminish. To illustrate the thermodynamics of expansion, this phenomenon is illustrated in T-s and h-s diagrams in Figure 13. Additional loss comes from the fact that throttling through the extraction control valve also has a higher impact on power production at lower pressures.

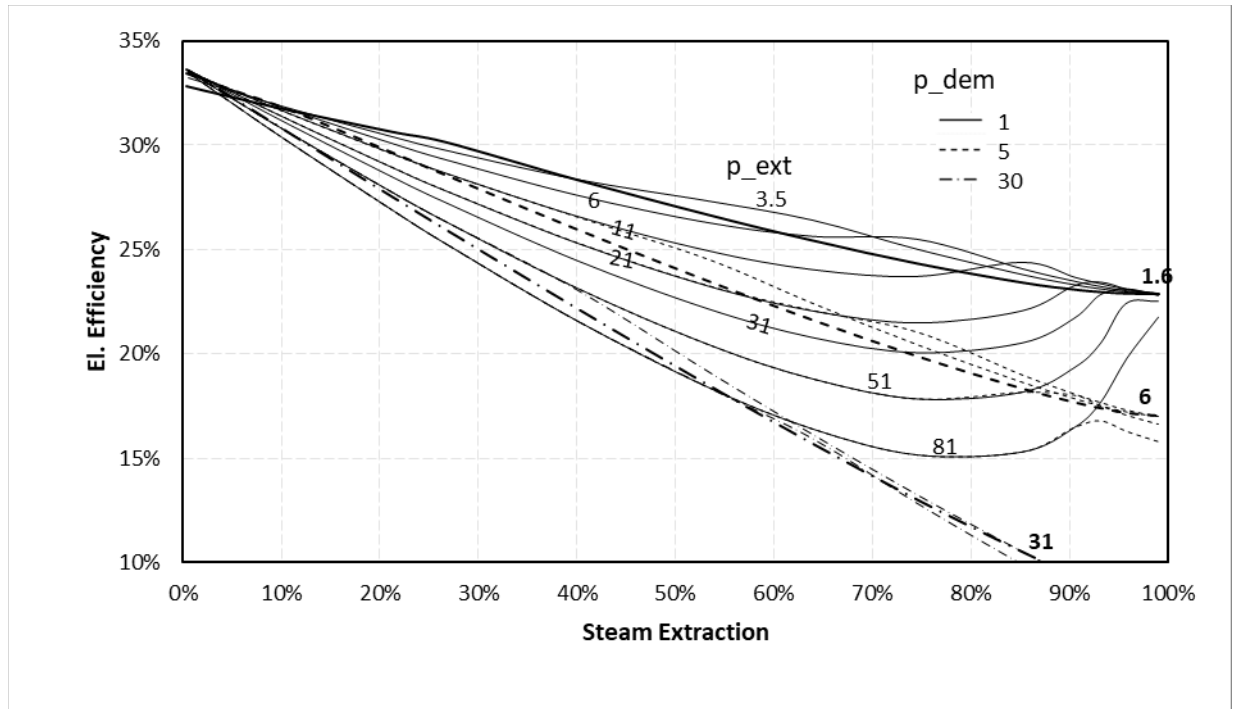


Figure 27. Valve-controlled extraction for a range of design extraction pressures and three different demand pressures.

Valve- and PA-controlled extraction can be compared against each other in a full-range chart similar to the one in Figure 28. It highlights, via the region of practically identical performance and the region of difference in the regimes, that the extraction is actually controlled. As the PA-controlled extraction corresponds to the ideal case, PA at a minimal pressure difference between extraction and demand always enables the highest performance.

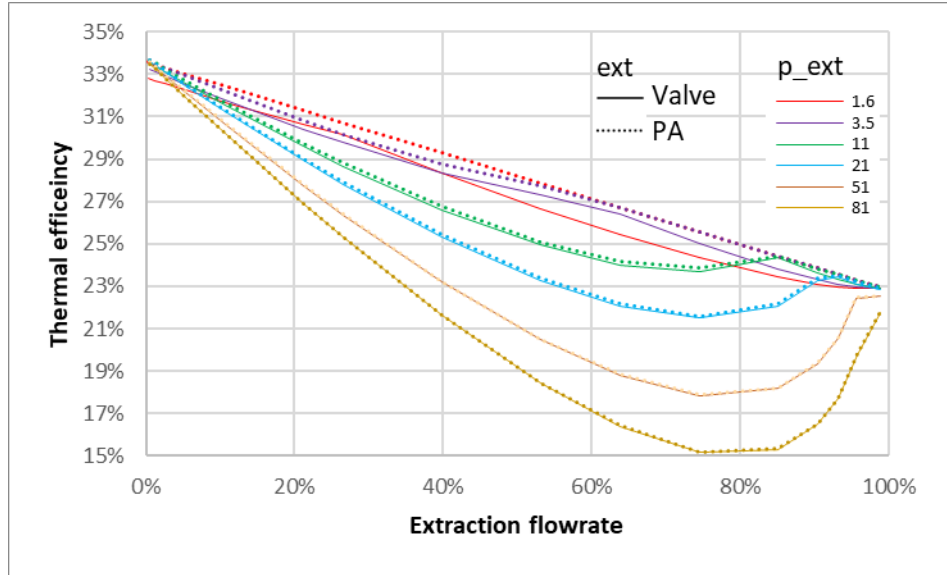


Figure 28. Comparison of valve- and PA-controlled extraction over the full explored range, with a demand pressure of 1 bar.

Arguably, one of the most valuable results of this analysis, in regard to the general comparison between valve- and PA-controlled extraction, is to see the impact of these extraction methods on efficiency, for the minimal pressure drops over a full range of active extraction control. Plotting these values clearly shows the difference (loss) as a result of throttling, as compared to the ideal case represented by PA (with zero decrease in turbine efficiency). This comparison is presented in Figure 29. Note that the efficiency values become closer at higher extraction, as the very low flow rate to the LPT and condenser reduces the impact of PA. In 100% expansion, the values are identical, as both configurations reduce to effectively just a single backpressure turbine section.

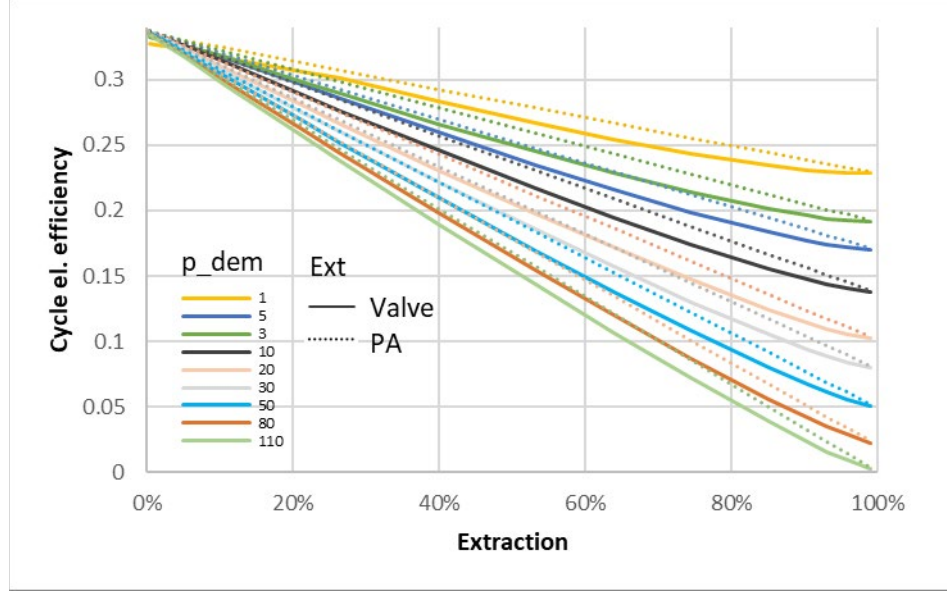


Figure 29. Comparison of PA- and valve-controlled extraction for a minimal (0.5 bar) design pressure difference between extraction and demand. Parameters for the SFR steam cycle.

Note that all systems here consider the design point at 0% extraction. Designing the valve-controlled extraction system to nominally operate with extraction flow would improve the system efficiency, effectively shifting it closer to the ideal case considering constant turbine efficiency under PA.

Lastly, for CHP systems, overall efficiency is commonly considered, accounting for both produced useful heat and power. Overall efficiency can be defined according to Equation 10. For the purpose of this analysis, the reference enthalpy for the heat demand outlet corresponds to saturated liquid at condensation pressure. Note that for a specified extraction, once the system operation makes it on the whole chart, the extraction pressure (and thus the enthalpy) is higher, increasing the amount of extracted heat. Thus, for a single demand pressure and a specified extraction regime, the decrease in efficiency with high extraction pressure is compensated for by the increase in extracted thermal energy, leading to effectively identical values. Practically identical values are also obtained at different extraction pressures. The only decrease in efficiency, based on the control regime, is observed between operation in PA-controlled extraction and valve-controlled extraction as a result of the throttling loss between the extraction and the downstream turbine. Figure 30 illustrates this parameter between the lowest and highest extraction pressures, and compares PA- and valve-controlled extraction at those pressures. Figure 31 shows the CHP efficiency in uncontrolled extraction for different limits of operation.

$$\varepsilon_{CHP} = \frac{W_{net} + Q_{thermal}}{Q_{in}} \quad (10)$$

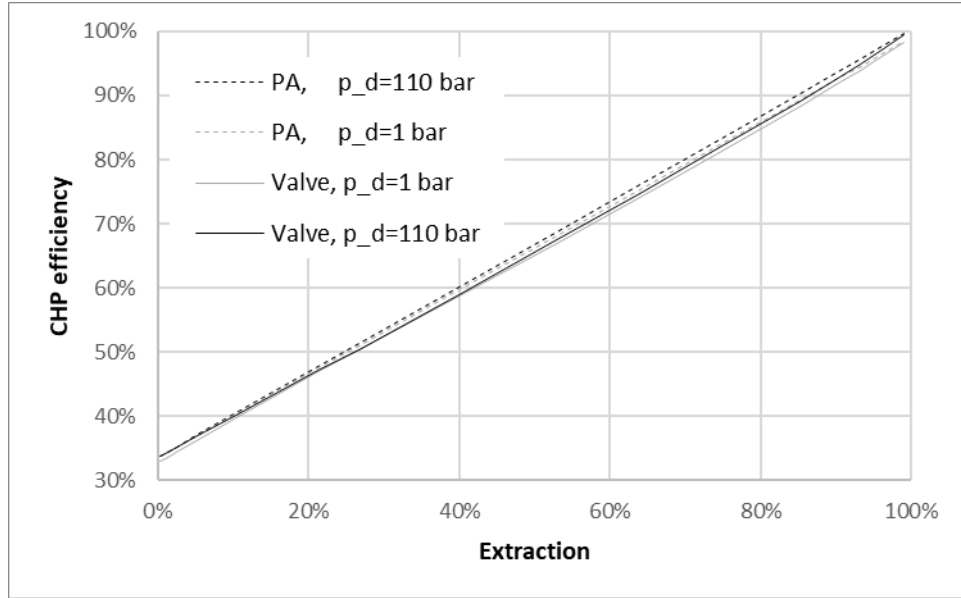


Figure 30. CHP efficiency, parameters for SFR steam cycle.

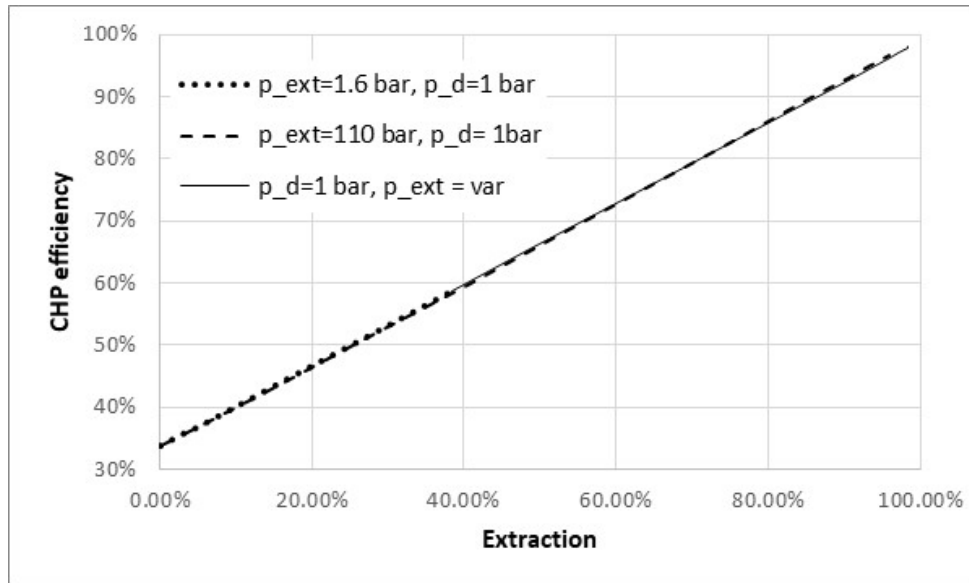


Figure 31. CHP efficiency for SFR steam cycle in uncontrolled extraction.

As with the SFR case, the parameters of a CHP cycle for a highly simplified LWR cycle were evaluated. The efficiency curves are now plotted in Figure 32—though for the sake of brevity, only for the minimal pressure drop between the design extraction pressure and the demand pressure. The analogous efficiency curves for the HTGR oversimplified steam cycle are presented in Figure 33.



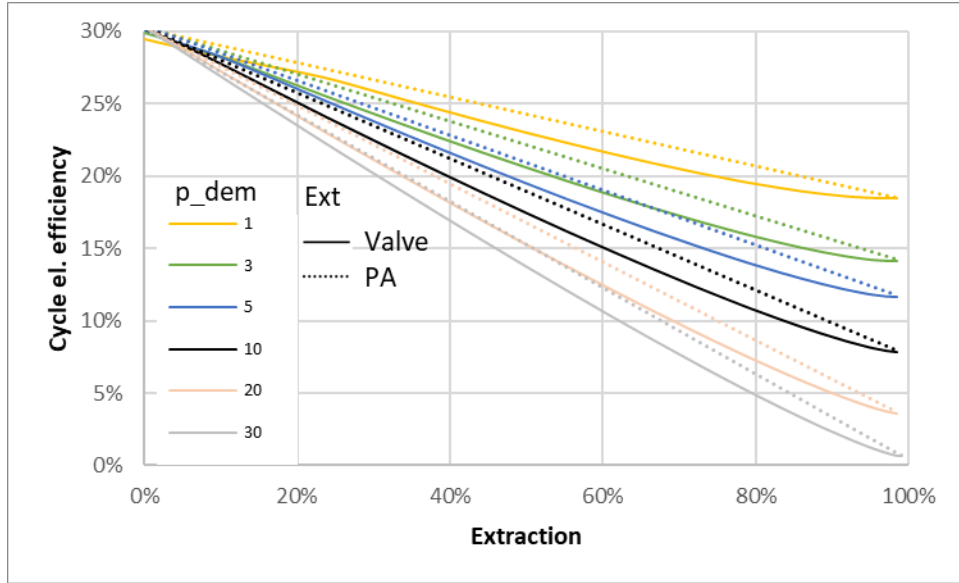


Figure 32. Comparison of PA- and valve-controlled extraction for a minimal (0.5 bar) design pressure difference between extraction and demand. Parameters for the LWR oversimplified steam cycle.

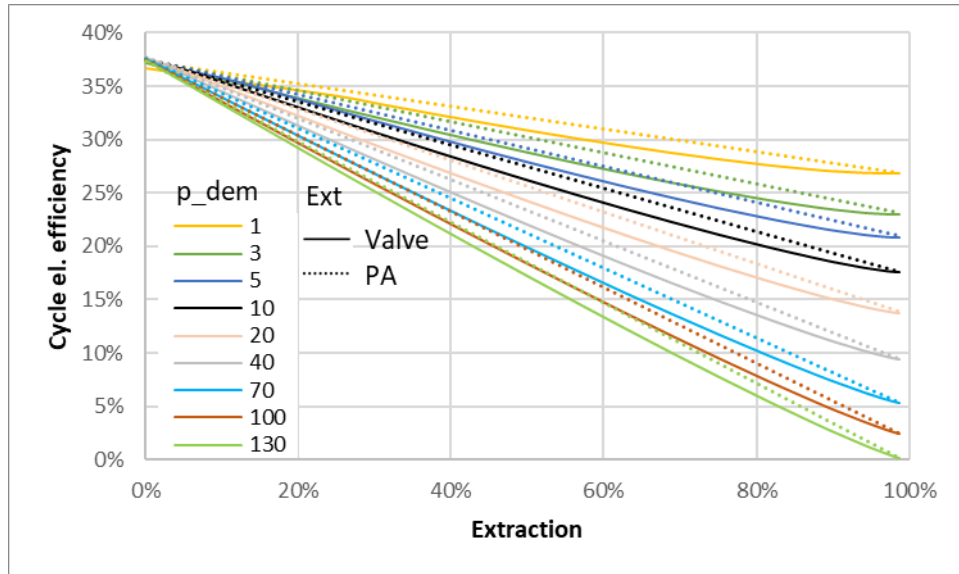


Figure 33. Comparison of PA- and valve-controlled extraction for a minimal (0.5 bar) design pressure difference between extraction and demand. Parameters for the HTGR oversimplified steam cycle.

Finally, the CHP cycle efficiency curves for the MSR are presented in Figure 34. The reference cycle for MSR was chosen to be supercritical and highly regenerated, with the same assumptions as the prior models [9]. Among the simplifications are a reduction from the reheat cycle (the original design considers a single reheat) to a simple cycle, and the absence of any thermodynamic benefit of feedwater heating, as it is performed by a bypass from the turbine inlet steam mixing with feedwater. Again, this is done so as to be consistent with previous work; however, the value of these results is highly limited.

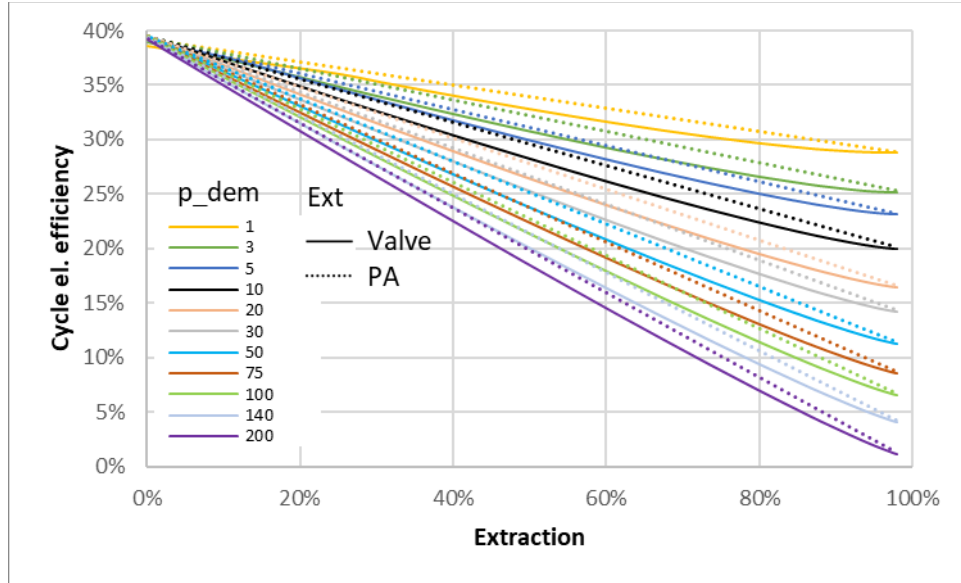


Figure 34. Comparison of PA- and valve-controlled extraction for a minimal (0.5 bar) design pressure difference between extraction and demand. Parameters for oversimplified MSR steam cycle.

## 5 THERMAL DELIVERY MODELING

Thermal delivery modeling is needed to quantify the impact of transferring heat across potentially impactful distances within tightly—meaning thermally—integrated energy parks. Modeling within the Modelica language, and thus allowing these models to interface with existing nuclear heat generators and various heat consumers already described within the HYBRID repository, enables fast parameterization and object-oriented model manipulation. While the initial problem statement of this work is centered on static system operation, by executing an engineering analysis capable of solving dynamic problems, the IES team is well-prepared for the next logical step of analysis.

The thermal delivery model produced within the HYBRID repository can flex parameters to calculate thermodynamic losses across many design dimensions, including power rating, piping length/diameter, heat transfer fluid, inlet temperature/pressure, insulation thickness, insulation material conditions, and ambient conditions. There are many degrees of freedom within this analysis, leading to computational difficulty in terms of the multi-dimensional sensitivity analysis and challenges in presenting the results. Many variables must be held constant in order to map the impact of changing conditions in a visually understandable manner. The goal of this work is not only to characterize the steady-state impacts of thermal delivery but also the dynamic responses to changes in supply and demand. Figure 35 shows how this new thermal delivery can be integrated into a future IES model.

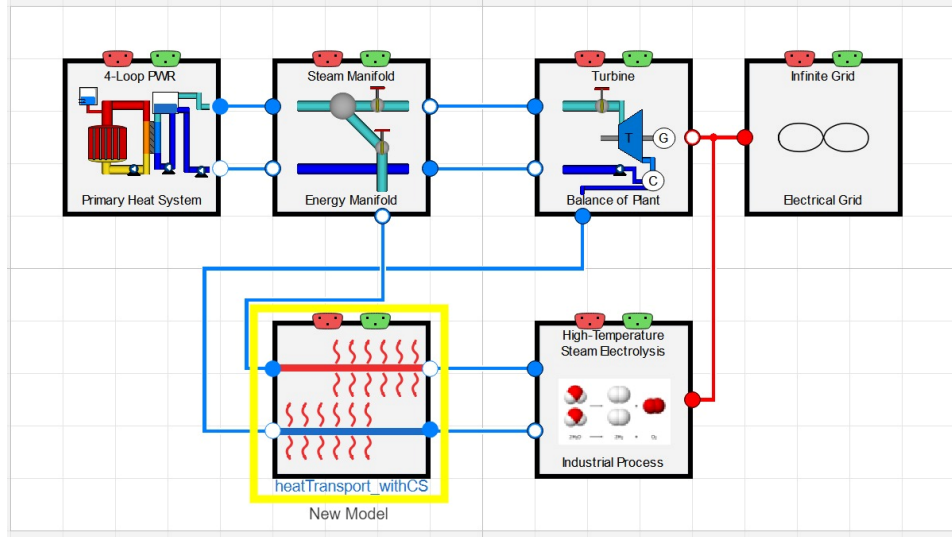


Figure 35. Possible future IES model, using the heat transport model to model long-distance heat transport for IES applications. The yellow box shows the thermal delivery location and integration.

## 5.1 Modeling Theory

Figure 36 shows the new transient thermal delivery model. The four fluid ports in the model, seen on the sides of the modeling box inside the yellow outline in Figure 35, can be used to connect two other systems together, while modeling the dynamics of long-distance heat transport and the losses incurred. The model is constructed around two configurable pipes: one for supplying heat to the heat application via a heat transfer fluid (HTF), and another for returning the HTF to the heat source.

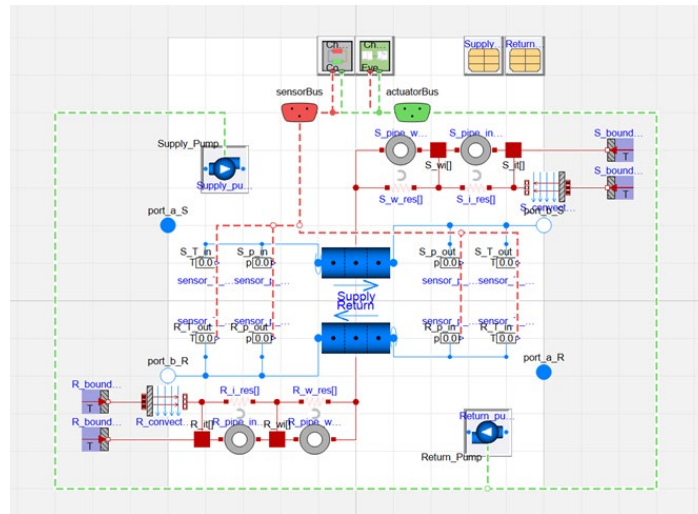


Figure 36. NHES.Systems.HeatTransport.HeatTransport\_withCS (some conditional connections are not shown).

The other model components are either selectable or conditional, meaning for example that the user can decide whether the pumps should be modeled internally to the heat delivery model or externally within the heat supply or heat use areas. The user can also select between different thermal boundary calculations, thereby simulating different approaches to insulation.

### 5.1.1 Piping Geometry Description

The piping geometry for the supply and return sides was defined independently, using two data blocks. The data block graphic user interface (GUI) for the supply side is shown in Figure 37. There are six geometric parameters for each side: length, diameter, pipe wall thickness, insulation thickness, change in height, and number of nodes. By default, the parameters for the return side are set to be identical to those of the supply side, but can be changed independently. These parameters, and more, are used to calculate the pressure drops across the system, as well as the heat transfer to the environment.

The screenshot shows a software window titled "Supply\_pipe\_data in HeatTransport.HeatTransport\_withCS". It has three tabs: "General", "Add modifiers", and "Attributes". The "General" tab is active. It contains several input fields and a table of parameters.

**General Tab Fields:**

- Component:**
  - Name: Supply\_pipe\_data
  - Comment: (empty)
- Model:**
  - Path: HeatTransport.data.pipe\_data\_1
  - Comment: (empty)
- Icon:** A small icon labeled "pipe\_data\_1" showing a yellow square divided into four smaller squares.

**Supply Pipe Geometry Table:**

| Parameter | Value | Unit | Description                           |
|-----------|-------|------|---------------------------------------|
| L         | 100   | m    | Supply Pipe Length                    |
| D         | 1     | m    | Inner Diameter Of Supply Pipe         |
| pth       | 0.1   | m    | Thickness Of Supply Pipe              |
| ith       | 0.1   | m    | Thickness Of Supply Pipe Insulation   |
| nV        | 10    |      | Number Of Volume Nodes In Supply Pipe |
| dH        | 0     | m    | Elevation Gain In Supply Pipe         |

At the bottom of the window are three buttons: "OK", "Cancel", and "Info".

Figure 37: Pipe geometry parameter input GUI.

### 5.1.2 Heat Transfer Fluid

The HTF for both sides can be easily changed via a drop-down menu, seen in Figure 38. The fluid can be any media from the Modelica standard library or from HYBRID. This includes water, steam, molten salts, gases, and liquid metals. The choices of fluid for the supply and the return side are independent of each other.

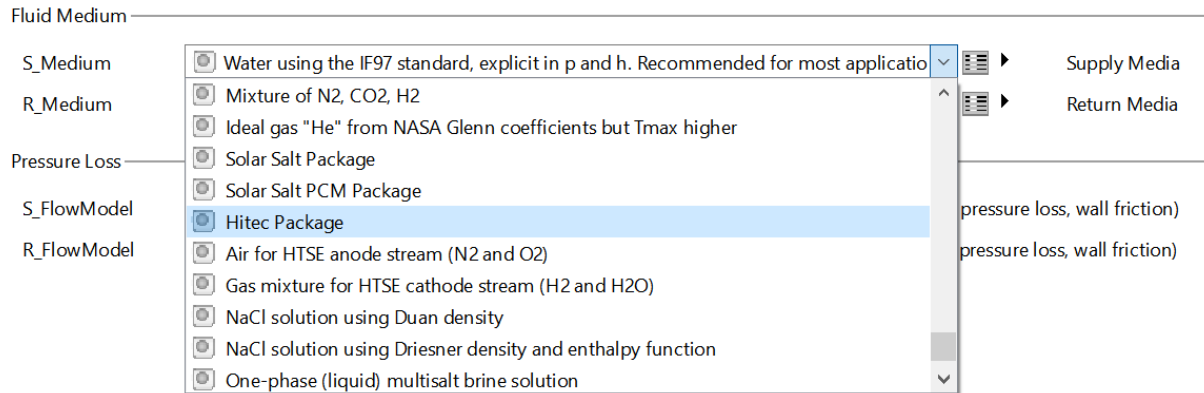


Figure 38. HTF menu in the model parameter GUI.

### 5.1.3 Thermal Losses

Heat transfer from the pipe to the external environment can be calculated using this model. Users can change the manner in which this is modeled, via the conditional components. Heat loss to the environment is calculated based on a user-defined heat transfer correlation in the pipes connected to a conduction model for the pipe wall and insulation. The heat loss calculates via connection to either a convective boundary or a conductive boundary. There are two options for the condition models: solid media or thermal resistance. For the conduction boundary, a simple constant temperature boundary is used. For the convective boundary, the heat transfer is calculated using a constant external temperature and a user-defined convective heat transfer coefficient. Options can be mix-and-matched independently for each side, and the heat paths are shown in Figure 39.

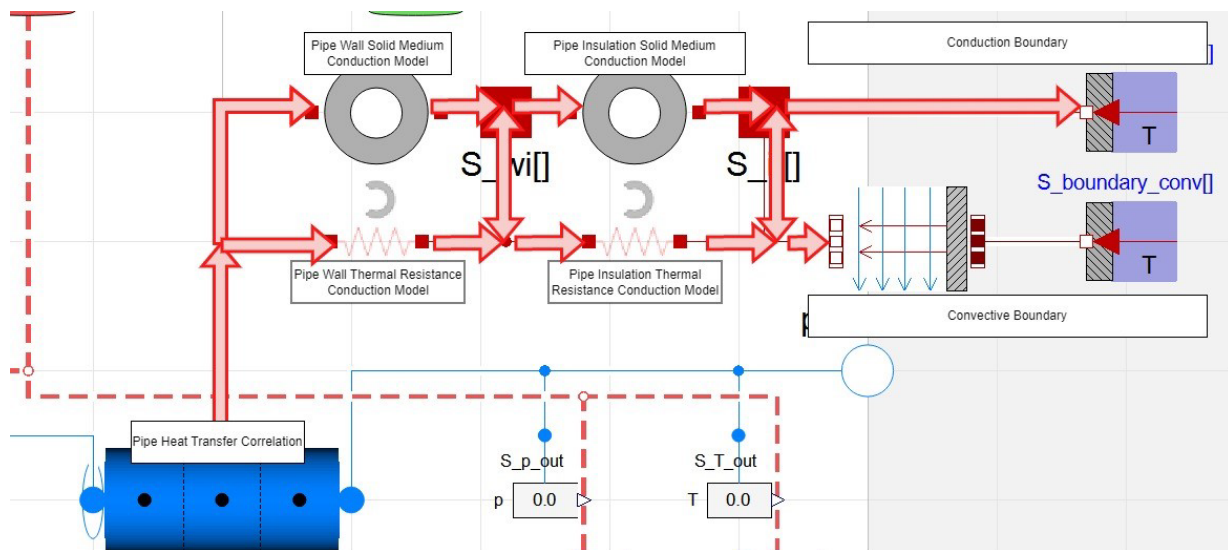


Figure 39: Heat transfer paths for heat loss.

Calculating total heat loss will be key in evaluating insulation requirements for heat delivery.

### 5.1.4 Pump Selection

There is an optional pump on both the supply side and return side. These pumps are replaceable, and the user can select the type of pump desired for a given use case. The selection of pumps is shown in Figure 40. These pumps can be set to have constant values or be controlled through a control system.

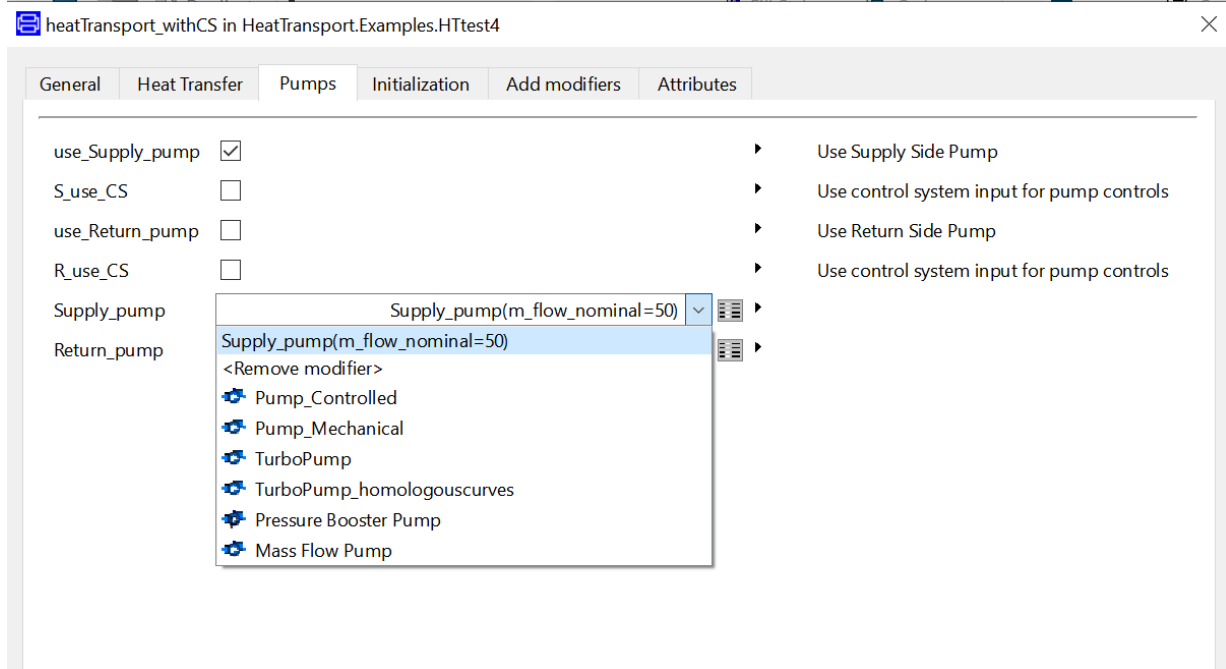


Figure 40: Pumps tab in the parameter GUI.

## 5.2 Results

Some preliminary results are presented in this section, showing that the results change in response to changes in a single variable. The nominal results are discussed in Sections 5.2.1 and 5.4. Section 5.3 presents how the results change when the geometry of the piping system is varied.

### 5.2.1 Nominal Setup Results

To test the model, an example model was created using pressure boundaries for the supply-side inlet and return-side exit. This model is shown in Figure 41. The supply-side and return-side inlets are connected by a volume that is cooled to a desired temperature. A constant mass flow rate pump is selected for the supply side, dictating the flow rate through both sides. The nominal conditions for this model and the resulting pressure drops are given in Table 8.

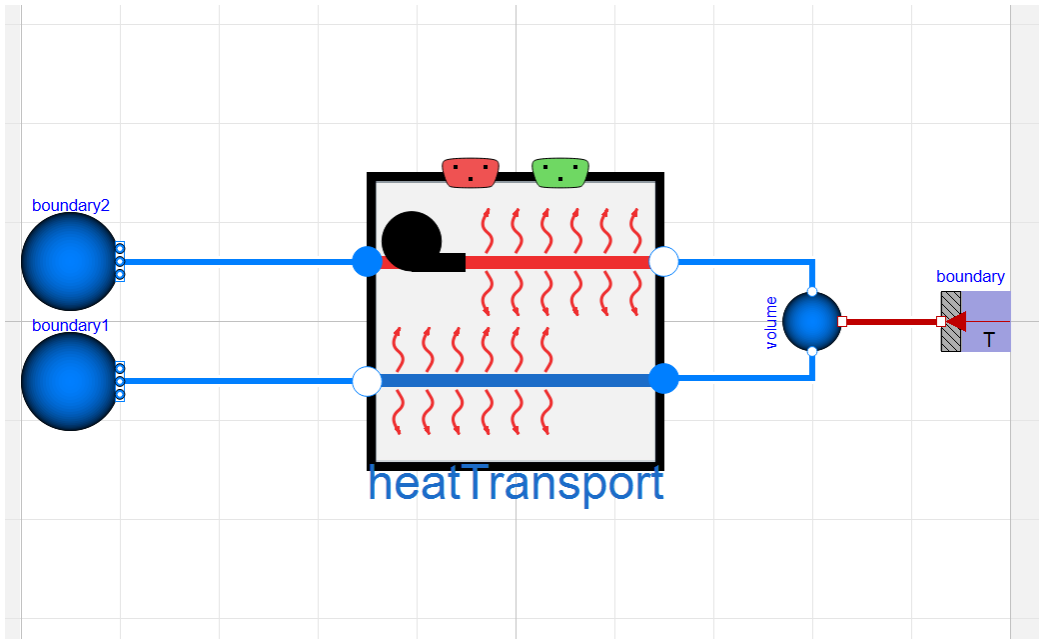


Figure 41. The initial test harness for the heat delivery model involves setting the inlet pressure and energy conditions, the heat removal rate at the delivery point, and pressure at the condensate return. The model is found at NHES.Systems.HeatTransport.Examples.HTtest6.

Table 8: Nominal parameters for the heat transport model.

| Physical Parameter              | Supply Side Value (unit)   | Return Side Value (unit)   |
|---------------------------------|----------------------------|----------------------------|
| Pressure Drop                   | 0.0295 (bar)               | 0.0312 (bar)               |
| Heat Transfer Fluid             | Water                      | Water                      |
| Inlet Temperature               | 90°C                       | 40°C                       |
| Pipe Length                     | 100 (m)                    | 100 (m)                    |
| Pipe Diameter                   | 0.25 (m)                   | 0.25 (m)                   |
| Pipe Wall Thickness             | 0.1 (m)                    | 0.1 (m)                    |
| Pipe Insulation Thickness       | 0.1 (m)                    | 0.1 (m)                    |
| Change in Height                | 0 (m)                      | 0 (m)                      |
| Flow Rate                       | 50 (kg/s)                  | 50 (kg/s)                  |
| Pipe Wall Material              | 304 Stainless Steel        | 304 Stainless Steel        |
| Pipe Insulation Material        | Fiber Glass                | Fiber Glass                |
| Ambient Temperature             | 30 (°C)                    | 30 (°C)                    |
| Boundary Convective Coefficient | 10 (W/(m <sup>2</sup> •K)) | 10 (W/(m <sup>2</sup> •K)) |

### 5.3 Parameter Sweep: Pipe Geometry

A parameter sweep was run with various pipe lengths and diameters to measure the pressure drop across the supply side. The supply-side inlet was set for 90°C water, which was pumped at a constant 50 kg/s to a heat exchanger that cooled it to 40°C. The cooled water then flowed through the return side to a 1 bar pressure sink. Pressure was measured on the supply at the inlet of the pipe (pump outlet) and at the outlet of the pipe. This simulation was run for a range of supply pipe diameters and lengths, and the

pressure drop across this pipe was measured. The results are shown in Figure 42. As expected, the pressure drop increased with increasing length and decreasing diameter.

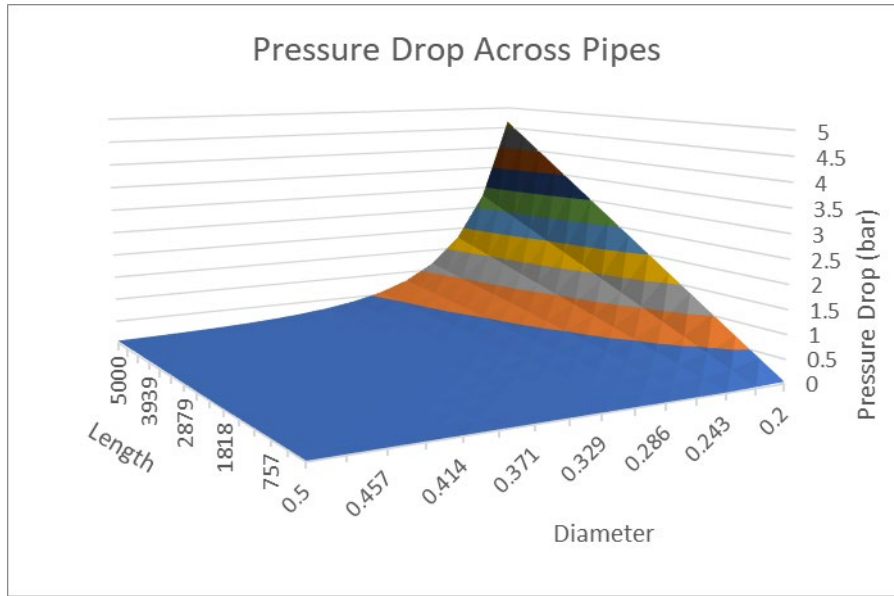


Figure 42. Pressure drop calculations sweeping across various pipe lengths and diameters.

### 5.3.1 Data Generation

To understand the effects that the various input parameters have on the thermodynamic losses, the model was run with a large array of inputs. This was done using RAVEN on INL's HPC system. Using the HPC allows for many more Dymola calculations to be run in parallel than would otherwise be possible on a single machine. Instructions on this procedure are included in Appendix B. Seven different input parameters were swept for three different heat transfer fluids. Table 9–Table 11 show the ranges and number of points for each fluid. For these runs, a convective heat boundary was used, along with a coefficient of  $20 \text{ W/m}^2\text{-K}$  and a temperature of  $20^\circ\text{C}$ , simulating a pipe operating outside in ambient air conditions. The conductive heat transfer was simplified to a single thermal resistance calculated for each set of parameters by using the pipe diameter, insulation thickness, and insulation thermal conductivity. The diameter of the pipe was also calculated for each set of parameters by using the velocity and mass flow parameters and the outlet density. There was also no pump or compressor in this model, and only a single direction was modeled. In the simulation, the inlet enthalpy was controlled using a PI controller, enabling the desired steady-state outlet enthalpy to be achieved. A flow source was used to generate a constant mass flow rate, which allowed for the inlet pressure to float, thereby generating a resulting pressure drop in order to achieve the delivery pressure. A finer mesh and more fluids will be simulated in future modeling.

Table 9. Heat transport input parameters for steam.

| Parameter                             | Min Value | Max Value | Number of Points |
|---------------------------------------|-----------|-----------|------------------|
| Sink Pressure (bar)                   | 1         | 25        | 6                |
| Degree Superheat ( $^\circ\text{C}$ ) | 20        | 60        | 3                |



|   |       |       |       |
|---|-------|-------|-------|
| Mass Flow Rate (kg/s)                   | 8     | 80    | 6     |
| Length (m)                              | 500   | 5000  | 11    |
| Velocity (m/s)                          | 5     | 40    | 5     |
| Insulation Thickness (m)                | 0.01  | 0.1   | 3     |
| Insulation Thermal Conductivity (W/m-K) | 0.022 | 0.115 | 3     |
| Total Number of Runs                    |       |       | 53460 |

Table 10. Heat transport input parameters for carbon dioxide.

| Parameter                               | Min Value | Max Value | Number of Points |
|---|-----------|-----------|------------------|
| Sink Pressure (bar)                     | 1         | 25        | 6                |
| Demand Temperature (C°)                 | 250       | 750       | 3                |
| Mass Flow Rate (kg/s)                   | 8         | 80        | 6                |
| Length (m)                              | 500       | 5000      | 11               |
| Velocity (m/s)                          | 5         | 40        | 5                |
| Insulation Thickness (m)                | 0.01      | 0.1       | 3                |
| Insulation Thermal Conductivity (W/m-K) | 0.022     | 0.115     | 3                |
| Total Number of Runs                    |           |           | 53460            |

Table 11. Heat transport input parameters for sodium.

| Parameter                               | Min Value | Max Value | Number of Points |
|---|-----------|-----------|------------------|
| Sink Pressure (bar)                     | 1         | 2         | 2                |
| Demand Temperature (C°)                 | 240       | 650       | 3                |
| Mass Flow Rate (kg/s)                   | 8         | 80        | 6                |
| Length (m)                              | 500       | 5000      | 11               |
| Velocity (m/s)                          | 5         | 40        | 5                |
| Insulation Thickness (m)                | 0.01      | 0.1       | 3                |
| Insulation Thermal Conductivity (W/m-K) | 0.022     | 0.115     | 3                |
| Total Number of Runs                    |           |           | 17820            |

The outputs of these runs were combined into a spreadsheet, enabling the creation of a lookup table for future analysis. Some of these results are shown below. Figure 43 shows how the velocity in the pipe affects the thermodynamic losses. Increasing the speed increases the pressure drop, temperature drop, and power loss. Note that, nominally, there is 132.2 MW of latent heat in the steam at the delivery pressure and mass flow rate.

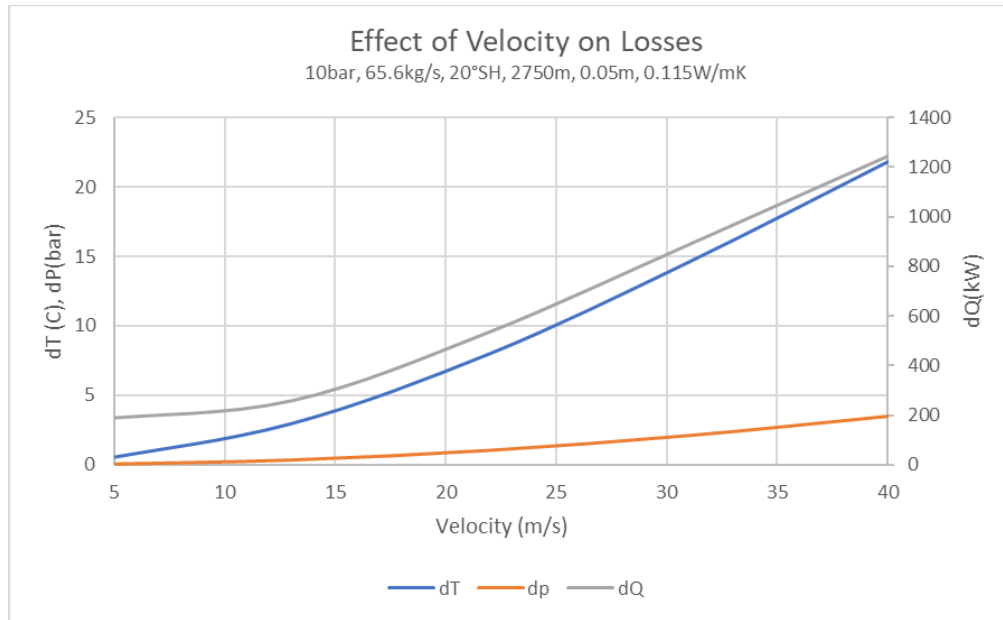


Figure 43: The effect of velocity on thermodynamic losses for steam transport.

## 5.4 HTF Comparison

Multiple heat transfer fluids can be compared using this model. Under nominal conditions, and with the supply length changed to 1000 m, a parameter sweep was conducted to compare the supply-side pressure drop to the pipe diameter. This was done for several different HTFs. Figure 44 shows the results of the parameter sweep for each HTF tested.

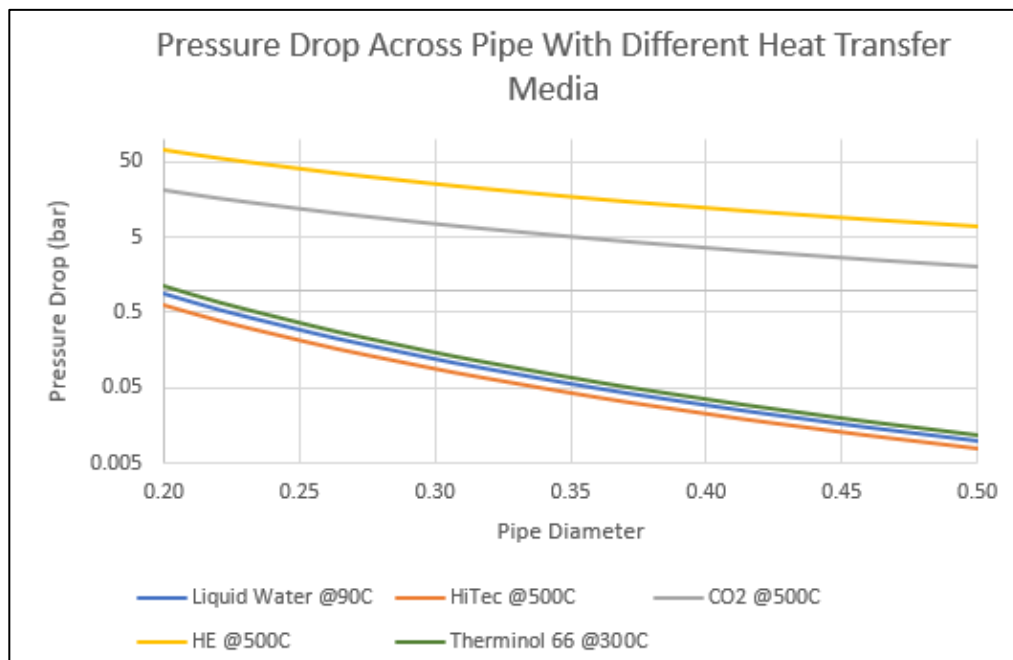


Figure 44: Comparison of multiple HTFs over a range of pipe diameters.

The results from the HPC RAVEN runs, with eight input parameters and several output variables, makes it not feasible to show all of the results graphically. To show how this dataset can be used, several figures were generated to highlight certain relationships. Figure 45 and Figure 46 show pressure and heat loss as a function of velocity for several HTFs.

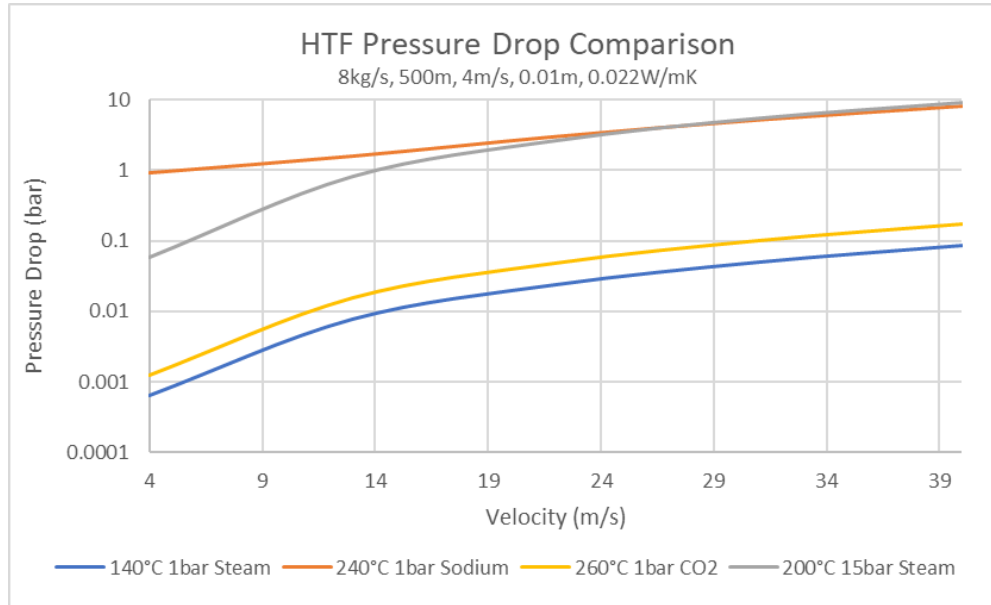


Figure 45: Effect of velocity on pressure loss for several HTFs.

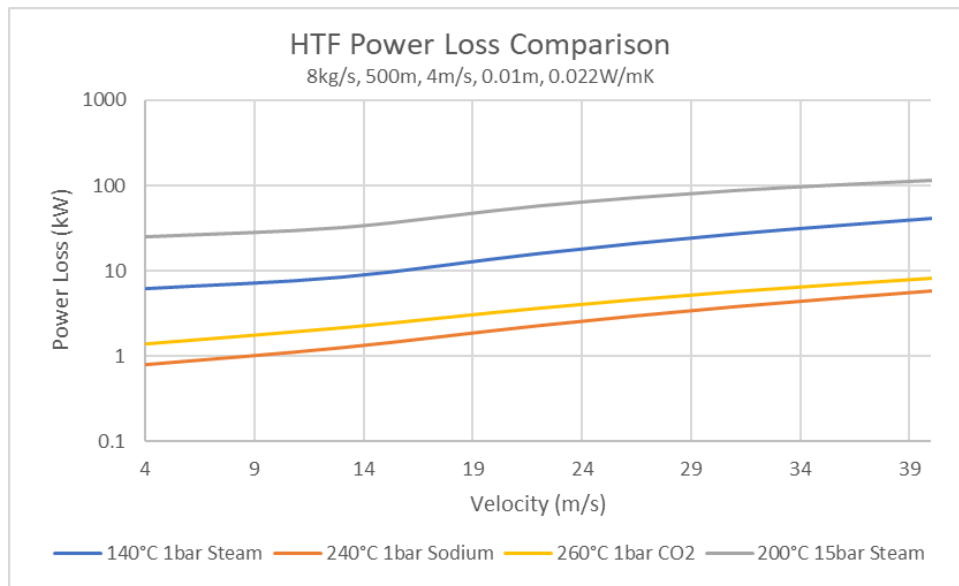


Figure 46: Effect of velocity on power loss for several HTFs.

Figure 47–Figure 49 show the linear heat rate loss, as a function of power delivered, for steam, sodium, and CO<sub>2</sub> at different temperatures. Steam shows a positive linear relationship between higher temperatures and increased heat loss. CO<sub>2</sub> shows behavior similar to that of steam, except that

temperature has a negligible effect on the loss rate. Sodium shows different behavior, with increasing power delivery leading to lowered heat loss. The heat supplied from sodium and CO<sub>2</sub> is much lower than that from steam, as the same flow rates were tested (8–80 kg/s). However, sodium and CO<sub>2</sub> have much lower specific heat capacities than steam, which can utilize latent heat.

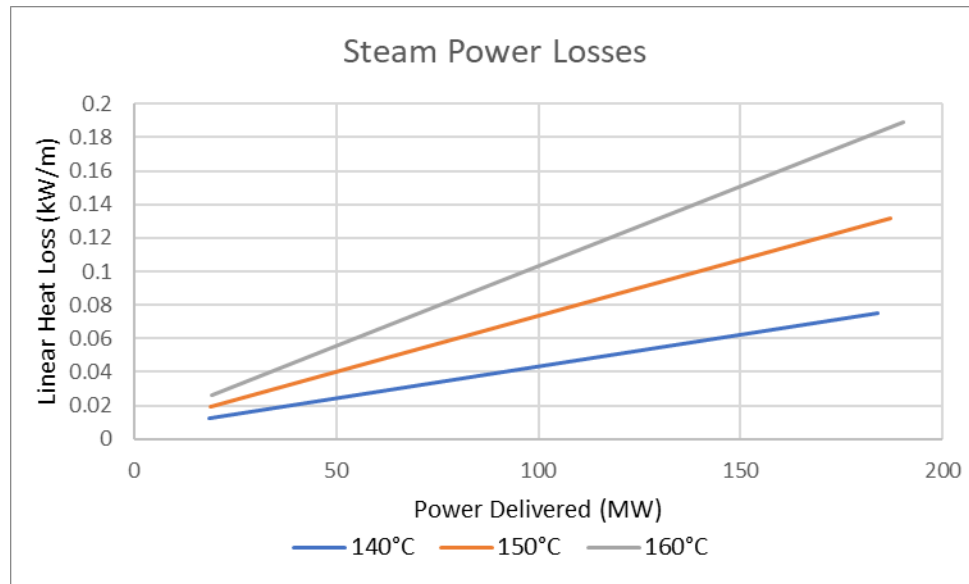


Figure 47: Power loss of steam per unit length, with different power delivery rates.

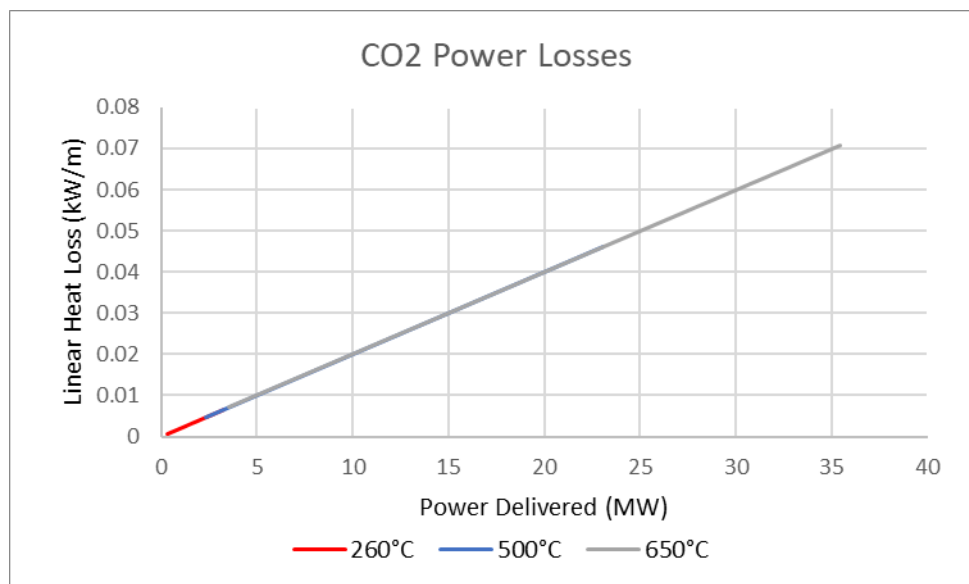


Figure 48: Power loss of CO<sub>2</sub> across different power rates and temperatures. Note that only one line is visible, as the values are nearly identical.

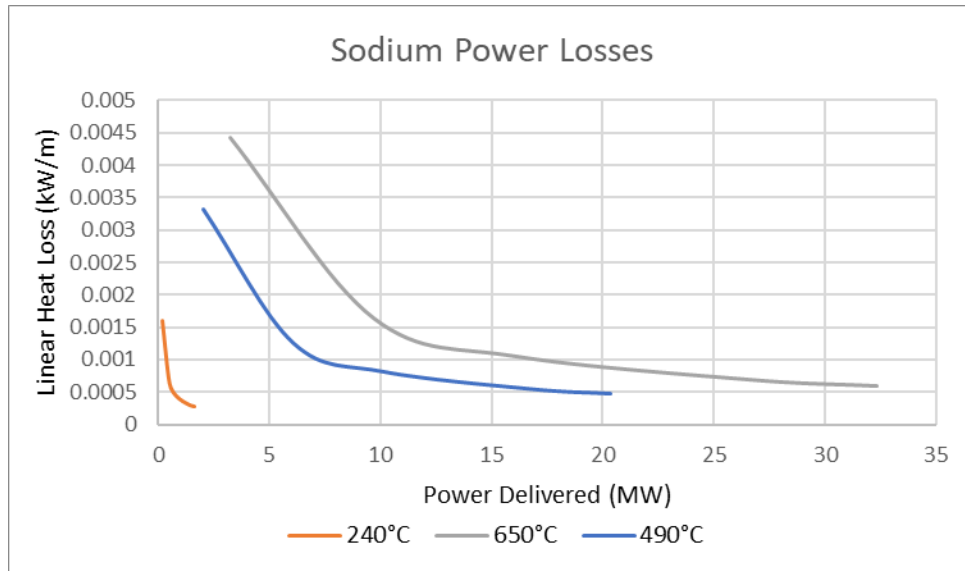


Figure 49: Power loss from sodium delivering power at various temperatures.

The results shown represent initial examinations of the tabulated parameter sweeps conducted for the various fluids. The tabulated results will be able to be interrogated as a lookup table to help define specific thermodynamic losses for investigated deployment scenarios. Furthermore, these values will be able to be combined with costing information to produce price curves for these systems as well.

## 6 FUTURE WORK

This document describes the capabilities of the IES program and showcases generated results. As the IES program continues to look toward analyses of specific reactor-industrial pairings, wherein specific thermal delivery and thus thermal extraction conditions are known, the capabilities presented in this report can be specifically applied to characterize the optimal integration method.

Looking forward, it is anticipated that the IES program will investigate various advanced reactor pairings with industrial systems such as oil refineries, pulp and paper mills, steel manufacturing, and synthetic fuels production. Each of these systems presents very different integration opportunities, with different temperatures, power rates, thermal-to-electric balances, and possibly even load profiles. The dynamic analysis capabilities developed here will be applied to thermodynamically optimize integration schemes.

Additionally, further validation and verification work is planned for the BOP models. While prior work has shown that Modelica on-design modeling aligns very closely with other state-of-the-art thermal and chemical calculation codes, the off-design calculations will still require some validation using outside codes or data.

## 7 CONCLUSIONS

This work explored the limits of the uncontrolled extraction of steam from the turbine at off-design steady states so as to simplify steam cycle matching for selected advanced reactor parameters. The results were summarized to show the maximum steam extraction for a given nominal extraction pressure and for a given demand pressure, in relation to the thermal efficiency of the cycle. The resulting whale charts show the limits of the extraction and corresponding efficiency. These results can allow analysts to have preliminary mapping of thermal requirements to various reactor types. The work is further extended to controlled extraction, performed either by a PA (ideal case) or by a valve (typical approach, often realized by screens). Parameters are plotted to full extraction, neglecting—across all analyses—certain minimal

requirements for the turbine to be operated and cooled safely. Many of the explored limits are, however, pushing turbine operation to highly off-design and potentially choked flow conditions, for which certain system assumptions can be questioned. Additional cycle details are intended for future analyses, primarily using steady-state codes on a case-by-case basis, so as to flesh out details without expending excessive resources on general analysis using computationally expensive dynamic models.

Thermal delivery data have been generated, calculating the thermodynamic requirements of meeting heat delivery conditions across a variety of swept parameters. So far, there appear to be trade-offs between using specific HTFs, and no easy overarching rules for preferring one fluid over another have been observed. Further analysis of the data across additional thermal delivery conditions may generate such rules in the future.

Though the models presented herein have only produced results under steady-state conditions, they are all fully capable of dynamic analysis. Selecting this over-capability method for this year made the IES team well set up for executing advanced analyses in future years, without having to construct all the building blocks of the dynamic system.

## **8 ACKNOWLEDGEMENTS**

This work was supported by the IES program at Idaho National Laboratory under Department of Energy Operations contract no. DE-AC07-05ID14517. This research made use of Idaho National Laboratory computing resources, which are supported by the Office of Nuclear Energy of the U.S. Department of Energy and the Nuclear Science User Facilities under contract no. DE-AC07-05ID14517.

## 9 REFERENCES

- [1] S. M. Bragg-Sitton, "Next generation nuclear energy: Advanced reactors and integrated energy systems, INL/MIS-22-66708 Rev.0," Idaho National Lab. (INL), Idaho Falls, ID (United States), 2022.
- [2] D. Mikkelsen, J. Kim and A. Epiney, "Status Report on Thermal Extraction Modeling in HYBRID, INL/RPT-23-03062 Rev. 0," Idaho National Lab.(INL), Idaho Falls, ID (United States), 2023.
- [3] K. L. Frick, A. Alfonsi, C. Rabiti and D. M. Mikkelsen, "Hybrid user manual, INL/MIS-20-60624 Rev.1," Idaho National Lab.(INL), Idaho Falls, ID (United States), 2022.
- [4] S. M. Greenwood, B. R. Betzler, L. A. Qualls and J. Yoo, "Demonstration of the advanced dynamic system modeling tool TRANSFORM in a molten salt reactor application via a model of the molten salt demonstration reactor," *Nuclear Technology*, vol. 206, no. 3, pp. 478-504, 2020.
- [5] A. Stodola, Steam and gas turbines: with a supplement on the prospects of the thermal prime mover. Vol. 2, McGraw-Hill, 1927., 1927.
- [6] S. A. Korpela, Principles of turbomachinery, John Wiley & Sons, 2019.
- [7] J. Wright, Steam Turbine Cycle Optimization, Evaluation, and Performance Testing Considerations, GE Power Generation, 1994.
- [8] C. Rabiti, A. Alfonsi, J. Cogliati, D. Mandelli, R. Kinoshita, S. Sen, C. Wang, P. W. Talbot, D. P. Maljovec and M. G. Abdo, "RAVEN user manual. No. INL/EXT-15-34123-Rev. 07," Idaho National Lab.(INL), Idaho Falls, ID (United States), 2021.
- [9] Thorcon US, INC., "Status Report," International Atomic Eenergy Agency, 2020.

## **APPENDIX A**

This appendix is added into this report to demonstrate the potential capabilities of future dynamic analyses. All of the presented results in this report were for steady-state results. However, the models are setup to analyze dynamic transient conditions. This section of the report not only includes some related transient results, but shows how future systems can be optimized for particular dynamic operation.

### **A. Model Based Reinforcement Learning for Improved Control of Transient Nuclear Operations**

The work described above on thermal extraction relies on operating large-scale BOP systems transiently. These systems are strongly thermally coupled to both industrial processes and reactor primaries. In changing the extraction setpoints we cause short term transients to propagate through the system affecting the safety of the coupled processes. As we will see below, often proportional-integral-derivative (PID) control is inadequate to deal with such transients due to the slow thermal feedback of large systems such as steam generators. This work looks to perform an innovative approach based on reinforcement learning to combat these thermal transients when making a large operating point maneuver.

#### **A.1. Motivation**

When attempting complex maneuvers PID feedback for process control can often significantly lag the speed that the system requires to maintain safe operating regimes. This has been discussed previously with respect to integrated energy system transient control [1][2]. This slow response of the control system forces operators to move to longer transients in order for the inherent timescales of the feedback control to be shorter than the desired speed of optimal dispatch. This slow operation can harm the economics and thermal source desirability of nuclear based integrated energy systems by limiting their dispatchability compared with more traditional gas fired industrial heat sources.

Machine learning algorithms, specifically reinforcement learning, have shown an improved ability to control industrial processes compared with PID control or rule-based controllers [3]. Their prevalence in the nuclear industry has however been restricted by the safety implications of letting “black box” neural networks take control decisions that may ultimately affect the safety of the plant and consequently the licensing process. It is hoped that improved transient modelling capabilities can demonstrate the ultimate safety of reinforcement learning (RL) trained controllers and may help address these concerns.

This work looks to build on previous works with RL trained controllers using Modelica [4] and apply it to the nuclear industry. To maintain model transparency while utilizing machine learning we employ a pre-trained RL feedforward signal to allow faster operation of the existing feedback controllers in set maneuvers. This simultaneously allows faster transients to be performed whilst maintaining the simplicity and easy regulation approach desirable in equation-based feedback control.

#### **A.2. Methodology**

##### **A.2.1. Model Selection**

We can highlight the undesirable transients seen in BOP control using the two-stage balance of plant Modelica model from the HYBRID library. The model operates with a constant reactor power and follows a load demand by throttling the turbine control valve (TCV). A full diagram of the model set up is shown in Figure A1 with the control set up described in Table A1.



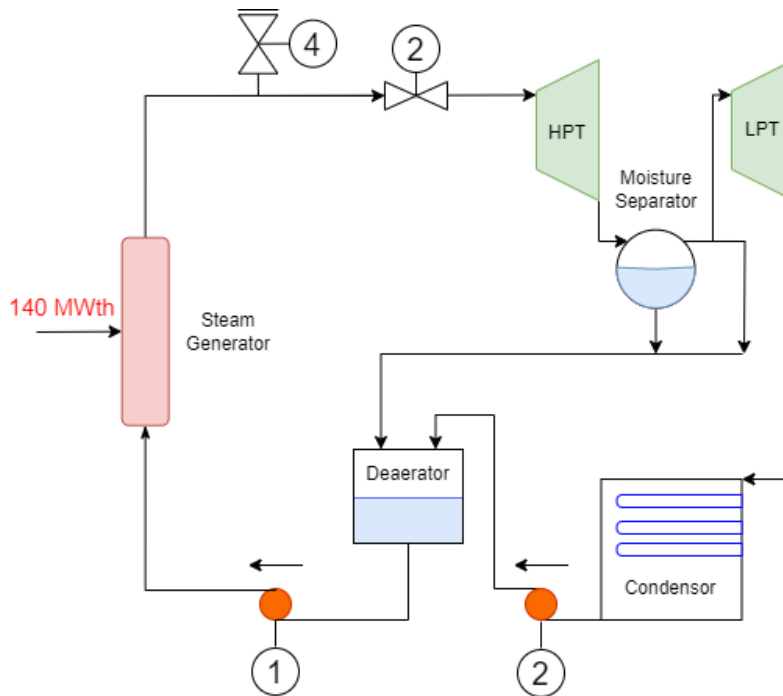


Figure A1. Simplified system diagram showing modeled components and controlled components.

The reactor steam generator (SG) input for simplicity is modelled as a constant heat input of 140 MW. The Deaerator maintains saturation conditions at around 3-4 bar and 300°C. The condenser is held at 0.08 bar and 42°C.

As such the three key manipulated variables involved in the transient thermal load follow are the opening of the TCV (to follow demand power), the deaerator level (to maintain pressure and feedwater temperature) and the feedwater coolant pump (FWCP) to maintain SG outlet temperature.

Table A1. Controlled components and system setpoints.

| Label | Name                  | Controlling             | Setpoint                       |
|-------|-----------------------|-------------------------|--------------------------------|
| 1     | Turbine Control (TCV) | Demand Electrical Power | Manipulated                    |
| 2     | Condensate Pump (CP)  | Deaerator Level         | 5 m ( $P_{sat}$ approx. 4 bar) |
| 4     | FWCP                  | SG Outlet Temperature   | 400°C                          |
| 10    | Pressure Relief       | Pressure Overloads      | Release at 150 bar             |

### A.2.2. Reference Case

To demonstrate the difficulty of maintaining a constant outlet temperature of the SG using just PID control, a transient maneuver is performed on the system with a demand power of 40 MWe dropped to 30 MWe in 100s. The results are shown in Figure A2 - Figure A6.

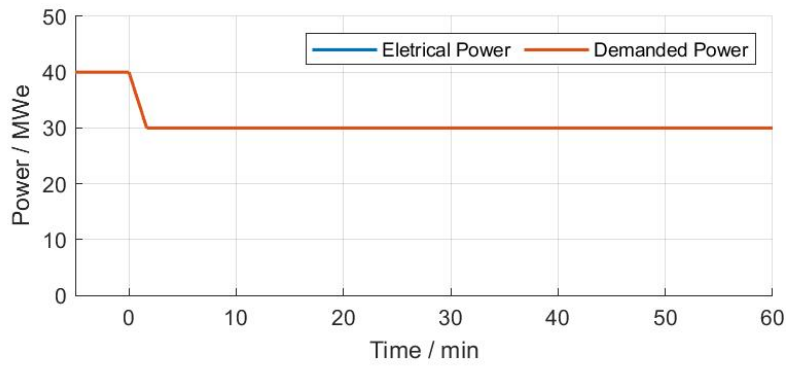


Figure A2. Electrical power thermal load follow imposed transient.

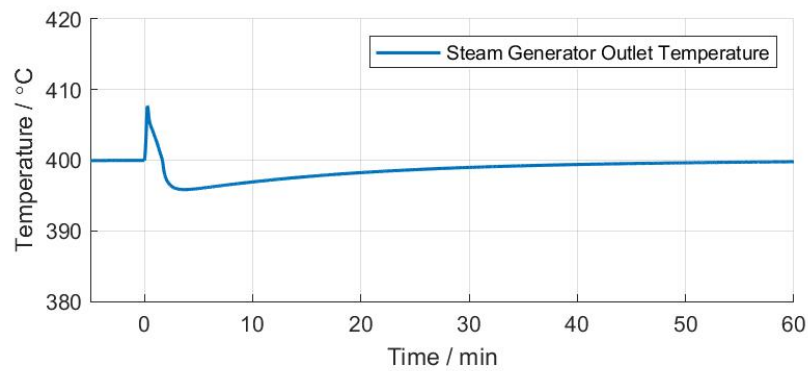


Figure A3. Steam generator outlet temperature with no FWCP feedforward control showing initial peak and slow temperature rebalancing.

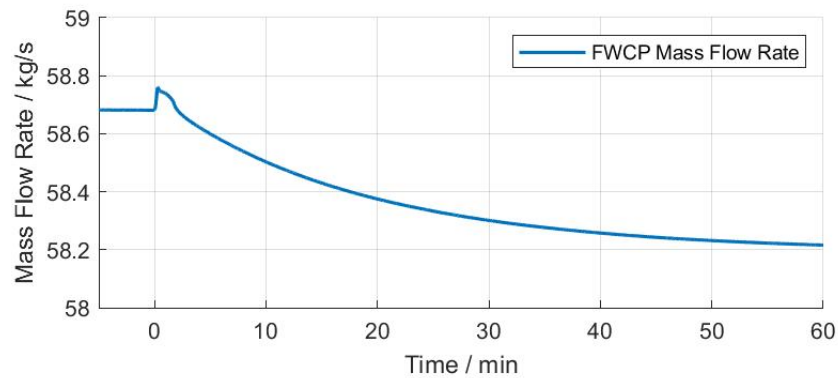


Figure A4. FWCP response rate using PID control showing slow integral feedback to achieve steady state temperature at 400°C/

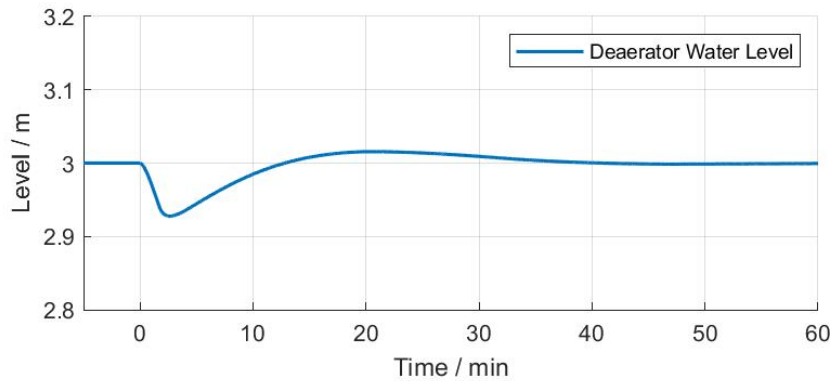


Figure A5. Action of CP to maintain the deaerator tank level showing initial fall and slow return to operating level with some overshoot.

We can see that the TCV responds very quickly to maintain demanded power. In doing so it restricts the mass flow rate through it and causes the pressure at its inlet to rise thus expelling additional mass through the pressure relief valve. The temperature at the steam generator exit rises rapidly as the steam builds up in the header. At this point the feedback of the temperature rise causes the FWCP to initially increase its mass flow rate to reduce this temperature change further increasing the pressure in the header until the pressure relief valve can remove the excess steam. Once this flow is established the temperature falls once more and the pump must respond by reducing the mass flow rate in order to increase the temperature back to 400°C. During this transient the temperature remains significantly above 400°C for 2 min and then falls below for 30 min while the pumps flow is reduced. Both the temperature spike and the long period below desired output temperature last long enough to have an impact on the primary side and thus should be avoided in normal operation. Typically, this would be counteracted by reducing the ramp rate on power such that the pressure build up in the header is reduced and consequently eliminating the temperature spike. However, if the pump was able to respond before it saw feedback from the temperature rise the initial pressure build up could be avoided. This feedforward control signal can be derived for equation-based models and linear physical system but is not easily come to in such a non-linear system of equations seen in this case and much of the IES designs considered. It is therefore desirable to use reinforcement learning to develop such a signal.

### A.3. Implementation using Gymnasium and the Python Dymola Interface

To interface a RL algorithm with the reactor environment, the application programming interface standard developed by OpenAI – Gymnasium [5] was used. Gymnasium provides a Python application programming interface in which a reactor environment can be defined with the key attributes required to interface with a training agent. The initial solution takes the form of individual episodes which are formed of up to 620 steps of 5 seconds each. At each step the agent can make a new action decision and apply it for the next time step. After 5 episodes the agent is updated.

The reactor environment is formed of the following main classes.

1. **Step:** The step class initializes the Dymola simulation model with the outputs from the previous step. It then takes a feedforward action from the agent and applies it to the FWCP PID controller in Dymola. The step then calls Dymola to perform a 5 second simulation run with 0.01s internal timesteps. The final state is recorded in a dsfinal.txt file and the class returns an observation, reward, and a Boolean as to whether a terminal state has been reached.

2. **Reset:** The reset class is called at the beginning of each episode and initializes the Dymola model with a feedforward signal of zero and starts the simulation 100s prior to the application of the power transient.

The reactor environment also contains attributes to allow the implementation of reinforcement learning.

1. **Action Space:** The action space is a 7-value array determining the actions an agent can take. In the reactor environment this takes the form of the array: [-0.7, -0.2, -0.1, 0, 0.1, 0.2, 0.7]. At any given time step the agent can choose to add or subtract either 0.03 or 0.25 to the feedforward signal or keep it the same as the previous time step.
2. **Observation Space:** The observation takes the form of a four-element array consisting of the SG outlet temperature, the pump mass flow, the electrical power out and the feedforward signal at the previous time step. The observations are roughly normalized such that their magnitudes fall in the range of -10 to +10. This process for each variable is shown in Table A2. Normalization is required to aid initialization of the weights of the neural network and ensure smooth updating of the network. The observation space is a box from the limits shown in Table A2.
3. **Reward:** The reward takes the form of a scalar variable that adds a contribution to the score at each time step dependent on how close the output temperature is at the end of that time step to the goal condition of 400°C. This takes the form of a linear function described by equation 1.

$$R[t] = 8 - |T_{out}[t] - 673.15| \quad 1.$$

4. **Terminal State:** The episode is terminated, and the score returned under two conditions. The first is if the SG output temperature at the end of any given time step does not lie in the range:  $664.15 < T_{out} < 682.15$ . This reduces the time the simulation takes to fully learn the sub space by penalizing bad states. The simulation has a run time set to 310 steps. After this the change in the feedforward signal is assumed to be zero as the temperature should have returned to its nominal state.

Table A2. Observations with normalization equations and normalized limits for reactor environment.

| Observation                        | Normalization                                  | Limits   |
|------------------------------------|--|----------|
| SG Outlet Temperature              | $T_{out} - 673.15$                             | -8, +8   |
| FWCP mass flow rate                | $\dot{m}_{pump} - 58$                          | -10, +10 |
| Turbine Electrical Power Output    | $\frac{(Q_e - 30 \times 10^6)}{1 \times 10^6}$ | -6, +6   |
| Pump Controller Feedforward Signal | No normalization                               | -10, +10 |

### A.3.1. Deep Q-Learning Algorithm

The reinforcement learning algorithm is based on a feed neural network formed of an input layer corresponding to the 4 observation states, 2 hidden layers, the first of 64 nodes the second consisting of 128 nodes, and then an output layer of a single action. This is implemented in python using the 'nn' class from the package PyTorch. The form of the solution is based on the deep Q-learning algorithm with the use of PyTorch softmax as described here [6][7]. The solver evaluates the Q-values from the neural network and produces an array of probabilities of the best action to take based on a temperature value. As this temperature is reduced, the more likely the agent is to choose the optimal action. Over the course of a

number of runs, the temperature is reduced exponentially to converge on an optimum solution. The neural network can be then evaluated with an epsilon-greedy strategy with a low epsilon value to find the final solution.

The neural network is updated every 5 episodes with uncorrelated action-observation pairs from a replay memory stack. The learning takes the form of 500 runs with an optimizer learning rate of 0.001. The temperature is initialized at 5 and is reduced exponentially over the simulation to a final value of around 0.007.

## **A.4. Results and Discussion**

### **A.4.1. Learning Speed and Hyperparameters**

To achieve the fastest possible learning, a two-step process is used. An initial learning of the full 3000s post transient is performed. This is used to demonstrate a reasonable time at which the temperature remains constant and the change in the feedforward signal is zero. After this initial sweep the region of interest is reduced, and a more detailed run is performed.

The final profile for the first step of this process is shown in Figure A6. The original temperature profile from Figure A3 is shown in blue with the new signal shown in orange, an acceptable temperature band of  $\pm 2^\circ\text{C}$  is shown in green with the simulation limits shown in red. In Figure A6 it can be seen that a steady state temperature can be achieved quickly in the first 500 seconds. Having performed this learning run we can then go back and locally optimize the first 500 seconds to achieve the optimum feedforward signal in this crucial region. This prevents the need to simulate the last 2500 seconds every time and hence significantly reduces computational effort.

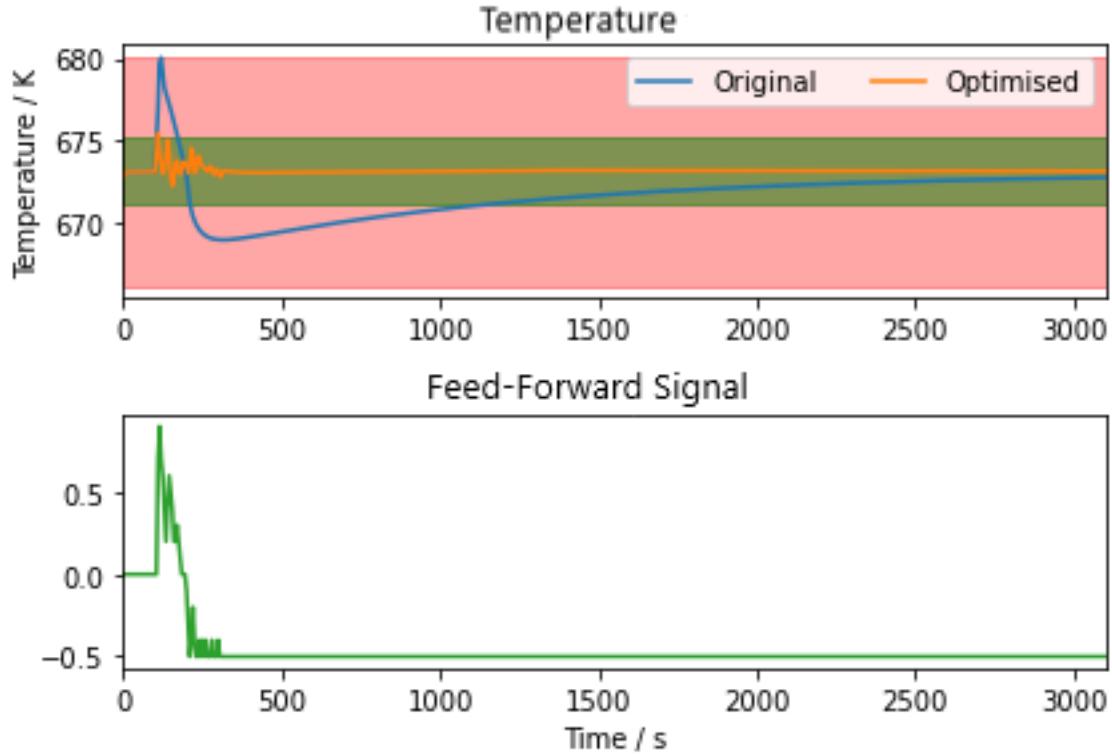


Figure A6. Initial long length run to scope settling time for temperature signal. The applied feedforward signal is shown below in green with the resulting temperature profile shown in orange. It can be seen that after the first 500 seconds in the optimized profile the temperature profile has returned to steady state.

The learning trajectory for this second step of 500 seconds long episodes is shown in Figure A7. This plots the rewards for each episode against the episode number. The learning is initially very good at finding the rough trajectory of the signal but finding the final optimum is slow requiring significantly more episodes. In this simulation we start by performing 500 runs with an exponentially decreasing temperature. This slowly converges to a signal close to the optimum but becomes trapped in a local maximum. To counter this, we then use the final result memory and optimized policy network to rerun the learning starting from a higher temperature again and more slowly reducing this temperature. This allows for the final optimum state to be found faster as it can quickly converge close to the true maximum and then be allowed to settle more slowly. With more powerful computation effort this hyperparameter tuning is unnecessary but in this trial, it allows good results to be found with less computational effort.

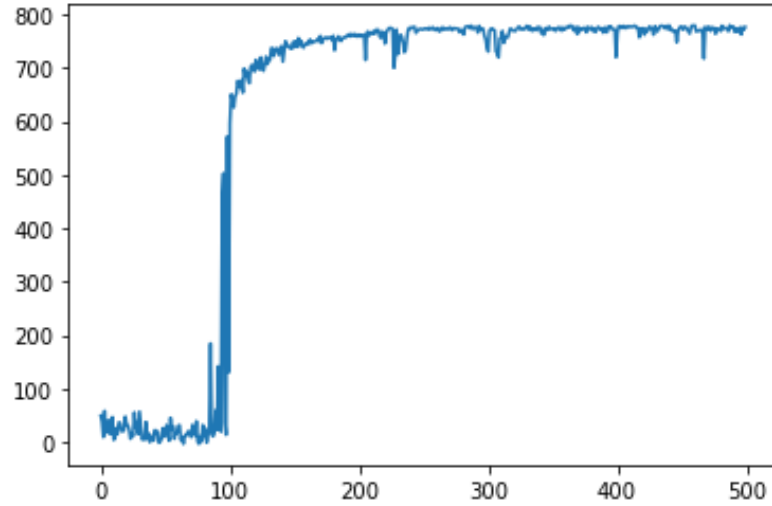


Figure A7. Rewards vs episodes for the first 500 episodes and the second 500 episodes with a simulation temperature increase mid-way through the simulation.

#### A.4.2. Transient Results.

The transient results for the final optimized run are shown in Figure A8 - Figure A10. These results demonstrate the effect of the new feedforward signal for the power transient in question.

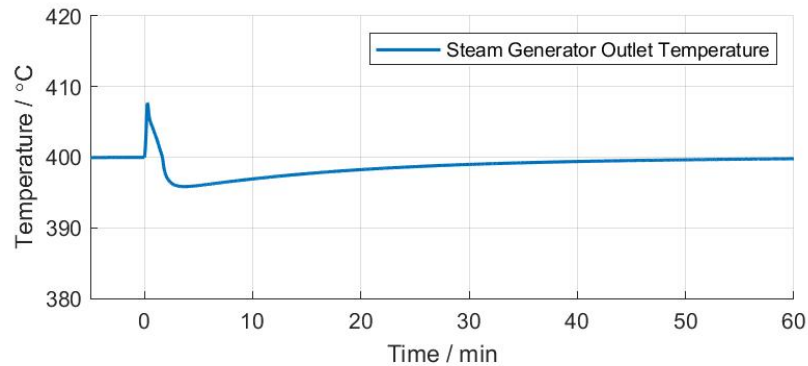


Figure A8. Steam generator outlet temperature with FWCP feedforward control showing a reduced initial peak and a much improved return to nominal operating temperature.

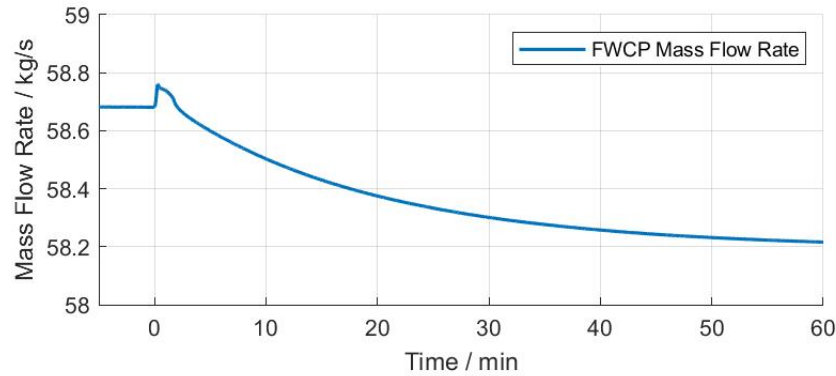


Figure A9. FWCP response rate using the added feedforward control showing a much faster steady state temperature at 400°C.

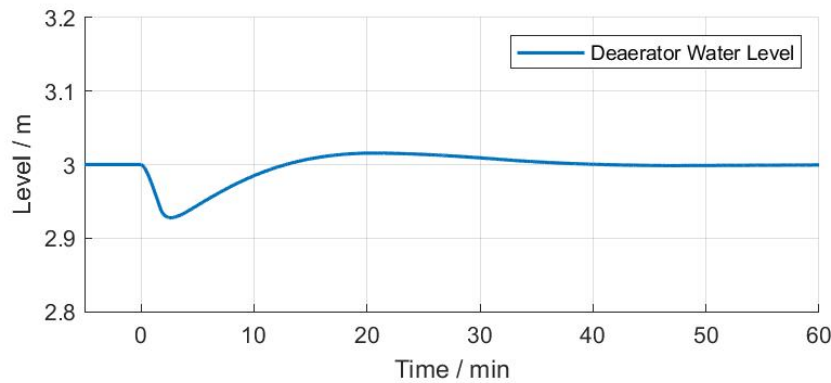


Figure A10. Action of CP to maintain the deaerator tank level showing initial fall and slow return to operating level with some overshoot.

The feedforward signal significantly reduces both the magnitude of the short-term upwards temperature transient and the duration of the long-term low temperature experienced when trying to return to the operating point. It can also be seen how this change does not significantly affect the pressure. It is clear therefore to see how this operating may work on a real integrated energy system, if we know that the power transient is to be applied, we can simultaneously apply the pump feedforward signal and thus counteract the temperature change.

A concern in this process is whether in applying the feedforward signal we breach physical limits imposed by the pump mechanics or whether the power draw is limited by our power electronics. More detailed simulations would be able to add these in as signals and impose these limits in the controller.

## A.5. Conclusions and Future Work

This work has shown that by using reinforcement learning and Modelica simulated transient physics we can derive complex feedforward signals in a multi-controlled non-linear system. It is hoped this work has relevance to control of thermal delivery but also for real time control of Modelica digital twins and improved physical optimization for integrated energy system design. Future work may include parallelizing the interface to perform either real time optimization or significantly faster feedforward control design. It would also be beneficial to consider more complex dispatch profiles and signals to see



how performance is affected. Finally tuning of the hyperparameters to achieve faster learning and studies that use higher fidelity signal simulation by allowing for shorter time stepping in key transients would be beneficial.

## A.6. References

1. Saeed, Rami M., Shigrekar, Amey, Mikkelson, Daniel Mark, George Rigby, Aidan Christopher, Yang Hui Otani, Courtney Mariko, Garrouste, Marisol, Frick, Konor L., and Bragg-Sitton, Shannon M.. Multilevel Analysis, Design, and Modeling of Coupling Advanced Nuclear Reactors and Thermal Energy Storage in an Integrated Energy System. United States: N. p., 2022. Web. doi:10.2172/1890160.
2. Rigby, Aidan Christopher George and Wagner, Mike and Lindley, Ben, Dynamic Modelling of Flexible Dispatch in a Novel Nuclear-Solar Integrated Energy System with Thermal Energy Storage (April 11, 2023). Available at SSRN: <https://ssrn.com/abstract=4528600> or <http://dx.doi.org/10.2139/ssrn.4528600>
3. Jeon, S., Abate, A., & Cullen, J. M. (2023). Low Emission Building Control with Zero-Shot Reinforcement Learning. *Proceedings of the AAAI Conference on Artificial Intelligence*, 37(12), 14259-14267. <https://doi.org/10.1609/aaai.v37i12.26668>
4. Pigott, K. Baker, S. A. Dorado-Rojas and L. Vanfretti, "Dymola-Enabled Reinforcement Learning for Real-time Generator Set-point Optimization," 2022 IEEE Power & Energy Society Innovative Smart Grid Technologies Conference (ISGT), New Orleans, LA, USA, 2022, pp. 1-5, doi: 10.1109/ISGT50606.2022.9817464.
5. Gymnasium, Zenodo, Towers, Mark and Terry, Jordan K. and Kwiatkowski, Ariel and Balis, John U. and Cola, Gianluca de and Deleu, Tristan and Goulão, Manuel and Kallinteris, Andreas and KG, Arjun and Krimmel, Markus and Perez-Vicente, Rodrigo and Pierré, Andrea and Schulhoff, Sander and Tai, Jun Jet and Shen, Andrew Tan Jin and Younis, Omar G., 2023, 10.5281/zenodo.8127026
6. Paszke, A., Gross, S., Massa, F., Lerer, A., Bradbury, J., Chanan, G., Killeen, T., Lin, Z., Gimelshein, N., Antiga, L. and Desmaison, A., 2019. Pytorch: An imperative style, high-performance deep learning library. *Advances in neural information processing systems*, 32.
7. <https://towardsdatascience.com/deep-q-network-with-pytorch-and-gym-to-solve-acrobot-game-d677836bda9b>

# APPENDIX B

## B. Raven and Dymola Usage on the INL's HPC

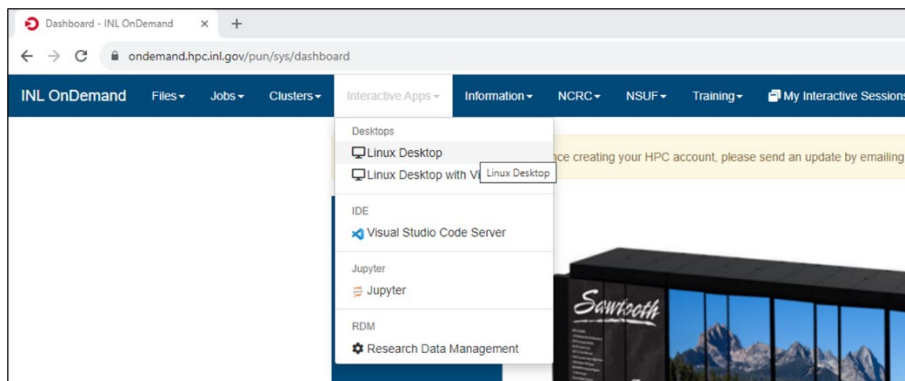
Computational expense from FORCE runs, especially runs using holistic energy resource optimization network (HERON) is a significant impediment to performing large RAVEN runs. Using INL's High Performance Computing (HPC) can reduce the run time. The following is a list of instructions for accessing HPC resources, setting up Dymola, and using RAVEN.

### 1. Accessing HPC On Demand

HPC OnDemand is used to access INL's HPC resources at <https://ondemand.hpc.inl.gov/>. An HPC account can be requested at <https://ncrcaims.inl.gov/Identity/Account/Register>.

### 2. Launching a Linux Desktop

Dymola's graphic user interface requires a Linux Desktop on the HPC. It can be launched in the interactive 'Apps' tab of HPC OnDemand.



You will be prompted for a project code, cluster selection, and job type. For the project code, check with project leads to ensure the code selection is appropriate, within the IES program, use is low enough that 'ne\_gen' can be used. A complete list of project codes can be found at <https://hpcweb.hpc.inl.gov/home/pbs#specifying-a-project>.

For RAVEN usage, choose Sawtooth as the cluster. The login job type is sufficient for Dymola setup.

After launching, your desktop will be placed in the job queue before it is available for usage.

**Linux Desktop**  
This app will launch a linux desktop on an INL HPC resource.

**Project**  
ne\_gen

This is the project argument provided to the job schedule. For a complete list of projects, go to [projects page](#) on hpcweb

**Cluster**  
Sawtooth

Select what cluster you want to run your desktop on.

**Job Type**  
Login

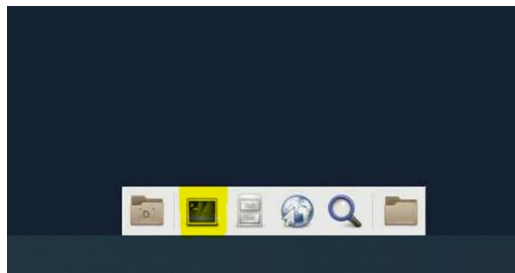
| Job Type    | Purpose                                |
|-------------|--|
| Login       | File editing, compiling, basic testing |
| Compute CPU | Tasks that may require more than 1 CPU |
| Compute GPU | Tasks that require GPU resources       |

**Launch**

\* The Linux Desktop session data for this session can be accessed under the data root directory.

### 3. HYBRID Installation

HYBRID must be cloned into your user space. First, create or choose the folder where you would like to place HYBRID, for example 'projects'. A file explorer is available as an icon on the bottom of the Linux Desktop. Then, open a terminal in the Linux Desktop with the icon at the bottom of the screen.



Clone HYBRID using the following command.

```
Terminal - costkr@sawtooth4: ~/projects
File Edit View Terminal Tabs Help
(base) [costkr@sawtooth4 ~]$ cd projects/
(base) [costkr@sawtooth4 projects]$ git clone https://github.com/idaholab/HYBRID.git
```

### 4. TRANSFORM setup

There are multiple ways to setup TRANSFORM. Only one of options a and b is necessary.

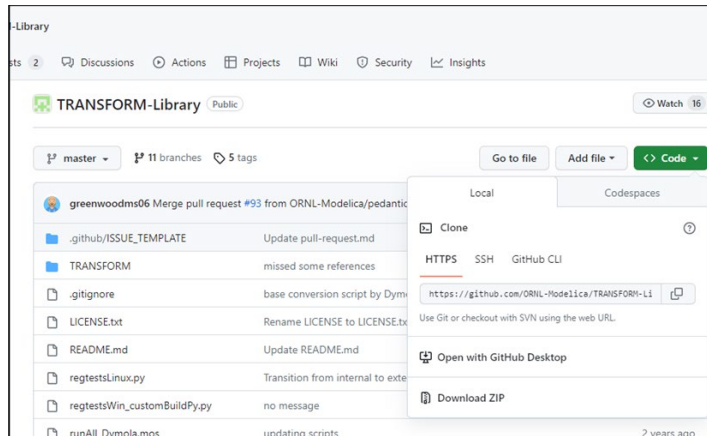
- a. Use git clone to install TRANSFORM

First, navigate to the HYBRID folder, then clone TRANSFORM.

```
Terminal - costkr@sawtooth4: ~/projects/HYBRID
File Edit View Terminal Tabs Help
(base) [costkr@sawtooth4 ~]$ cd projects
(base) [costkr@sawtooth4 projects]$ cd HYBRID/
(base) [costkr@sawtooth4 HYBRID]$ git clone https://github.com/ORNL-Modelica/TRANSFORM-Library.git
```

- b. Using the web browser available as an icon on the Linux Desktop, download the TRANSFORM zip file from Oak Ridge National Laboratory's GitHub page.

<https://github.com/ORNL-Modelica/TRANSFORM-Library>

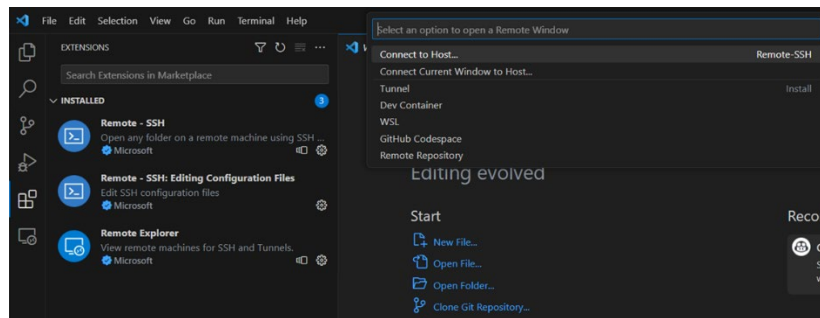


In the file explorer once the download is complete, extract the files from the zip file. Rename the extracted folder to exactly 'TRANSFORM-Library' if it is named differently.

After cloning, the HYBRID folder already contains a folder named 'TRANSFORM-Library'. Delete this folder in HYBRID and insert the folder you extracted and renamed in its place.

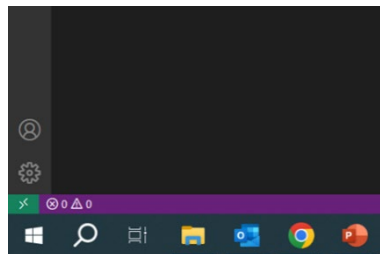
##### 5. Accessing the HPC in Visual Studio Code

The Remote – SSH extension in VS Code is required for this. On the left side of the screen in VS Code, there is an extensions panel. Select that and add the Remote – SSH extension.

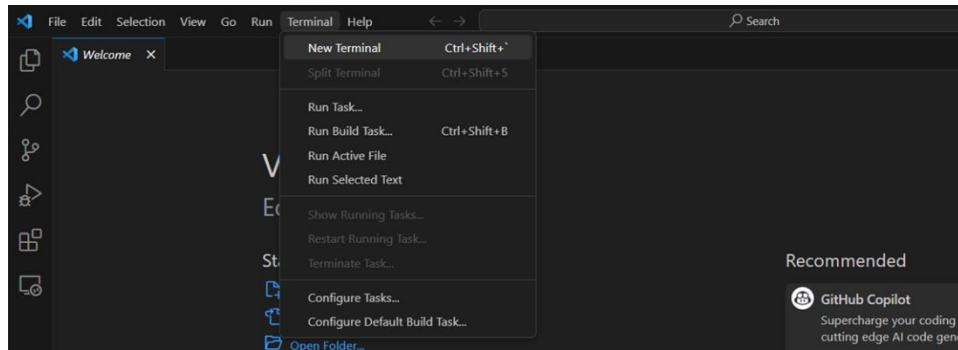


Once the extension installs, the option to start a remote connection appears on the bottom left of VS Code. Click this, and at the top of the screen, an option to Connect to Host appears. Select it. Enter the following, substituting in your HPC username:

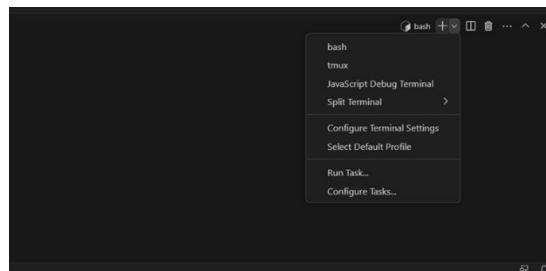
`Ssh -p 22 [HPCusername]@sawtooth1.hpc.inl.gov`



The top ribbon of VS Code contains a terminal option. Select this to open a new terminal.



Ensure this terminal is a bash terminal by checking the drop down on the right side of the terminal.



## 6. Editing your .bashrc file

Editing your .bashrc file ensures that the necessary modules to run RAVEN and Dymola are loaded automatically when you connect to Sawtooth. First, ensure that you are in the correct directory. In the terminal, type the command:

Pwd

pwd shows your current directory. You should be in /home/[username]. If you are not, navigate to it. Now, you can see a list of all files and folders in the directory with the command

ls -la

(Note, use lowercase 'L's in ls -la)

```
(base) [kimj5@sawtooth1 ~]$ pwd
/home/kimj5

(base) [kimj5@sawtooth1 ~]$ ls -la
total 1528
drwx----- 27 kimj5 kimj5 1062 Aug 18 16:27 .
drwxr-xr-x 64 root root 0 Aug 22 15:41 ..
-rw----- 1 kimj5 kimj5 5299 Aug 18 17:20 .bash_history
-rw-r--r-- 1 kimj5 kimj5 529 Aug 3 11:32 .bash_profile
-rw-r--r-- 1 kimj5 kimj5 735 May 4 13:31 .bashrc
-rw-r--r-- 1 kimj5 kimj5 81 Jun 1 2015 .bashrc_local
drwxrwxr-x 8 kimj5 kimj5 180 Aug 7 07:06 .cache
drwxrwsr-x 4 kimj5 kimj5 78 May 2 15:43 .conda
drwxrwxr-x 12 kimj5 kimj5 345 Aug 17 09:05 .config
-rw-r--r-- 1 kimj5 kimj5 304 Jun 30 2014 .cshrc
-rw-r--r-- 1 kimj5 kimj5 58 Jun 1 2015 .cshrc_local
drwxrwxr-x 3 kimj5 kimj5 24 Aug 10 11:58 .dassaultsystemes
drwx----- 3 kimj5 kimj5 29 Aug 7 07:06 .dbus
drwxr-xr-x 2 kimj5 kimj5 0 Aug 7 07:06 Desktop
drwxr-xr-x 2 kimj5 kimj5 0 Aug 7 07:06 Documents
drwxrwxr-x 3 kimj5 kimj5 24 May 3 17:00 .dotnet
drwxr-xr-x 2 kimj5 kimj5 0 Aug 7 07:06 Downloads
drwxrwxr-x 3 kimj5 kimj5 25 Aug 10 11:58 Dymola
-rwxrwxr-x 1 kimj5 kimj5 47 Aug 18 16:27 .flexlmrc
drwx----- 3 kimj5 kimj5 64 Aug 7 07:06 .gnupg
drwx----- 2 kimj5 kimj5 0 Aug 7 07:06 .gvfs
-rw----- 1 kimj5 kimj5 1252 Aug 10 11:58 .ICEauthority
drwxrwxr-x 3 kimj5 kimj5 23 May 2 17:07 .local
```

In the terminal, enter the command:

```
vim .bashrc
```

This opens the bash file. Press ‘i’ to enter insert mode and enter the following lines at the bottom of the file:

```
module load dymola/2022.1
module load python/3.7-anaconda-2019.10
module load raven/2.0
```

```
if [ -f /etc/bashrc ]; then
    . /etc/bashrc
fi

# Source local definitions
if [ -f ~/.bashrc_local ]; then
    . ~/.bashrc_local
fi

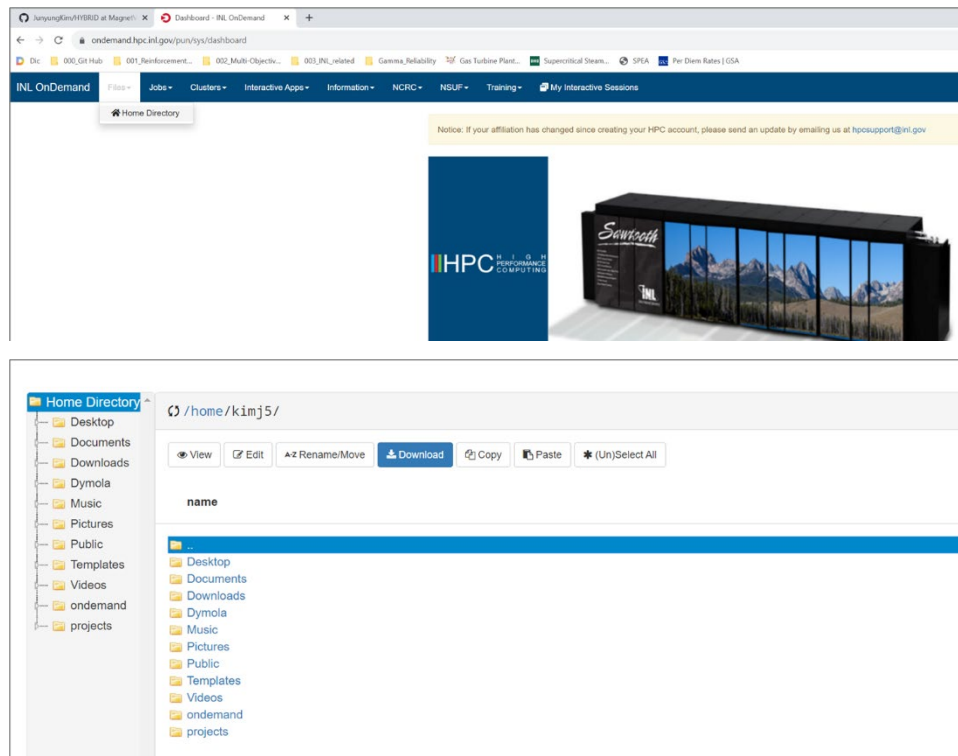
module load dymola/2022.1
module load python/3.7-anaconda-2019.10
module load raven/2.0

```

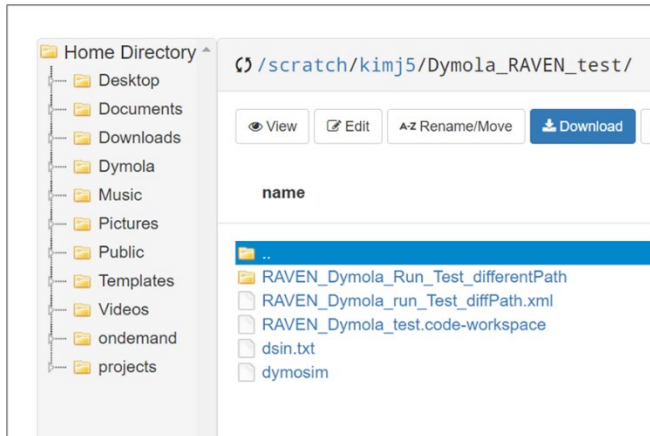
Once the lines have been added, enter ‘wq’, which will save (‘w’) and quit (‘q’) the vim editing.

## 7. Storing required input files to use RAVEN

Using RAVEN on the HPC is a similar process to using RAVEN on a personal machine. The dsin.txt and dymosim files generated by a Dymola simulation are still required. However, they must be generated from the Linux version of Dymola in the HPC. They must also be stored in a specific directory. You can access your working directory on the HPC from HPC OnDemand.



RAVEN requires that the dsin and dymosim files are not stored in this directory, but in /scratch/[user]/ instead. You can access scratch by selecting the ‘.’ to go back a directory.



8. To use multiple cores on the HPC, one should submit jobs using the Qsub command of PBS professional. Assuming that one would like to submit a job related to general nuclear energy project (i.e., ne\_gen) to use 48 cores in 1 cluster and kill the job submitted after 1 hour, following command should be typed:

```
(base) [kimj5@sawtooth1 constellation]$ qsub -I -l walltime=01:00:00 -P ne_gen -l select=1:ncpus=48
qsub: waiting for job 5924299.sawtoothpbs to start
qsub: job 5924299.sawtoothpbs ready

(base) [kimj5@r2i7n7 ~]$
```

For details of PBS, PBS command, and project names in PBS, it is recommended to visit the following website:

[https://hpcweb.hpc.inl.gov/home/user\\_guide/pbs\\_professional#Documentation](https://hpcweb.hpc.inl.gov/home/user_guide/pbs_professional#Documentation)

9. One can identify the jobs submitted using the command `qstat -u <userID>`.

```
(base) [kimj5@r2i7n7 ~]$ qstat -u kimj5

sawtoothpbs:

Job ID      Username Queue  Jobname  SessID NDS TSK  Memory Req'd Req'd Elap
-----
5924299.sawtoo* kimj5  short  STDIN    215711  1  48  188gb 01:00 R 00:01
(base) [kimj5@r2i7n7 ~]$
```